The University of Manitoba

A Model Study for Influence Surfaces of Curved Elastic Isotropic Bridge Decks

by

G. L. Asoka J. De Silva

A Thesis

Submitted to the Faculty of Graduate Studies

in Partial Fulfillment of the Requirements for the Degree

of Doctor of Philosophy

Department of Civil Engineering

Winnipeg, Manitoba

October, 1974

A MODEL STUDY FOR INFLUENCE SURFACES OF CURVED ELASTIC ISOTROPIC BRIDGE DECKS

by

G. L. Asoka J. De Silva

A dissertation submitted to the Faculty of Graduate Studies of the University of Manitoba in partial fulfillment of the requirements of the degree of

DOCTOR OF PHILOSOPHY

SUMMARY

This dissertation deals with the development of a simple but precise experimental technique that can be used effectively in model analysis as a means of studying the more complicated structural systems. The inadequacy of the analytical methods is discussed, indicating how these deficiencies point to the importance of considering structural model analysis and testing as a design tool. After a brief review of the experimental techniques available for model analysis, a detailed description of the technique used in this work is presented. The combination of versatility and simplicity offered by this technique makes it suitable for use even in remote field design offices. A unique curvature meter was developed as a part of the work and details of its design are presented. This design has many advantages over those used by other investigators. One of the main advantages of the writer's design is that a twisting curvature associated with the two orthogonal bending curvatures can be obtained without rotating the meter. The need for rotation of the meter through 45^{o} is inconvenient and time consuming and is required in all other curvatures reported in the literature.

After a brief discussion on the necessity of the use of curved bridge decks in modern highway systems, the results of tests on three aluminium models of curved bridge decks are described and used to show the effectiveness of the experimental technique. Two

of the models chosen represent the two extremes of the simply supported curved slab bridges that are popular in practice. The third model is used to study the effect of an intermediate support on one of the simply supported slabs mentioned above.

The concept of influence surfaces for slab-, or slab-like structures is reviewed. Non-dimensional curvature influence surfaces are prepared from the model results. A brief description is given of how these influence surface could be used as aids in bridge designing as well as in checking existing curved slab bridges for abnormally heavy moving loads.

The validity of the application of model results to prototype slabs has been discussed. The limits and the method of incorporating any difference in between the Poisson's ratio of the model material and that of the prototype material are also included. The model results are compared with the exact solution results obtained from the computer programme developed and are found to be in good agreement.

The influence surfaces so prepared for the curved slabs are compared with each other and with the influence surfaces that have been published for rectangular bridge decks and are discussed. Finally, thirty-five influence charts are presented in Appendix II to be used as a permanant record.

NOTATIONS

The following includes the notations generally used throughout this work. Occational deviations are defined where they occur in the text.

C_θ, C_R, $C_{\theta R}$	Calibration constants
D	Plate stiffness
E	Modulus of elasticity
H	Height of the curvature meter
I_θ, I_R	Non-dimensional bending curvature influence values
$I_{\theta R}$, $I_{R\theta}$	Non-dimensional twisting curvature influence values
K	Curvature
K_θ, K_R, $K_{\theta+45°}$	Bending curvatures
$K_{\theta R}$, $K_{R\theta}$	Twisting curvatures
L	Gauge length of the curvature meter
L_M	Span of the model
L_T	Micrometer carriage gauge length
M_θ, M_R, $M_{\theta+45°}$	Bending moments per unit length
$M_{\theta R}$, $M_{R\theta}$	Twisting moments per unit length
P	Load
R	Orthogonal axis in radial direction
R_1	Radius of curvature
f, f_θ, f_R, $f_{\theta+45°}$	Relative deflections
h	Plate thickness
θ	Orthogonal axis in tangential direction
μ	Poisson's Ratio

ACKNOWLEDGMENTS

The writer wishes to express his thanks to his supervisor, Dr. A. M. Lansdown, for the help, guidance and encouragement offered by him during the writer's four year research programme at Manitoba University.

He also would like to express his thanks to Dr. K. R. McLachlan, for his invaluable advice and assistance, particularly during the experimental work. His superior knowledge in instrumentation and electronics is sincerely appreciated.

He also would like to express his thanks to the Civil Engineering Laboratory staff, particularly Mr. E. Lemke and Mr. V. Nowoselski for their assistance in constructing the curvature meter and the models.

The writer wishes to offer his special thanks to his wife for her help in proof reading, tabulating test results and her tolerance during his many disappearances, particularly during testing and the preparation of the manuscript.

During his four years of research at Manitoba University, the writer has been sponsored by the Commonwealth Scholarship and Fellowship Division of the Association of Commonwealth Universities. For their assistance he is most grateful.

TABLE OF CONTENTS

CHAPTER Page

LIST OF FIGURES

LIST OF TABLES

CHAPTER I

INTRODUCTION

With the increasing demands for the use of statically indeterminate structures, especially for modern highway systems, refined and more accurate methods of analysis of these structures are required. In applying existing structural theories to the analysis of structures, quite often the design engineer is required to incorporate simplifying assumptions with regard to the deformed shape and structural behaviour. Even with the finite element technique which is considered to be the most powerful analytical tool at the present time, one has to work with a structure that corresponds to presumed deformations or stress distributions. Usually it is difficult to visualize and to predict the behaviour which is the governing factor of the accuracy, that leads to optimum designs. Simplifying assumptions always tend to be taken on the conservative side for safety, and the economy of the structure depends on how conservative they are. It is always essential to verify the efficiency as well as the reliability, before an analytical method is made available for the use of others.

One may suggest checking the reliability by applying the selected analytical method to a problem, where the exact solution is available. In most practical cases, however, numerical solution of these equations utilizing a digital computer is the only practicable method.

Such a method of solution will be referred to as the "exact" method in this thesis.

Also, in general, the problems that have exact solutions are not complex. Therefore, in solving these problems, even by the so-called approximate analytical methods, it may not be necessary to make severe assumptions as in a complex problem. Hence, this method of checking will not verify the reliability of an analytical method truly. In addition these exact analyses are really only a better approximation to the exact theory because the practical accuracy depends on the convergence of the hyperbolic and trigonometric series employed. Although one finds perfect, rapid convergence for deflections, in the vicinity of the load the convergence becomes slow for bending moments and very slow for shear [(1)]. The series become divergent in the vicinity of a concentrated load [(2)], as mentioned in Chapter VII.

The numerical solutions to all these powerful approximate analytical methods, including finite element, finite strip, folded plate analysis etc., that require a matrix formulation are just not attainable without the aid of digital computers. At the same time an analytical method is only as good as the data fed in at the beginning since no computer programme will correct the poor assumptions made in the analysis.

With the development of the highly sensitive electronic apparatus, the method of model analysis becomes an answer to the above-mentioned shortcomings of the analytical methods. Many investigators particularly in Europe[3,4,5,6] have shown the reliability and scope of model analysis and testing as an indispensable design tool, particularly for structures of complex shapes and boundary conditions. The testing of models not only demonstrates the true structural behaviour under load, but also provides the stress and strain indirectly through the deformations such as deflections, rotations, elongations and shortenings which can be measured on the model.

The main objective of this dissertation is to demonstrate experimentally, how model analysis and testing can be used as a precise design tool in analysing structures of any shape and of any complex boundary conditions. Also its purpose is to build up a simple, but precise experimental technique which is efficient, but unsophisticated, hence could be used even in a remote field design office.

In Chapter II, some of the experimental methods that are frequently used in the model analysis, are briefly discussed along with a detailed description of the technique used in this work. The technique of direct measurement of relative deflections by curvature meters was used in this project. As a part of the project, a unique curvature meter was designed. The writer's design differs in many ways from the curvature meters that have been used by other investigators[5,7,8,9] so far. This is discussed in Chapter III. Minor but important design details such as the design of legs, the procedure to obtain correct center points for the legs and the transducer holes and the method of mounting the meter onto the model, that had to be considered in order to achieve a high level of precision, are also included in Chapter III. The writer's inverse approach of checking the meter analytically on an assumed worst case (a deflection equal to half the thickness of the plate which is considered to be the limit for small deflection theory) to obtain a quantitative idea of each individual error that he feels could be present in the actual testing, is included in Appendix 1.1. This is so-called the "inverse approach" because initially, the significance of each error was studied individually. Then, where appropriate, they were considered separately to obtain an optimum design, instead of checking the quality of the meter in a direct way (like most investigators have done), by using it on a situation with a known solution. The danger inherent in the latter method is that, by coincidence one may use a rare situation where the errors cancel out each other to give excellent results, which may not be the case in the actual testing.

The effect of the gauge length of the meter on the measured values and the size of the model are discussed in Chapter VII. An approximate idea of this effect was obtained analytically and the details are included in Appendix 1.2.

In the type of curvature meter designed, three displacement transducers were used on two orthogonal and one 45° axes to find the curvatures in those three directions. The curvature meter was calibrated along each axis, using a strain gauge testing beam apparatus. This apparatus also works on the same principle as the curvature meter. Details of the calibrations are included in Chapter V.

With the type of device described above, curvature only in one direction can be measured when the reference point is situated on or close to a boundary of the model. Hence another "edge meter" was designed to be used in these situations. This meter too is discussed in Chapter III though it was not used in the testing due to poor performance in one direction.

To demonstrate the suitability of model analysis, models of curved bridge decks were chosen. Curved bridges are required particularly in highly developed urban and suburban areas, where many railroad level crossings and highway intersections are being replaced by overpasses, underpasses and interchanges. Even in rural areas, alignment and site conditions may be such as to make it more economical to locate a curve on the bridge rather than on the approaches. As far as the writer knows, until a few years back curved slab bridges were analysed using the simple beam theory. Then came the more refined analyses for curved slabs, such as finite strip method(10), curved strip method(11) (or curved folded plate analysis) and discrete energy method(12). Basically all of these fall into the same approximate but conservative group of analytical methods discussed earlier. The writer feels that, comparatively very little research work has been carried out on curved bridges, although they have become increasingly common in modern highway systems as a result of smooth traffic flow requirements.

For straight and skew bridges of various boundary conditions, span/width ratios and opening angles, one can find an ample amount of published design data[6,13,14,15,16,17]. They are usually presented in a form that is more useful to the designer, namely "influence surfaces". But, so far no attempt has been made to provide the designer with this type of design data for curved bridges.

Therefore as a second objective, information on curved bridge decks was obtained from the study of models and is presented in a form, that may be useful as aids to the bridge designer. Such information was not previously available.

Many model tests particularly in North America have been used just to study a particular unfavourable case or cases of loading, as an aid of the design of the structure or just in verifying the design under "worst load"[18,19,20]. Such tests provide only qualitative information of the effect of other "heavy loads" that may cross the bridge from time to time. Hence these model tests are not of much use, particularly to a bridge engineer, who has been called upon to check existing bridges for the passage of abnormally heavy loads. Indivisible objects such as transformers, electrical generators, pre-cast highway bridge beams and turbines are few examples of the so-called "heavy loads", that are being transferred from one part of the country to the other. The 800 Megawatt generators for Bruce Nuclear Power Station in Ontario is a current example of heavy indivisible loads currently being built for Canada[35]. Out of the entire turbine-generator set, the stator core and the windings alone weigh about 240 tons. There will be a total of four of them at Bruce Nuclear Power Station.

The use of influence surfaces is an answer to the above-mentioned limitations of the model tests. These influence surfaces for two dimensional slab-like structures are analogous to the influence lines of one dimensional framed structures. An influence surface prepared for any action (moment, curvature, twist, shear, etc.) at a particular reference point on a slab, provides the designer with qualitative information of the considered action at the reference point due to a load or any pattern of loading at any place on the slab. Such surfaces have been used first by H. M. Westergaard[2]. A large number of such surfaces have already been prepared for standard cases of structures, such as rectangular and skew slabs of single span and also of continuous spans[6,8,13,14,15,16,17,21,22,23]. If a set of influence surfaces for the structure under consideration are available, all that the designer has to do is to draw the loading pattern on tracing paper to the same scale as the influence surfaces and move it about on each corresponding surface, until the critical location of the load is obtained. This may require more than one trial whereas a person familiar with influence surfaces will spot critical cases just by glancing through the set of influence surfaces. The method of evaluation of these surfaces is discussed in Chapter VII.

Thirty-five influence surfaces were prepared from the writer's model test results. They are presented in Appendix 2, in the form of contour plans which seems to be the most useful form of presentation for the assessment of the effect of heavy loads on bridges. All these surfaces are plotted in terms of nondimensional curvatures. The advantage of so doing, is discussed in Chapter VII. The investigator has to use his own judgement in selecting the reference points for influence surfaces. The points considered in this project are discussed in Chapter IV.

Initially two model curved bridge decks made out of high strength aircraft aluminium were studied experimentally. The model sizes were chosen such that they represented the two extremes of the simply supported curved slab bridges, popular in practice. A computer programme was developed for the exact analysis solution involving an infinite Fourier series. Model results were compared with the "exact" solution results and found to be in close agreement.

A two span continuous model deck was formed by locating a radial knife edge at the center of the span of the second model tested. The effect of presence of the intermediate support was studied experimentally and compared with the single span model results. No exact solution is available for the continuous case.

CHAPTER II

ELASTIC PLATE EQUATIONS AND REVIEW OF SOME FREQUENTLY USED EXPERIMENTAL METHODS IN MODEL ANALYSIS

2.1 Elastic Plate Equations

The general elastic plate theory is well established and has been known for years. Derivations and the limitations on the applications of elastic plate equations can be found in any standard text book on elastic plates(Eg. 1,24). However, the equations are given below since they are necessary for an understanding of how the experiments described later could be used in the analysis of plates. Attention is also drawn to two of the limitations, to the application of these equations since they are crucial factors in model analysis.

In a plate element, stressed in the elastic range, the following relationships exist.

$$M_R = D[K_R + \mu\ K_\theta] \tag{2.1}$$

$$M_\theta = D[K_\theta + \quad K_R] \tag{2.2}$$

and

$$M_{R\theta} = -M_{\theta R} = D(1 - \mu)\ K_{R\theta} \tag{2.3}$$

where, M_R, M_θ and $M_{R\theta}$ are moments per unit length of the plate as shown in Figure 2.1 on page 10; $K_R \left(= -\frac{\partial^2\omega}{\partial R^2}\right)$ and $K_\theta \left(= -\frac{1}{R}\frac{\partial\omega}{\partial R} - \frac{1}{R^2}\frac{\partial^2\omega}{\partial\theta^2}\right)$ represent the curvatures in the R and θ directions produced by the bending moments M_R and M_θ; and $K_{R\theta} \left(= \frac{1}{R^2}\frac{\partial\omega}{\partial\theta} - \frac{1}{R}\frac{\partial^2\omega}{\partial\gamma\partial\theta}\right)$ is the twisting

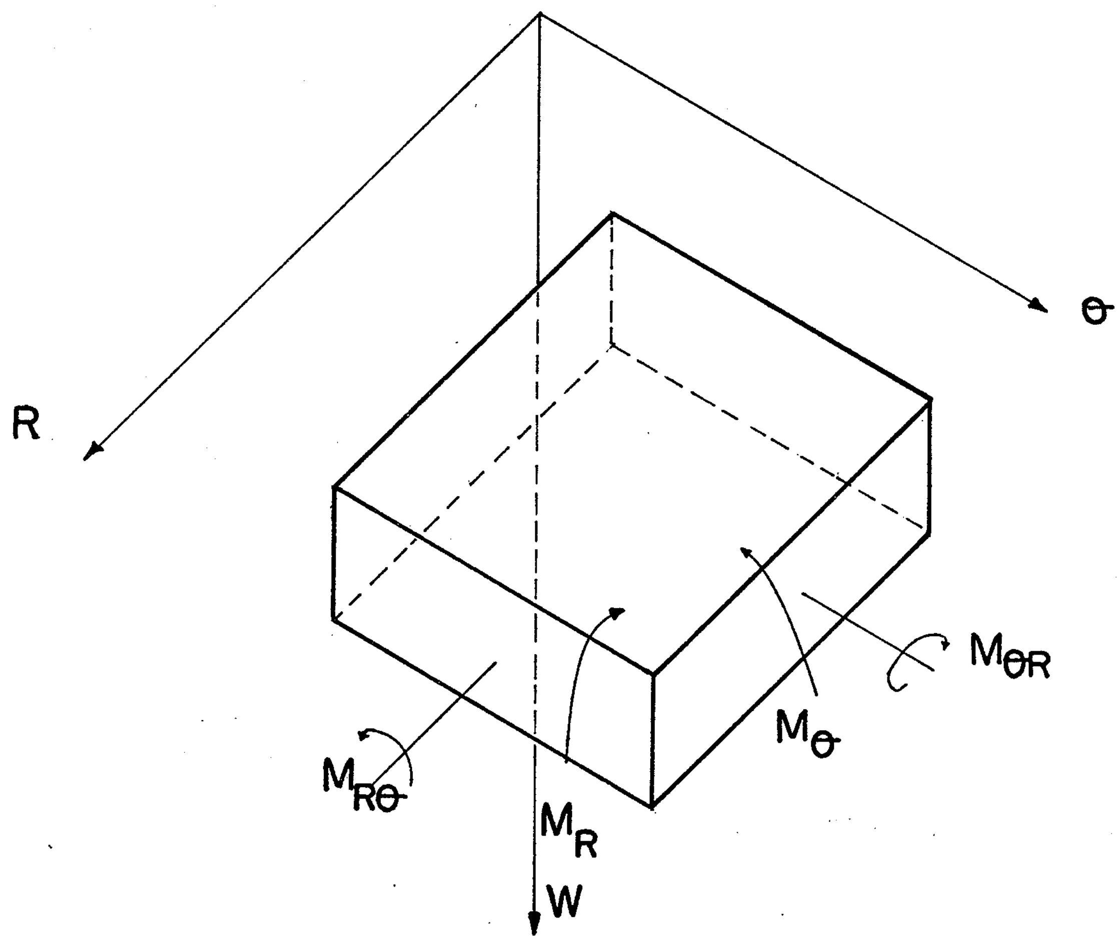

Figure 2.1 Moment Diagram
Terms Shown all Positive.

curvature due to the torsional moment $M_{R\theta}$.

$$D = \frac{Eh^3}{12(1 - \mu^2)}$$

is the plate stiffness per unit width where E is the modulus of elasticity, μ is the Poisson's ratio of the material and h is the thickness of the elastic plate.

Two limitations mentioned above are:

1) The model slab must be thin compared to the other dimensions, for the shear deformation to remain negligible in relation to the flexural deformation;
2) The deflection of the model must be small compared to the thickness, in order that the stresses corresponding to the stretching of the middle surface of the plate are negligible in comparison with the bending stresses.

2.2 Review of Some Frequently Used Experimental Methods In Model Analysis

2.2.1 Moire Method

The Moire fringe technique is now freqently used in model studies where the stress and strain can be derived directly from displacements.

A model made of reflecting material or coated with a reflecting surface is set up vertically, in front of an illuminated cylindrical screen, consisting of black and white parallel lines of equal width. The model is loaded from the back to obtain unobstructed fringes. Images of the screen reflected by the model in the loaded and unloaded states are photographed through a hole in the center of the screen. Both states are photographed on the same negative. Moiré interference fringe patterns appear on the photographic plate since when the model is loaded, the reflected array of lines deform following the surface displacements induced in the model and generally do not coincide with the lines reflected by the unloaded model. These interference fringes represent contours of constant slope normal to the screen line direction. By rotating the screen, the slope in any direction can be obtained. Numerical or graphical intergration and differentiation of the slope curves give the deflections and the curvatures in the plate respectively. Hence the bending and twisting moments at any location can be found making use of the relationship between curvatures and moments and knowing the flexural rigidity of the model as shown in Equations 2.1, 2.2 and 2.3. For more details, the writer refers the reader to F. K. Ligtenberg's paper on Moiré method(25).

This method is not suitable if very high accuracy is required since there is always a possibility of human error in finding the fringe centers and plotting the slope curves. This technique becomes less precise when the model has a shape other than a rectangle or a square, especially a curved model, such as the one considered in this work. In a curved bridge slab, it is more appropriate to present curvatures, moments, etc. using the polar coordinate system. Hence it is convenient to use curved and radial grid lines with a curved model. Since the black and white screen lines are parallel to one of the axes of an orthogonal system, the fringe patterns that appear on a photographic plate represent contours of constant slope in a direction parallel or perpendicular to only one radial grid line at a time. Therefore, one has to employ the conditions of equilibrium (Mohr's circle) to obtain radial and tangential curvatures at grid points on the other radial grid lines. The other alternative is the expensive method of taking two photographs with the screen lines parallel and perpendicular to each radial grid line. From his earlier experience on the application of Moire technique to models of curved bridge decks, the writer is aware of the amount of work and the errors involved in finding a slope along a curved grid line. The above method becomes relatively expensive if high accuracy is needed[8].

2.2.2 Strain Gauge Technique

The strain gauge technique is certainly the most widely used technique in model analysis and has been known for many years. Details of the technique can be found in any book on experimental stress analysis [Eg. 26], therefore will not be given here. Moments are calculated from the surface strains of the model that are obtained from the strain gauges affixed to the model. The magnitude of the reading and therefore its accuracy increases with the distance of the strain gauge from the middle surface of the slab.

For this reason relatively thick slabs are advantageous for strain measurements. At the same time one has to keep in mind the limitations imposed by the elastic theory on the thickness of the slab, as mentioned in section 2.1 above.

With strain gauges, high precision can be obtained with a little care. The development of modern electronic equipment has made the use of strain gauges in model analysis much easier in recent years. Typical of such high precision strain gauge study is the work of Yeginobali[27] where he used electric strain gauges to study a three-span continuous skew slab model to verify his theoretical results. But a total of 20,000 strain readings were required to complete the experiment. In 1961 Rüsch and Hergenröder[6] also made use of strain gauge technique to study models of skew slabs to produce 174 contour charts of influence surfaces for bending and twisting moments. A test of equilibrium showed a discrepancy of not more than 4 percent in the final results.

In most of the places on the model, except at free edges, interior supports and exterior supports, the gauges have to be applied in the form of "3-legged rosettes". There is a difficulty in finding the stress peak over the reference point (even if the gauge length is sufficiently small) if rosettes made of individual strain gauges are used, since these gauges will have to be applied at some distance from the theoretical reference point. This drawback can be avoided by using more expensive commercially made rosettes fabricated so that all the individual gauges coincide at one common point. Hence with this type of rosette, it is possible to have all the three gauges directly over the reference point. For better accuracy, it is preferable to have the same number of gauges on both sides of the slab to seperate axial from bending and for temperature compensation. Therefore a large number of gauges are required for a detailed model study of any structure. These high costs and the amount of labour involved become a significant drawback for the extensive use of strain gauges in detailed investigations.

2.2.3 Curvature Meter Method

As mentioned in the first chapter, in model analysis stresses and strains are not measured directly, but calculated indirectly from the deformations that are measured on the model and the elastic constants of the model material. Since the characteristics deformations produced by bending are curvatures, an obvious way of determining experimentally the moments in a model slab is by the use of curvature measurements. The relationships that exist between curvatures and moments have already been shown in Equations 2.1, 2.2 and 2.3. The curvature meter technique is based on the calculation of curvature from the measurement of relative deflections of points over a predetermined base length.

These curvature meters have been used in optics for a long time in curvature measurements, under the name spherometers.

Simple curvature meters were employed in model tests, as early as 1949[28]. W. Andra[5,9], R. Krieger[5], H. Weigler[29], H. Weise[8,29] and A. Mehmel[8] made improvements to the curvature meter to bring it up to its present advanced form. Some of the investigators employed the method of mechanical addition of deflections in order to include the Poisson's effect while others preferred the addition to be done electrically. The difficulties of machining for the case of mechanical addition has made the method of electrical addition more popular. In recent years, the advancement of highly sensitive electronic apparatus has made it even more suitable.

It was not necessary to employ any of the above-mentioned methods of addition with the work described in the dissertation since it was decided to present the results in the form of curvatures, and hence they are, independent of the Poisson's effect in the plate. The advantage of so doing is discussed in Chapter VII as mentioned previously.

The basic principle of the curvature meter is that of measuring the relative deflections at three positions on the surface of the slab. In Figure 2.2 (page 17), A, B and C are three equally spaced collinear points on a deflected surface having a local radius of curvature, R_1. If this spacing (L) is small compared to R_1, the curvature from A to C can be assumed to be constant. In other words, the three points A, B and C can be assumed to lie on a circular segment of radius R_1. Based on these assumptions, the relationship between the measured rise f over the chord length AC

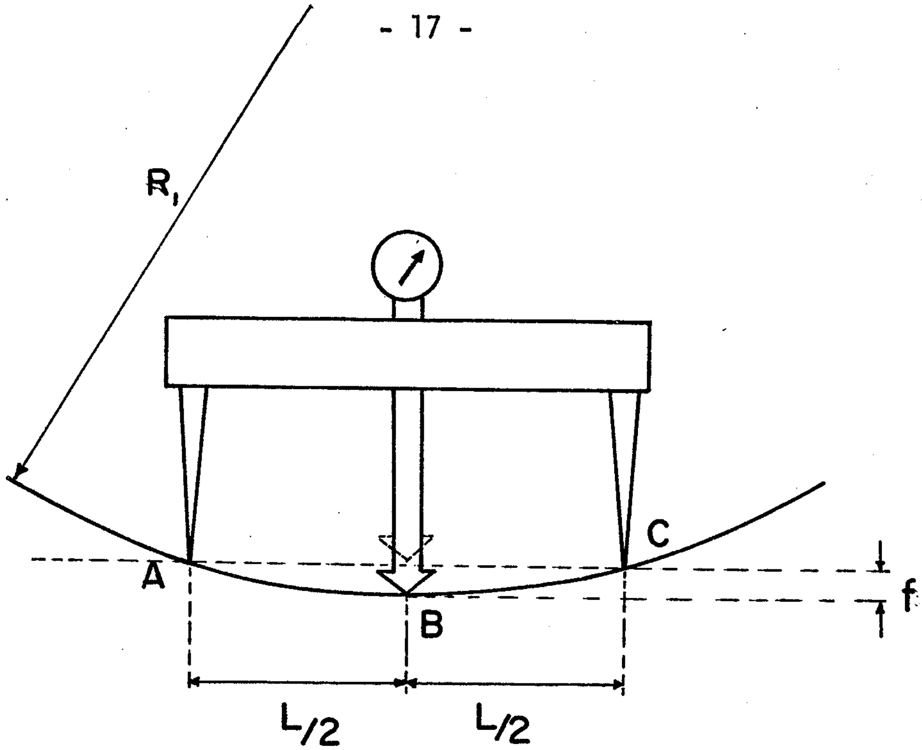

Figure 2.2 Curvature Meter Principle.

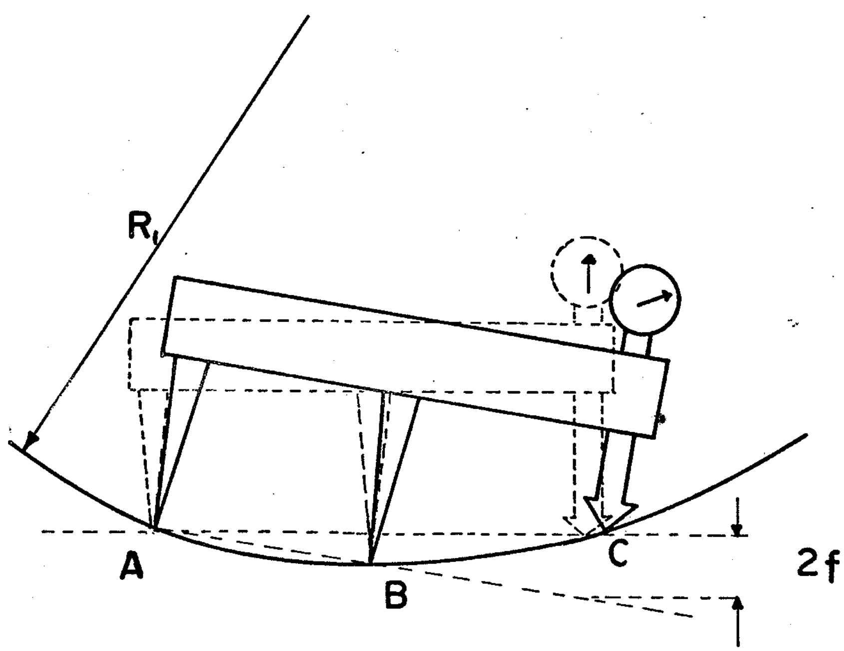

Figure 2.3 Position of the Deflection Measuring Transducer.

(as indicated in Figure 2.2, page 17) and the radius of curvature R is derived as follows:

$$\left(\frac{L}{2}\right)^2 + (R_1 - f)^2 = R_1^2$$

or $$\frac{L^2}{4} + R_1^2 - 2R_1 f + f^2 = R_1^2$$

where $$2R_1 f = \frac{L^2 + 4f^2}{4}$$

giving $$R_1 = \frac{L^2 + 4f^2}{8f}$$

since f is very small compared to L, $4f^2$ becomes negligible in comparison to L^2. Hence,

$$R_1 = \frac{L^2}{8f}$$

$$\text{Curvature } K = \frac{1}{R_1} = \frac{8f}{L^2} \qquad (2.4)$$

The displacement measured is 2f for the curvature meter used in the work since deflection measuring transducer was fixed at the outer point as shown in Figure 2.3 on page 17. Letting 2f be equal to the registered value f , then

$$\boxed{K = \frac{4f}{L^2}} \qquad (2.5)$$

Equation 2.5 is the basic expression used for bending curvature in the meters of the type used in this investigation.

2.3 Application of Elastic Plate Theory to Concrete

Many investigators[18,19,27,31] have shown the validity of the use of elastic plate theory in predicting the behaviour of reinforced concrete structures. Elastic behaviour of a structure can be obtained from a study of elastic model also. The results obtained from an elastic model study are limited in value to the same extent as the results obtained from an accurate mathematical study based on the theory of elasticity. Thus, we may state that the findings derived from a well conceived elastic model are no better than but as good as, those from a properly executed study of a mathematical model. Knowels and Huggins[19] from their model study on the behaviour of a three-span 60^{o} skew bridge with stiffened edges concluded that tests on a model made from a reasonably isotropic material, such as aluminum, can provide the necessary information for the design of a reinforced concrete strusture under both service and ultimate load conditions.

CHAPTER III

DESIGN OF CURVATURE METER

3.1 Rationale Behind the Design

In some recent types of curvature meters, the meter has to be rotated through 45° with respect to one of the main directions considered, in order to find the twisting moment associated with the two bending moments in those main directions. The meter developed for the present work does not suffer from this disadvantage and a twisting moment at any point can be found without rotating the meter. To avoid this extra rotation, an additional third transducer was placed on an axis 45° to the main axis θ as shown in the Figure 3.1b on page 20. This transducer measures the relative deflection between points O and E in the diagram. In Figure 3.1b, AOC and BOD form the gauge lengths of the meter in θ and R direction respectively.

For each meter position three deflection readings are recorded. From these deflection readings, curvatures K_θ, K_R and $K_{\theta+45°}$ at a point can be calculated and hence the bending moments M_θ,M_R and the twisting moment $M_{\theta R}$ can be obtained, without adjusting the meter. From Equations 2.1 and 2.2 it is clear that once K_θ and K_R are obtained, the calculation of M_θ and M_R is straightforward. But the calculation of $M_{\theta R}$ is not as easy since $K_{\theta R}$ is not known directly. But from equilibrium for curvatures in a plate (Mohr's

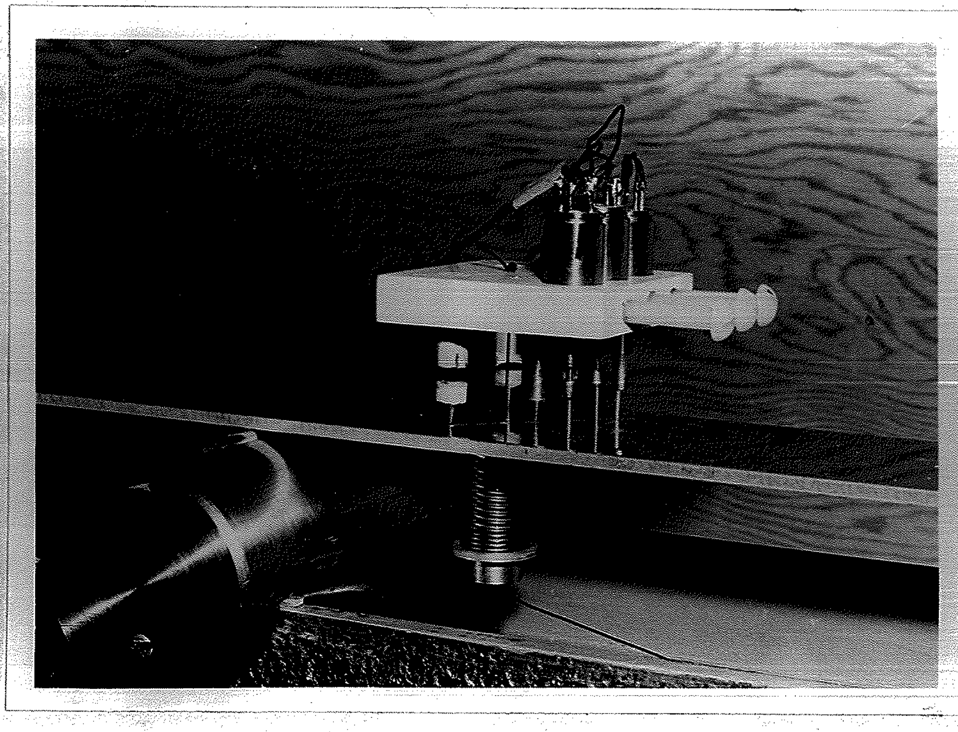

Figure 3.1a Curvature Meter.

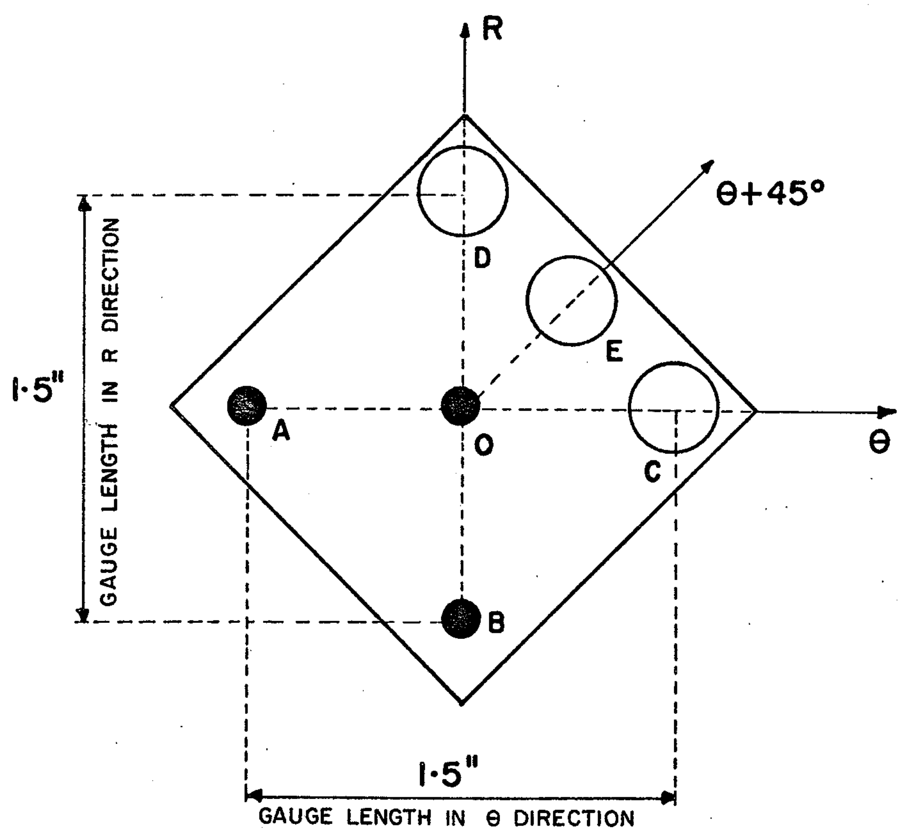

Figure 3.1b Details of the Curvature Meter Base.

circle), it is known that the following relationship exists.

$$K_{\theta R} = \frac{K_{\theta+45°} - K_{\theta+135°}}{2}$$

Hence, $M_{\theta R}$ is expressed in a different form, from that of Equation 2.3

namely $$M_{\theta R} = \frac{D(1 - \mu)}{2} (K_{\theta+45°} - K_{\theta+135°}) \tag{3.1}$$

However, only $K_{\theta+45°}$ can be obtained from the readings of the meter as designed. Therefore, equilibrium is used again to calculate $K_{\theta+135°}$. It is known that

$$K_\theta + K_R = K_{\theta+45°} + K_{\theta+135°}$$

hence, $$K_{\theta+135°} = K_\theta + K_R - K_{\theta+45°}$$

Substituting back into Equation 3.1 gives

$$M_{\theta R} = \frac{D(1 - \mu)}{2} [K_{\theta+45°} - (K_\theta + K_R - K_{\theta+45°})]$$

$$= D(1 - \mu)(K_{\theta+45°} - \frac{K_\theta + K_R}{2})$$

From the Equation 2.5

$$K_\theta = \frac{4f\theta}{L^2}$$

and

$$K_R = \frac{4f_R}{L^2}$$

Unfortunately the expression for $K_{\theta+45°}$ is not as straightforward as the above two. This is because the required relative deflection between the points O and E (Figure 3.1b, page 20) on the axis θ+45° cannot be obtained from the third transducer reading $f_{\theta+45°}$ alone without knowing the tilt of that axis θ+45°. This tilt of the axis θ+45° cannot be determined as easily as that for the other two axes since along the former, the curvature meter is supported only on one leg, i.e. the common center leg. To make this clear hypothetical and real examples are considered along the θ axis (or R axis).

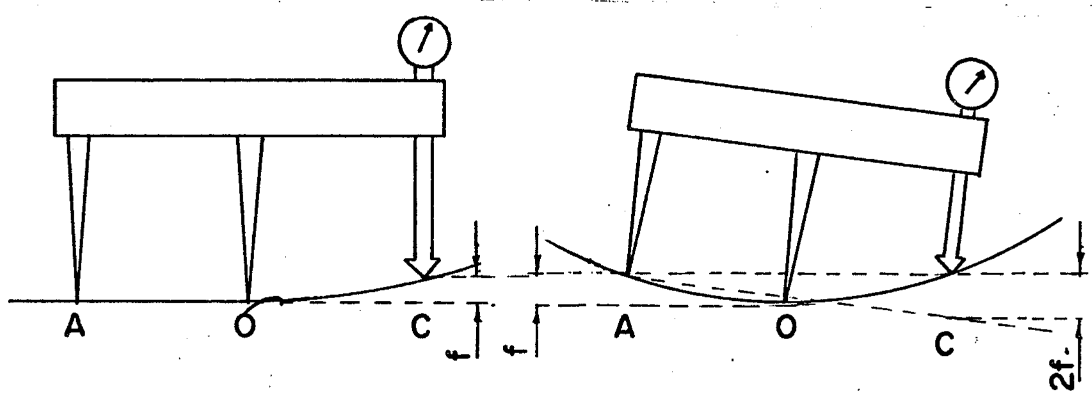

Figure 3.2 Hypothetical Case

Figure 3.3 Real Case

As shown in Figure 3.2 if only point C gets deflected and point A remains undeflected, the curvature meter will remain level. Then the registered reading of the transducer will be the true deflection of C relative to O. On the other hand, if points A and C both get deflected as shown in Figure 3.3, as occurring in the general case, the curvature meter will be tilted due to the uplift of the bottom tip of the outer leg. Here the registered reading therefore will not be the true deflection of C relative to O. To find the true relative deflection, the amount of uplift of the bottom tip of the outer leg has to be deducted from the registered reading. This uplift is equal to one half of the registered reading of the transducer and hence the true deflection is half the registered value, for both axes R and θ.

In the case of the axis $\theta+45^{o}$, this uplift, which gives the tilt of the axis can not be determined as easily, due to the absence of an outer leg. If we imagine an outer leg F on the axis $\theta+45°$ of length equal to that of the other three fixed legs A, O and B (as shown in Figures 3.4 and 3.5 below), then the uplift of the

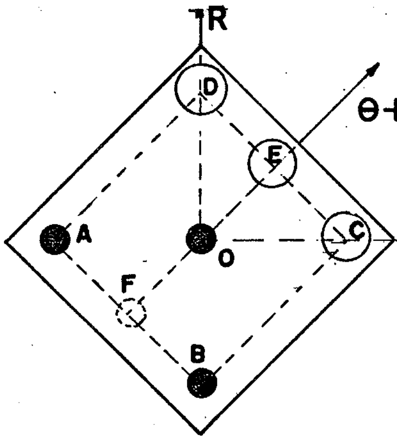

Figure 3.4 Imaginary Leg F

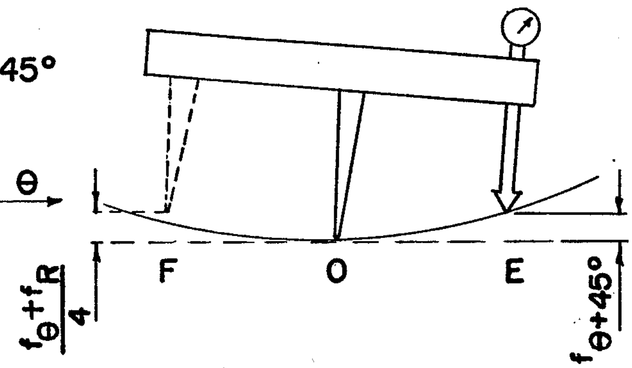

Figure 3.5 Tilt of $\theta+45^{o}$ Axis

bottom tip of the imaginary leg F will be defined by the uplifts of the legs A and B, since the tilt (inclination) of the solid base carrying these legs depends on those two uplifts. Uplift of F is the average of those of A and B since F is midway between those two points. As pointed out previously the uplifts of A and B are equal to one half the registered readings on the respective transducers opposite to them. Therefore the true deflection of E relative to O is the reading registered on the third transducer less one-fourth of the sum of the other two readings. Of course the signs must be taken into account.

Hence, from Equation 2.4

$$K_{\theta+45°} = \frac{8}{(L/\sqrt{2})^2}\left(f_{\theta+45°} - \frac{f_\theta + f_R}{4}\right)$$

$$= \frac{16}{L^2}\left(f_{\theta+45°} - \frac{f_\theta + f_R}{4}\right)$$

Substituting back into $M_{\theta R}$

$$M_{\theta R} = D(1 - \mu)\left[\frac{16}{L^2}\left(f_{\theta+45°} - \frac{f_\theta + f_R}{4}\right) - \frac{4}{L^2}\frac{(f_\theta + f_R)}{2}\right]$$

$$= D(1 - \mu)\frac{16}{L^2}\left[f_{\theta+45°} - \frac{(f_\theta + f_R)}{4} - \frac{(f_\theta + f_R)}{8}\right]$$

$$= D(1 - \mu)\frac{16}{L^2}\left[f_{\theta+45°} - \frac{3}{8}(f_\theta + f_R)\right]$$

The expressions that were used with the curvature meter designed, in order to calculate bending and twisting curvatures are given below

$$K_\theta = \frac{4f_\theta}{L^2} \qquad \text{(A)}$$

$$K_R = \frac{4f_R}{L^2} \qquad \text{(B)}$$

$$K_{\theta R} = \frac{16}{L^2}\left[f_{\theta+45°} - \frac{3}{8}(f_\theta + f_R)\right] \qquad \text{(C)}$$

3.2 Design of Main Body and Legs of Curvature Meter

It is preferable to make the curvature device as light as possible, in order to keep the deflection due to its selfweight a minimum. Although the initial curvature due to this selfweight has no effect on the final results, since the whole system can be "zeroed" electronically after applying the meter to the model, a light meter will help in allowing a greater portion of the total allowable deflection (for the small deflection theory) to be obtained only from external loading after the electrical "zeroing". A detailed discussion of this is included in Chapter V.

A piece of aluminium, 2" x 2" x 3/8", was used as a base for the legs and the housing for the transducers. The centers of the legs and the transducer holes (Figure 3.1b, page 20) were located using a universal milling machine (Maximat V-10, Canadian Edelstaal Limited). The carriage of this machine could be moved in two orthogonal directions, with a precision of 1/1000 of an inch, using the attached micrometers. It was ascertained that there was some back lash in the horizontal movement of the machine carriage. Therefore, care had to be exercised in locating the centers of the legs and the transducer holes. The transducer holes were bored out to obtain a close smooth fit. Hence, it was possible to move the transducers smoothly, easily and quickly in the vertical direction to obtain the zero position. Polyethylene screws were used to lock the transducer in place (Figure 3.1a, page 20).

In order to measure the minute changes in curvatures, the legs of the curvature meter should be pressed tightly against the surface but at the same time, its ability to adjust itself to the change in "gauge length" due to circular arc deformation of the plate should not be prevented. If the outer legs of the curvature meter were rigid and solidly fixed to the base, obviously they would offer some resistance to the deformation of the surface. Therefore, localized stress concentrations would be formed around the tips of these legs which could have a significant effect on the local final deformed shape of the plate. An answer to this is the use of legs with freely movable bottom tips.

Both outer legs of the meter were made of two parts, connected together at the middle by a high tensile leaf spring as shown in Figure 3.6 on page 27. The bottom part of each leg had a conical tip of 60° and was hardened. The center leg was made of one solid piece and this too had a hardened, 60° conical tip.

The outer legs were fixed on to the base as indicated in Figure 3.7 on page 27. A great deal of care was taken to ensure that the plane of each leaf spring was orthogonal to the respective meter axis through it. Each leaf spring offered stiffness in the direction along the plane of the spring, and little resistance in the direction normal to its plane. Therefore, the bottom part of each outer leg was allowed to move, only in the direction of its corresponding meter axis. Since the meter axes were orthogonal to each other, any rotation of the meter about a vertical axis was prevented.

To make sure that the distances between the tips of the outer legs and the center leg remained equal to half the gauge length, the tips of all the three legs were placed in precisely located 90° conical shaped punch marks on the model.

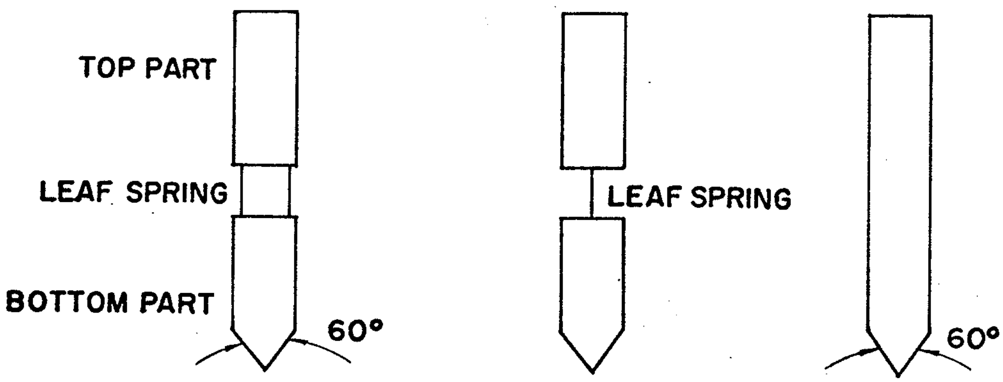

Two Views of an Outer Leg.

Center Leg.

Figure 3.6 Curvature Meter Legs.

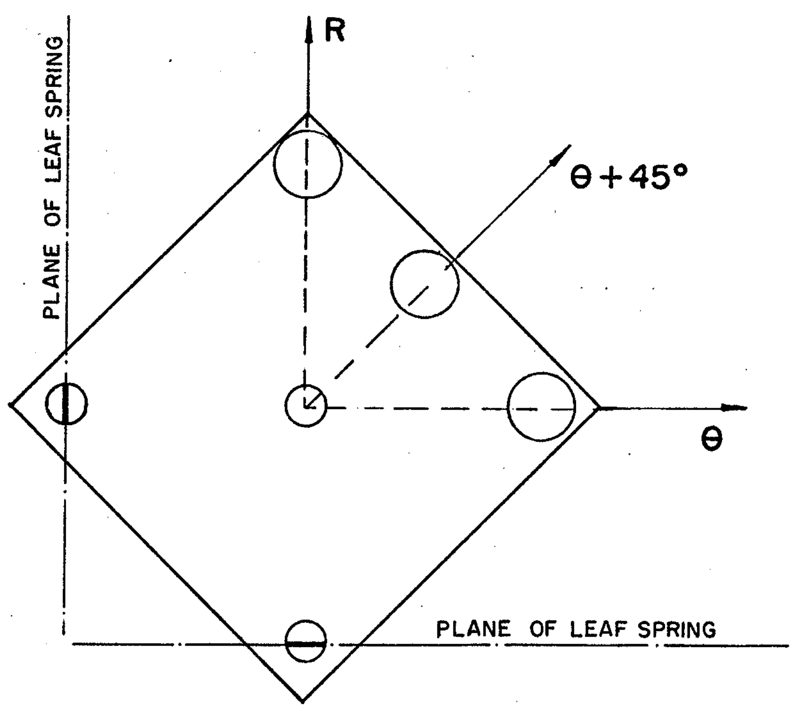

Figure 3.7 Alignment of the Legs on the Base of the Curvature Meter.

3.3 Curvature Meter Mounting Device

Due to the eccentric weights of the three transducers, it was not possible to support the curvature meter on its own three legs alone. Therefore, a method that would ensure stability and firm contact between the legs and the surface, without introducing significant restraints, was required to support the meter on the model.

A very efficient technique which had not been used in earlier work, was employed to meet this design requirement. The force required to hold the curvature meter against the model was obtained from the action of a "string and spring" arrangement as shown in Figure 3.8. First, a nylon fishing line, knotted at one end was passed through a hole of diameter 0.04" made in the base at the center of gravity of the meter. Then it was taken through a hole (diameter 0.04") made in the model, right beneath the center of gravity of the meter. After that it was passed through a helical spring. This spring was guided by a guide pin made of aluminium, with a restraining collar at the bottom. The purpose of the restraining collar was to compress the spring against the model plate. To obtain the force required, the line was tensioned and anchored against the inner wall of the guide pin with a set screw (Figure 3.8, page 29), with the spring in compression in between the plate and the collar. The tension in the line could be varied by varying the compression in the spring. It was tested and ascertained that, within reasonable limits, the amount of tension in the line was not an influential factor on the

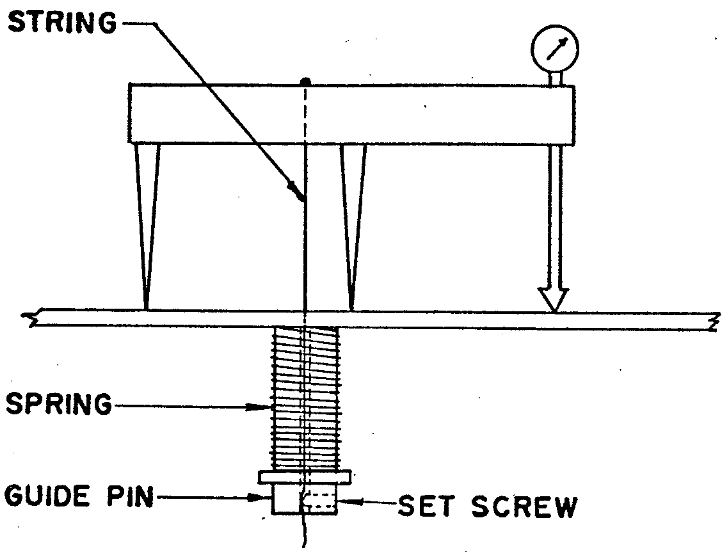

Figure 3.8 The Curvature Meter Mounting Device.

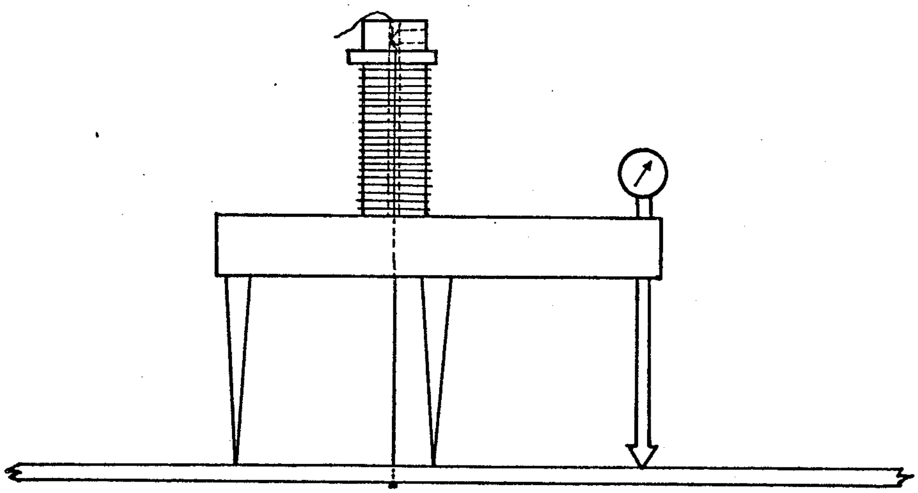

Figure 3.9 The Reversed Mounting.

results.

When it was required to load the model from underneath, closer to the reference point, the loading stem interfered with the guide pin. Then the "string and spring" arrangement had to be reversed as shown in Figure 3.9 on page 29.

3.4 Electronic Equipment Associated with the Curvature Meter

As mentioned earlier, the principle of the curvature meter was based on the measurement of relative deflection over a gauge length. Since these gauge lengths were kept as small as possible consistent with the required sensitivity, the magnitude of these relative deflections was generally in the neighbourhood of several microns. At the end of each gauge length of the meter, an inductive displacement transducer of the type WIE (Messrs. Hottinger Messtechnik, Darmstat) was installed to measure these minute relative deflections.

The transducer, type WIE, consisted of a probe connected to a ferrite core which could be moved axially in the bore of a coil assembly, placed in the cylindrical transducer housing. The coil assembly was made of two coils which were adjacent to one another on a common axis. These coils were electrically connected in series to form two branches of a Wheastone Bridge circuit. The Wheastone Bridge could be balanced by moving the ferrite core, so that its center coincided with the mid point of the transducer. Any axial displacement from this position resulted in a change of inductance in the two coils, causing a disbalance in the previously balanced

Wheastone bridge. The signal that would be available as a result of this disbalance, after amplification, could be read on the meter of a carrier frequency amplifier. For this purpose an amplifier of the type KWS/T-5 (Messrs. Hottinger Messtechnik, Darmstadt) was used in this work. The maximum sensitivity of the meter KWS/T-5 is 2×10^{-8} metre.

To connect simultaneously the three transducers used in the curvature meter to measuring bridge KWS/T-5, a switch box was constructed. This was capable of connecting one transducer directly to meter KWS/T-5 for one switch position. Then for the other switch position it connected a frequency mixing apparatus S A II (Messrs. Hottinger Messtechnick, Darmstat) to the meter KWS/T-5. The other two transducers were connected directly to the input of the mixing apparatus S A II (same manufacturer as the above equipment). The mixing apparatus S A II is simply a mixer, which has to be used always in conjunctionwwith KWS/T-5. In using the mixer S A II two seperate electric signals could be summed or subtracted using the appropriate sign settings. The incoming signals could be mixed to different proportions using the two proportionality settings.

In this experiment the mixer S A II was used to feed only one transducer impulse at a time, into the measuring bridge KWS/T-5. This was achieved by setting one of the proportionalty knobs to zero while the other was set to read 100 percent. Hence, with the aid of the switch box and the mixer S A II, it was possible to read the

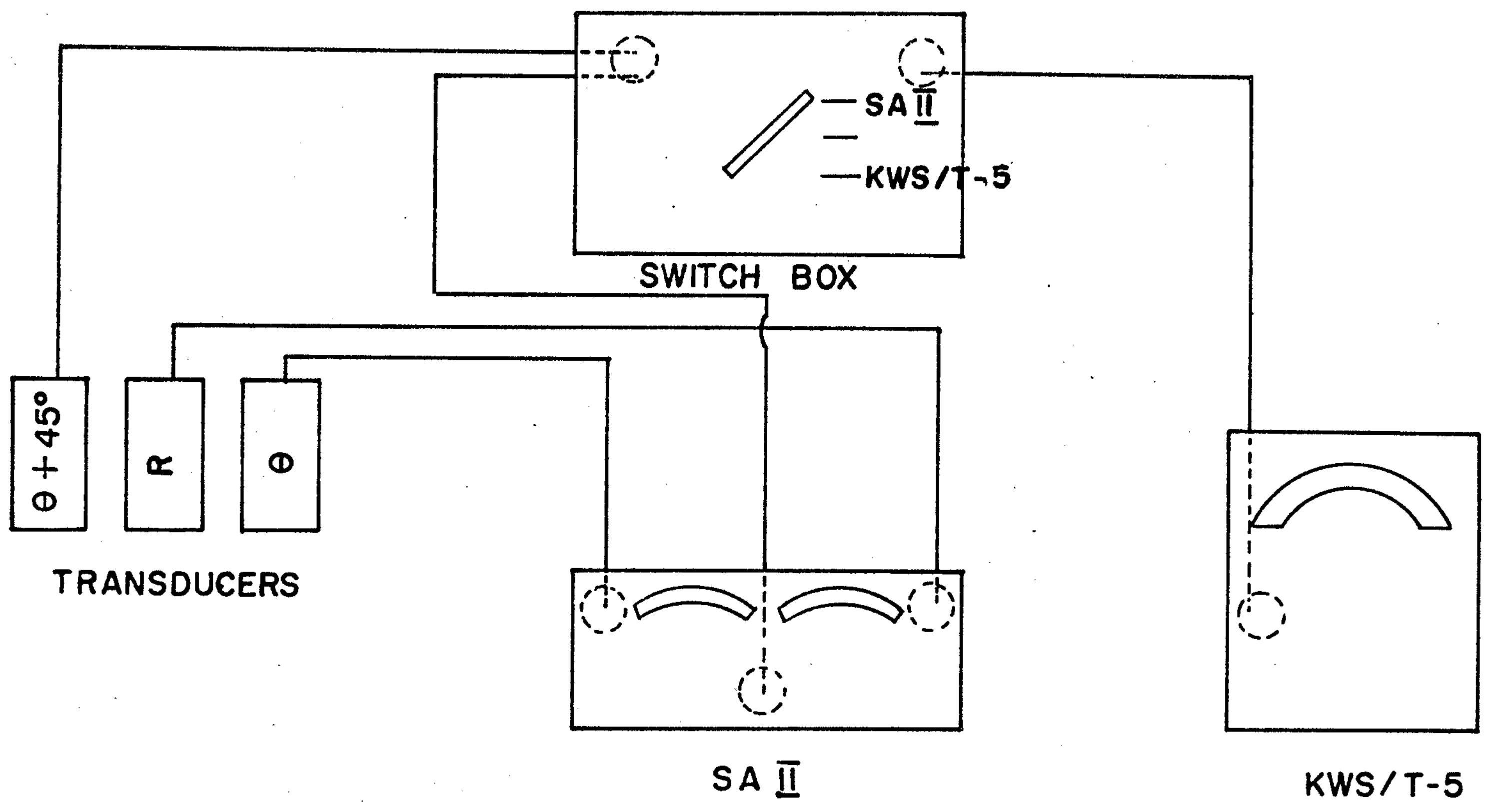

Figure 3.10 The Schematic Diagram of the Electronic Equipment Arrangement.

probe deflections of all the three transducers on the measuring bridge KWS/T-5 one at a time, without disturbing the meter, the leads or the connections. A schematic diagram of this arrangement is shown in Figure 3.10 on page 32.

3.5 Edge Curvature Meter

As mentioned previously, the curvature meter discussed above could not be used to measure all the three curvatures occuring on or close to a boundary, especially at a free edge. A special fixing clamp shown i- Figure 3.11 on page 23 was designed to carry the curvature meter and to support it on an edge, such that the tip of the center leg of the meter was right over the reference point (Figure 3.11, page 34). The conical bottom of the cylindrical hole in the clamp was made to coincide with the tip of the center leg when inserted. In machining the clamp, care was taken to make sure that the points A, B and C were solinear.

The tightness of clamping was found to have an effect on the results. This effect was found to be more significant on the reading $f_{\theta+45°}$ than on the other two, f_θ and f_R. This was because the magnitude of $f_{\theta+45°}$ was very low compared to the other two. The resulting inaccuracies caused this type of edge meter to be discarded. Instead the curvature K_θ in the θ direction was measured at the free edges using the ordinary currature meter as shown in Figure 4.26 (page 38). The other two curratures K_R and $K_{R\theta}$ were obtained from the measured K_θ value using the plate theory for free edge boundary conditions.

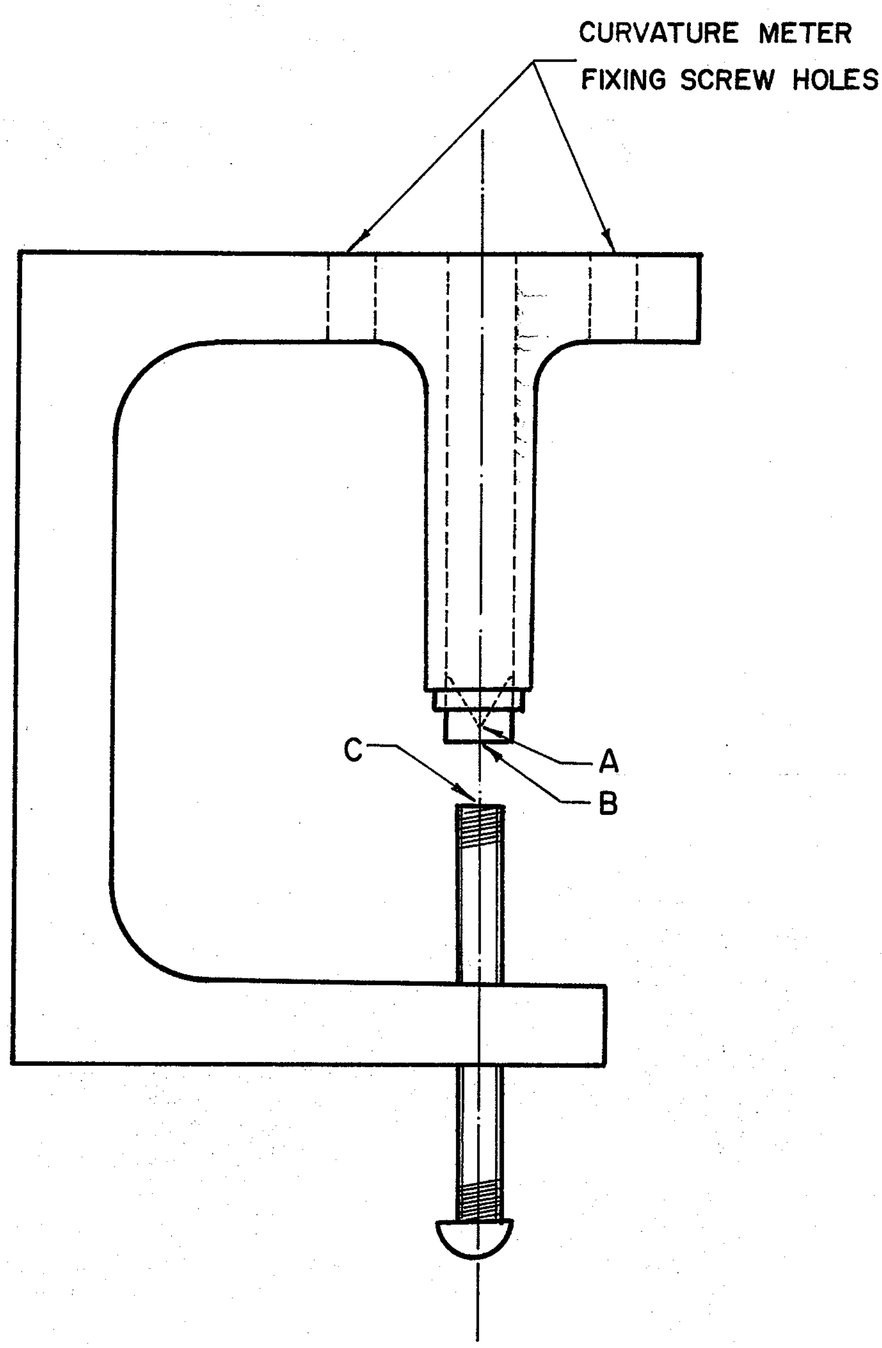

Figure 3·11 Fixing Clamp .

CHAPTER IV

MODEL AND TEST EQUIPMENT

4.1 Construction of Models

Out of the few model materials that have already been shown suitable for simulating the flexural behaviour of reinforced and prestressed concrete structures [5, 9, 21, 27, 29], air-craft aluminium alloy (ALCAN 2024-T-3) was chosen to construct the models. Its high modulus of elasticity ($E = 10.38 \times 10^6$ psi) enabled the achievement of adequate accuracy of measurements, with the equipment available, without requiring deformations so large as to alter the fundamental geometry of the model slab. Hence it was ensured that the small deflection theory of plates remained valid. In addition, its nature for easy fabrication to the required curved form was also considered to be important. Poisson's ratio (μ) was 0.322 for the aluminium alloy used and therefore higher than that for concrete. The effect of the difference in Poisson's ratios and the method of correcting the model results for varying Poisson's ratio, are discussed in Chapter VII.

The thickness of aluminium plate used was 0.125". The thickness chosen was such that the plate could be considered thin compared to the dimensions on plane. However this, at the zones of application of the load, where the "load spread" takes place, is not true. Thinness of the model assisted in correlating the model results to those of actual structure around these zones as discussed in Chapter VII. It also facilitated the measuring procedure because measurable deflections could be achieved with small values of applied load.

The layout of the models is shown in Figure 4.1, on page 37. As mentioned earlier, the model dimensions were chosen to represent curved slab bridges popular in practice. Along each radial boundary, a set of holes of diameter 0.04" were drilled through the model plate to pass the strings to hang the "pre-loads" that will be discussed later in this chapter.

The reference points investigated are indicated in Figure 4.1 on page 37. The reference points at the free boundaries were located as close as possible to the free edge. It was possible to locate all the "edge" points at distances less than one half the thickness of the plate from the edges. Around each reference point, three 90° conical shaped holes were punched (Figure 4.2b on page 38) to position the meter in place. As mentioned earlier, great care was taken to ensure that the distances from the center leg hole (i.e. the reference point) to the two outer leg holes were equal to one half the gauge length of the meter. For each meter portion, a hole of diameter 0.04" was drilled through the model plate at the appropriate place to mount the device as explained earlier. The loading schedule used is shown in Figure 4.1a on page 38.

4.2 The Pre-Loading

Due to the fact that the self weight of the aluminium plate

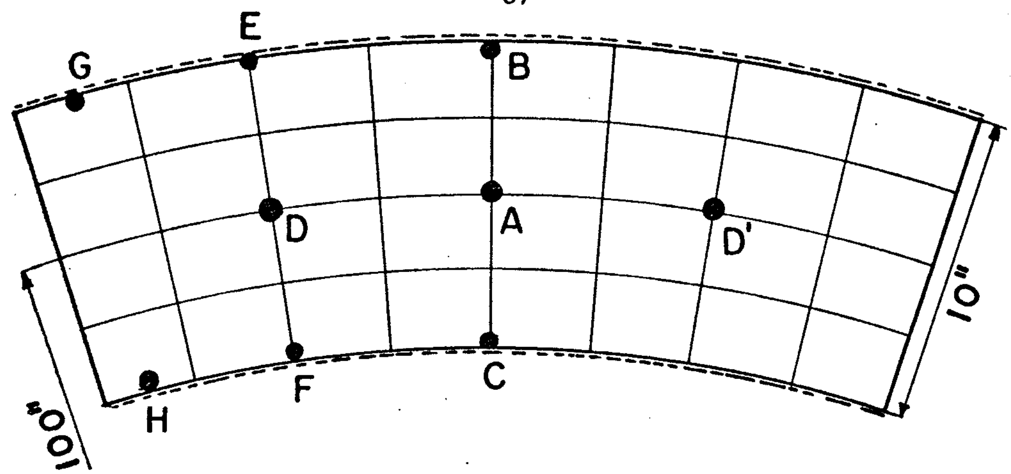

Model 1 - 15° Opening Angle.

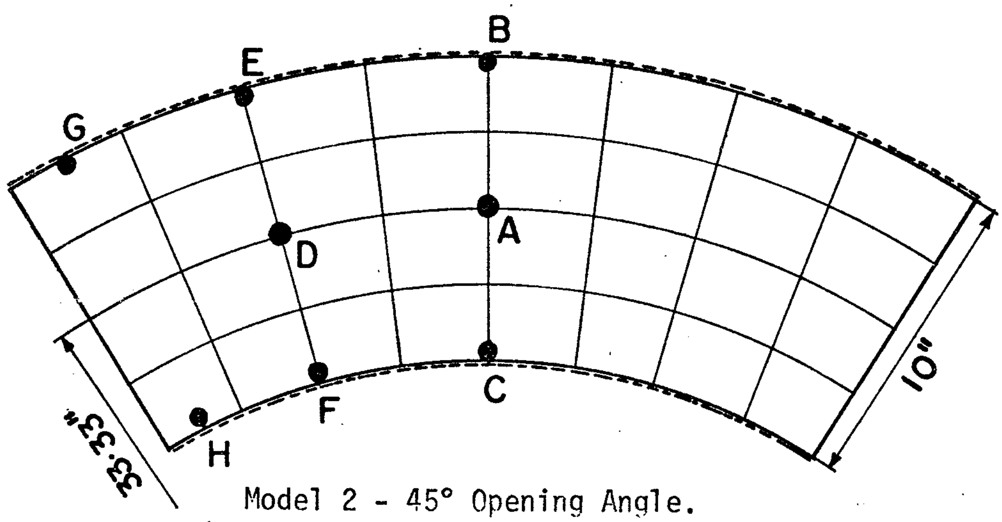

Model 2 - 45° Opening Angle.

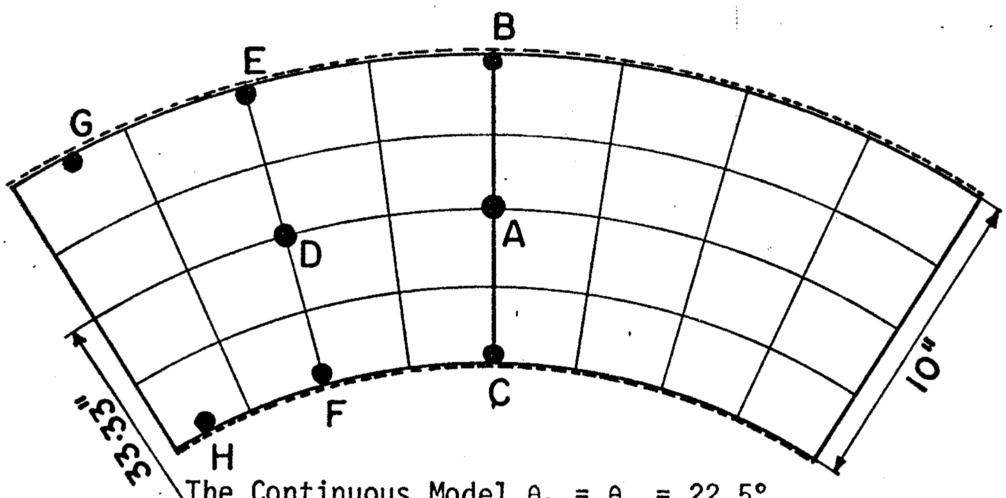

The Continuous Model $\theta_1 = \theta_2 = 22.5°$

Figure 4.1 Layout of Models.

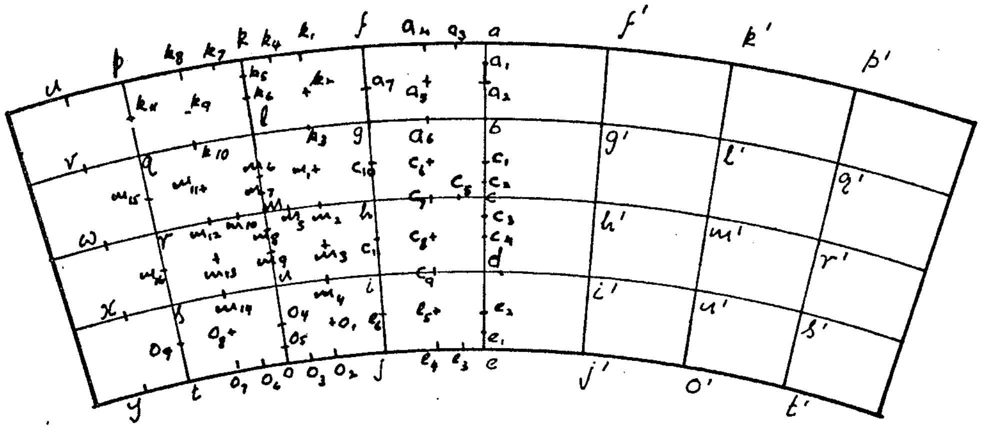

Model 1 and Model 2.

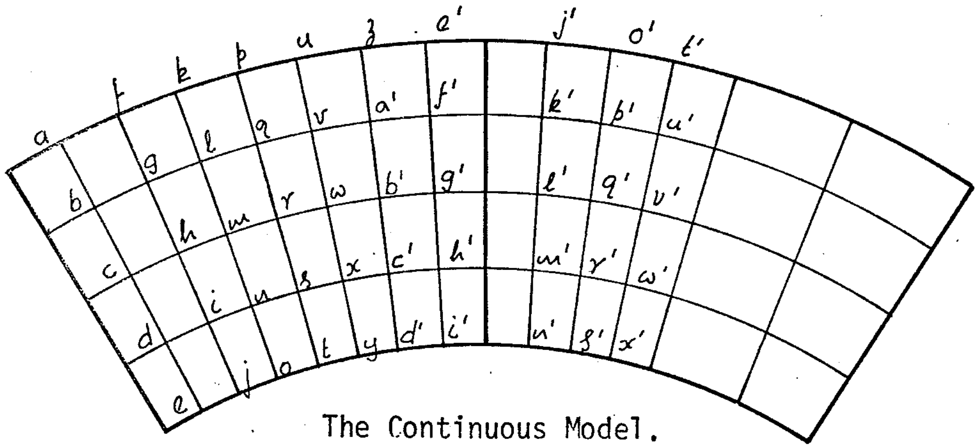

The Continuous Model.

Figure 4.2a   Loading Schedule.

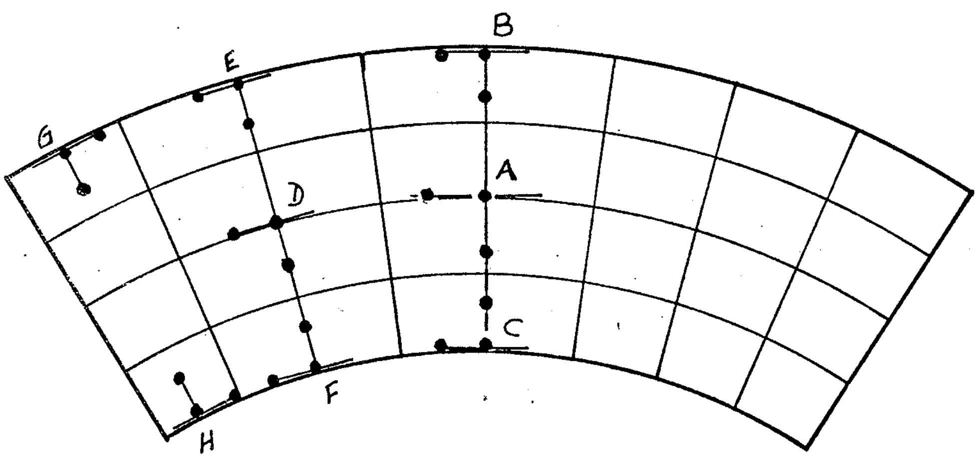

Figure 4.2b   Location of Punch Marks.

was not great enough to ensure firm contact between the model plate and the knife edge supports, some pressure was necessary to hold the model plate down. This was achieved by hanging weights from strings which were anchored to the upper surface of the model through tiny cones sitting at the edge, as shown in Figure 4.3 on page 40. In addition these pre-loads prevented any possible uplifts of the corners of the model due to loading. The question may arise as to whether these loads would affect the results because they cause some initial curvature in the model. However, this curvature was very small and its effect was eliminated by electronically "zeroing" the whole system after all the pre-loads were applied. This principle is explained in Chapter V.

4.3 The Knife Edges and the Testing Arrangement

The knife edges were made of solid steel. As shown in Figure 4.4 on page 40, slots were cut along the sharp edge of each knife edge. A set of holes of diameter 0.04" were drilled through them, to pass the strings carrying the pre-loads. These slots were cut to avoid the difficulties in aligning the holes through the sharp tips of the knife edges. The slots were machined to widths of dimensions less than one half the thickness of the plate to ensure that the localized stresses formed in the plate aroung the slots due to suspended pre-loads were insignificant.

The test bed consisted of two large steel channels champed across two leveled tables. Two double angles made of single angles fixed back to back were clamped across these two channels. In each

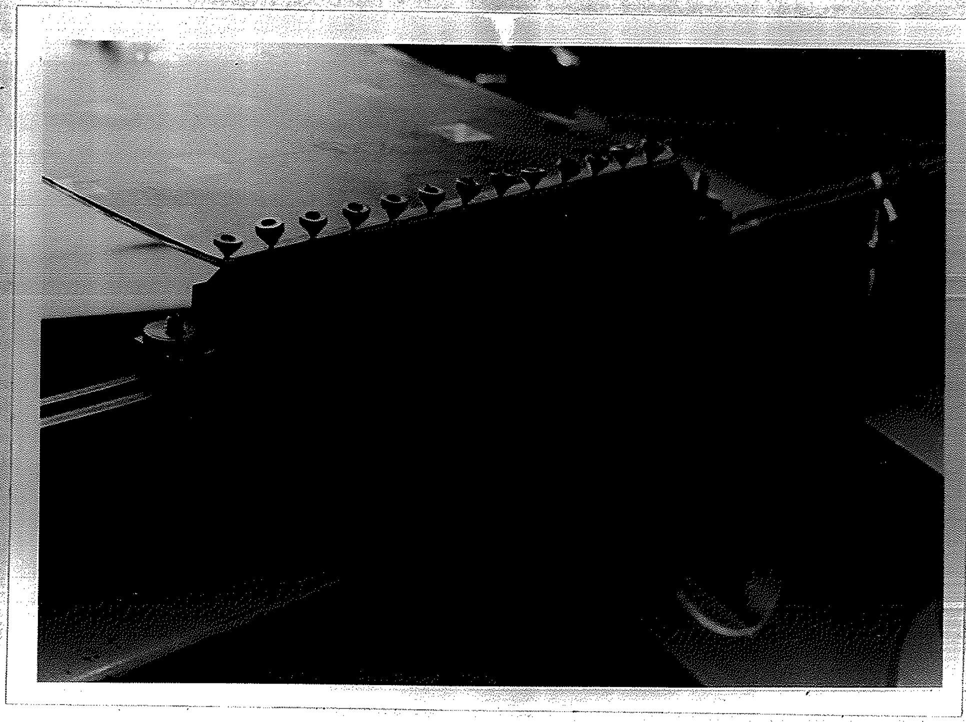

Figure 4.3   The Pre-Loading.

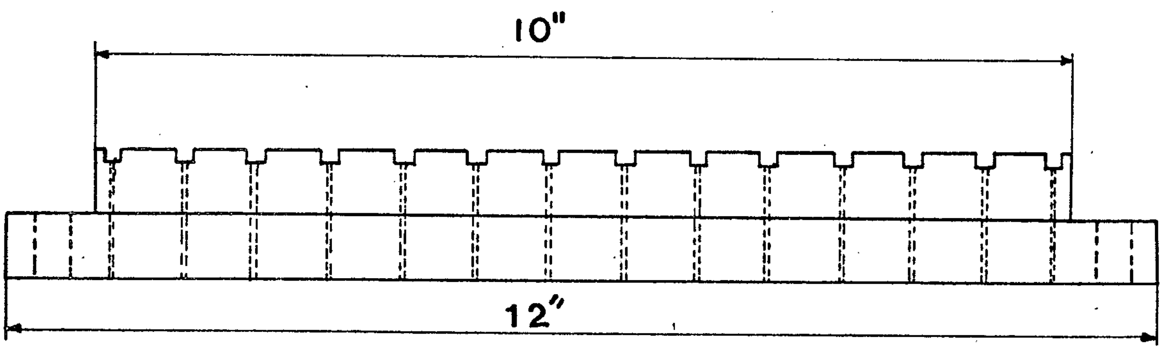

Figure 4.4   Knife Edge Support.

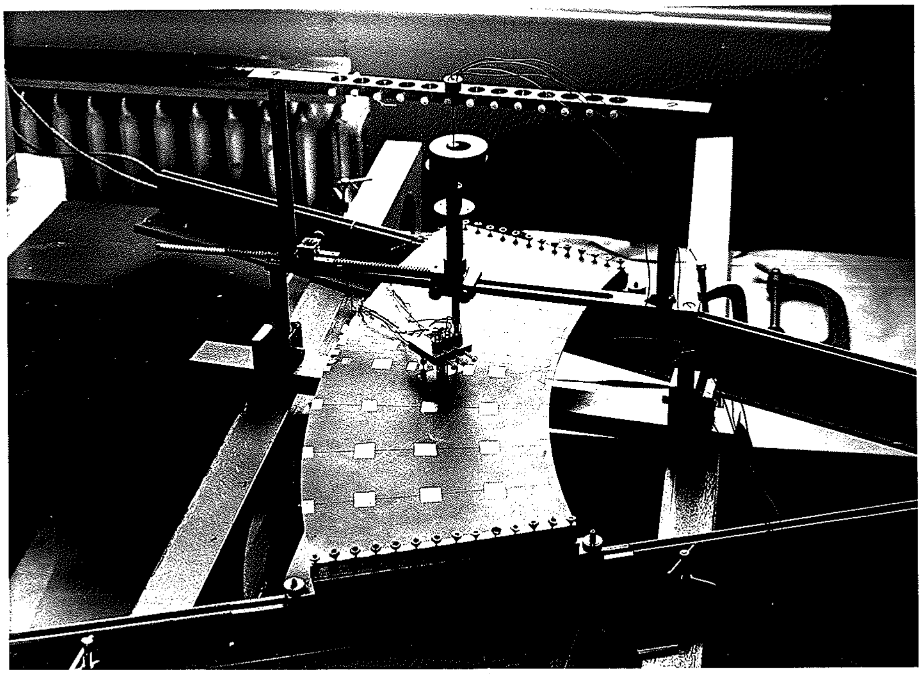

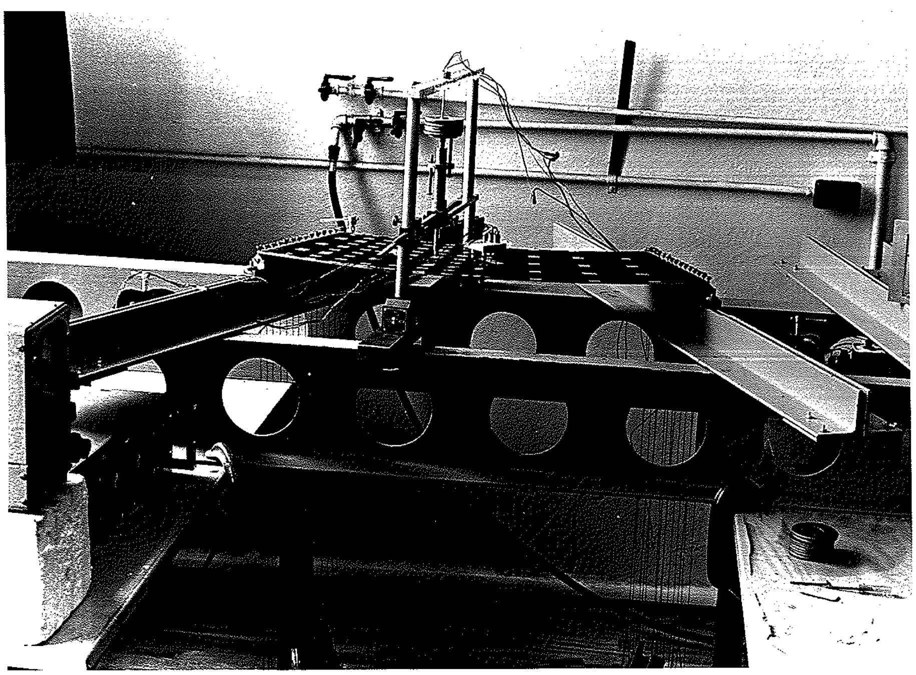

Figure 4.5 Test Set up.

of them, a gap was provided between the two single angles in order to pass the strings carrying the pre-loads. The two knife edges were fixed to the double angles. This test set up is shown in Figure 4.5, page 41.

4.4 Loading Mechanism

A vertical steel shaft with a ball transfer at the bottom was employed to load the model plate. This loading shaft was guided through two teflon bushings placed inside a cylindrical housing. As shown in Figure 4.6 on page 43 the cylindrical housing was machined as a part of a carriage that was designed to slide on a horizontal beam. The ends of this beam were fixed on to two vertical posts having magnetic bases. Another vertical frame was fixed on top of the previously mentioned horizontal beam. In the horizontal beam of the top frame, a number of holes were bored at pre-determined spacings to fix an inductive displacement transducer of the type 7DCDT-100, Hewlett Packard. The purpose of this transducer was to obtain the deflection directly under the load. A circular steel disc was fixed to the top of the loading shaft on which the loads were placed. Solid steel washers with a circular hole in the center to fit the shaft were used as weights. The loading shaft could be held at any vertical position using two long vertical screws placed against the bottom surface of the steel disc (Figure 4.6). Hence the ball transfer of the loading shaft could be made to be just in contact with the plate before loading. To obtain the deflection directly under the load, the bottom end of

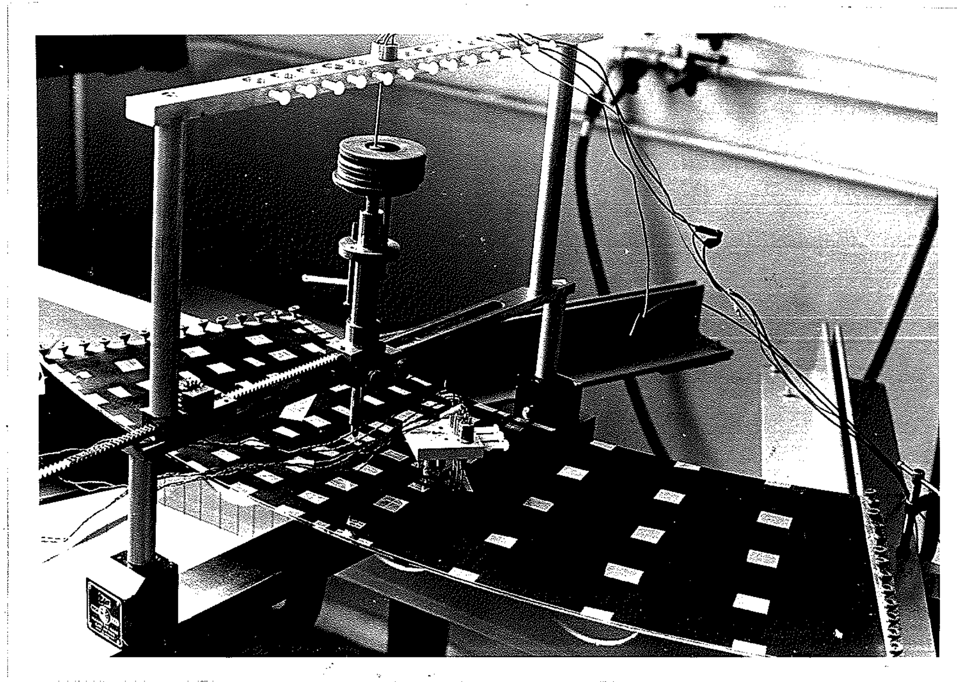

Figure 4.6 Loading Mechanism.

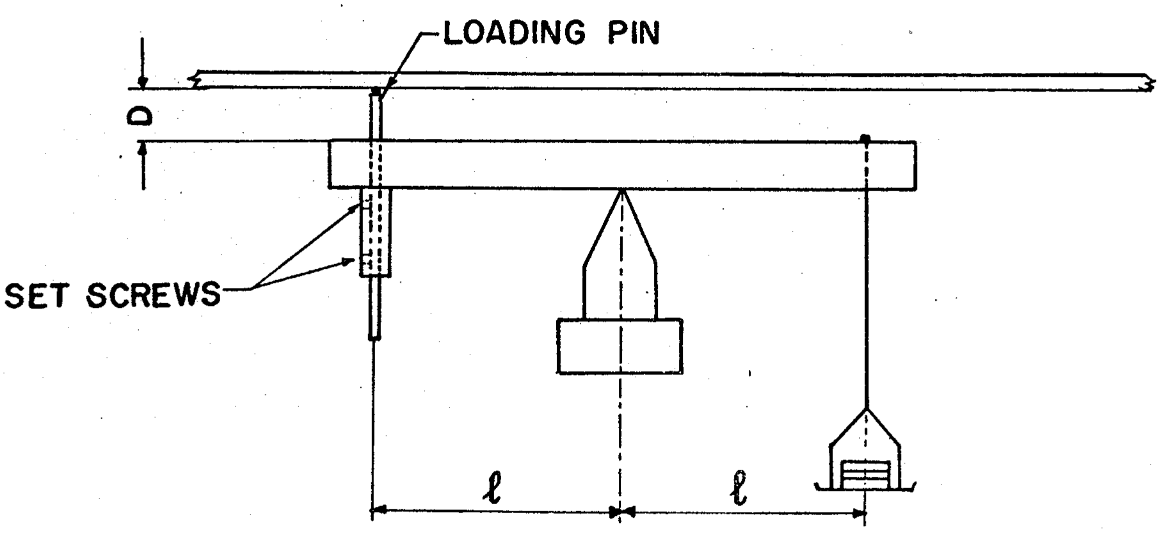

Figure 4.7 Cantilever System.

the transducer probe was kept on the loading shaft after it was adjusted to the above mentioned position. This transducer was connected to the Hewlett Packard Data Acquisition System machine to find the corresponding deflection.

As mentioned previously, at points close to the reference points,it was required to load the model from underneath. A cantilever system similar to that of a simple balance was employed to achieve this purpose. As shown in Figure 4.7 on page 43, a vertical steel needle with a ball transfer at the end was employed to load the model from underneath. This needle was guided through a steel tube fixed to an end of the horizontal balance beam. The needle could be adjusted vertically to ensure that the horizontal beam remained horizontal during loading and the deflecting of the plate. The purpose of this was to avoid the load being applied at an inclination to the vertical. To minimize the possible effect due to the horizontal frictional force that could exist between the ball and the model plate, the length D of the needle (Figure 4.7) was kept as short as possible. A tiny bit of grease on the ball transfer also helped to reduce the above mentioned friction to a negligible amount. When loading from below, instead of turning the knife edges to the top of the model, a technique of preloading the model was used and the procedures involved are given in Chapter V, page 55.

CHAPTER V

EXPERIMENTAL PROCEDURE

5.1 Calibration of Curvature Meter

Initially, the performance of the curvature meter discussed in Chapter III was tested on a plate that was subjected to pure bending. As shown in Figure 5.1, page 46 a 6" x 6" square plate made of aluminium alloy (ALCAN 2024 T-3) was supported at the opposite corners A and C from underneath and at the corner B from the top. The curvature meter was attached to the plate such that the two main axes of the meter were aligned along the two diagonals of the plate. Then the plate was loaded at the corner D. As expected, the two transducers on the main axes registered readings of equal magnitudes but of opposite signs indicating anticlastic curvatures along AC and BD. The third transducer registered a zero reading indicating that the plate remained undeflected along the lines X and Y (Figure 5.1, page 46) as expected in the case of pure bending. In addition the twisting curvature calculated from Equation [C] on page 24 using the three transducer readings was zero, which again satisfied the criterion of pure bending. Further, this confirmed the validity of Equation [D] that was developed in Chapter III. This experiment was repeated for two or three loading cases. For example the transducer readings obtained for a particular load were +0.00199, -0.0020 and 0.0 for the two main axis transducers and the third transducer

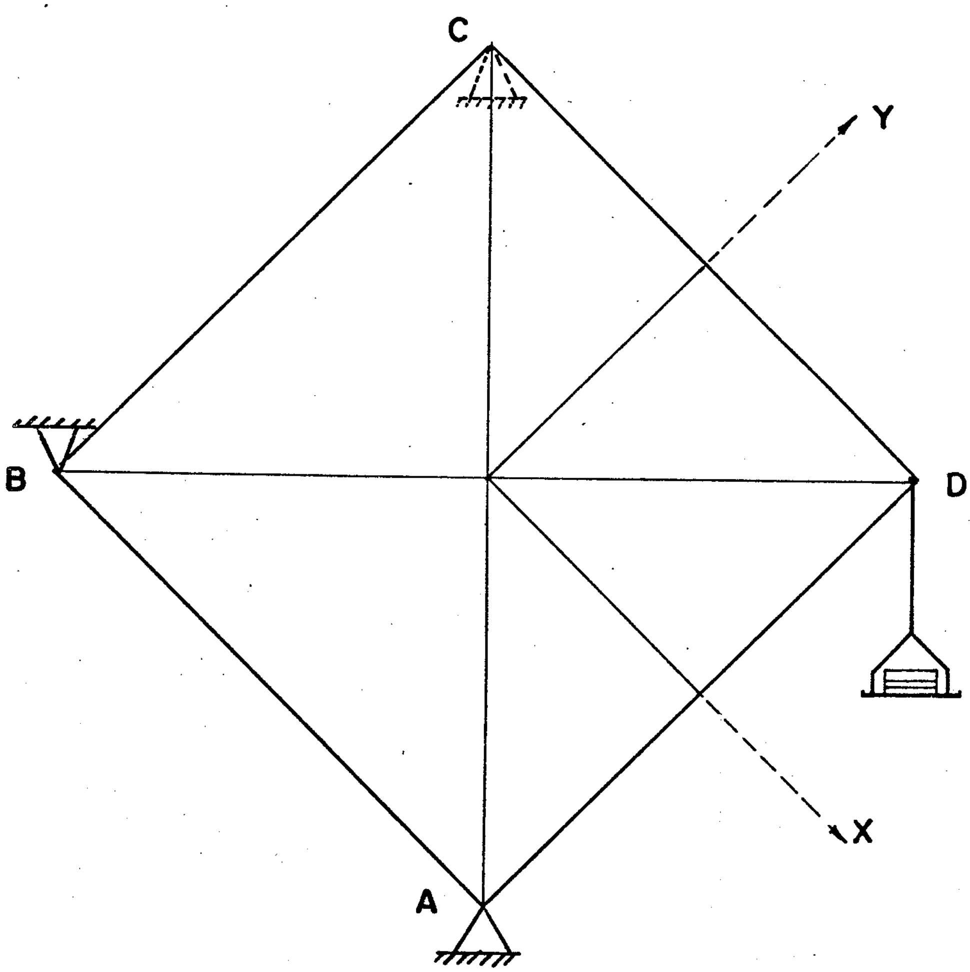

Figure 5.1 Plate Subjected to Pure Bending.

respectively. This experiment was repeated with the device rotated through 180° to be certain of the consistency of the curvature meter. The same readings were obtained with the signs reversed. Then the curvature meter was rotated through 45° such that the main axes of the meter were at 45° to the diagonals of the plate, i.e., in X and Y directions. As anticipated, the transducers on the main axes registered zero readings while the third transducer registered a non-zero reading. The curvature along the diagonal of the plate was calculated using Equation [C] developed for $K_{\theta+45°}$ in Chapter III, page 24. This value was found to be equal to the curvature obtained for the same diagonal for earlier meter set up using the more straightforward Equation [A]. Hence, the validity of Equation [C]was confirmed again. The curvature meter was rotated through 180° from this position. The same readings were obtained again with the sign reversed. Then the curvature meter was adjusted such that the main axes were 15° from the diagonals. All the three transducers registered non zero readings. From these readings curvatures along the diagonals were calculated using the equilibrium for curvatures in a plate (Mohr's circle). They were equal to those obtained with earlier set ups. Unfortunately, the above described experiment could not be considered as a general proof to show the validity of Equation [C] developed for θ+45° axis of the meter. This was due to the fact that in all the three meter set ups the meter axis θ+45° remained level as in the simple case considered in Figure 3.2 on page 22. Hence the term $(f_\theta + f_R)$ in Equation [C] always turned out to be zero unlike in the general case shown in Figure 3.3, page 22. On the other hand, this experiment did not produce data inconsistent with the equations developed for the meter axis θ+45° in Chapter III.

As mentioned earlier, the curvature meter was calibrated along each axis using a strain gauge testing beam apparatus, (H. Tinsley and Co. Ltd.). With this apparatus, a circular curvature could be obtained in the center portion of the beam by fixing the two adjustable roller supports A and B equi-distant from the respective screw jacks R and L provided at the ends of the beam, (Figure 5.2a page 49). This circular curvature could be calculated using the relative deflection measurement obrained from a micrometer mounted at a center of a special carriage. This carriage had been designed to work on the same principle as the curvature meter. The gauge length between the two fixed legs at the ends of the carriage was much larger than the gauge length of the curvature meter. The relative deflection measurements of the micrometer, therefore, were greater in magnitude than those of the curvature meter transducers. Hence, the micrometer sensitivity of 10^{-5} metre was quite adequate for calibration of the currature meter. For accurate measurements of deflections the micrometer should not exert any pressure on the beam while recording the readings. For this purpose the carriage was provided with two terminals which were connected to an electric buzzer actuated

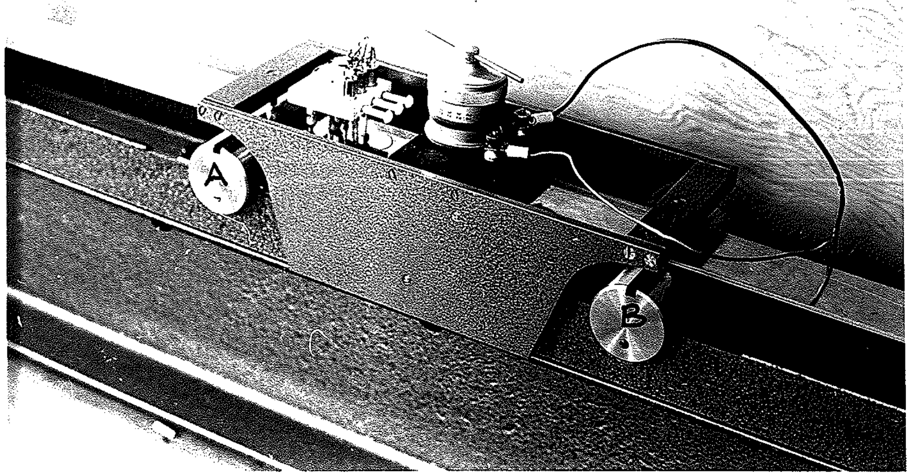

(a)

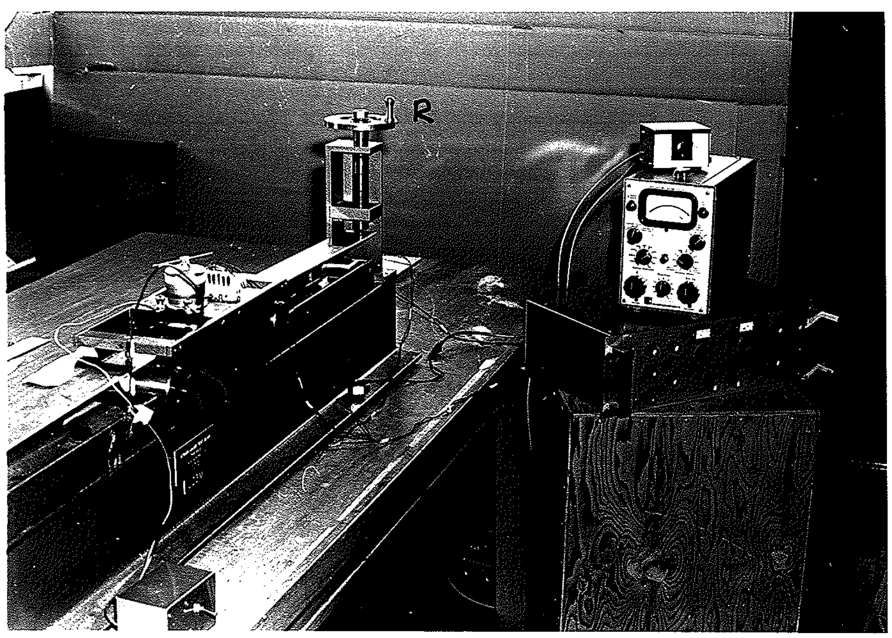

(b)

Figure 5.2 Calibration Set up.

by a high frequency current. Thus, the slightest contact between the micrometer and the test beam would at once be indicated by the buzzer sound.

The calibration set-up is shown in Figure 5.2b, page 49. A narrow strip of aluminium of length 48", of width 2" and of thickness 0.125" was used as the testing beam instead of the Beryllium Copper beam supplied with the apparatus. This strip was cut from the same sheet of aluminium that was used to make the models in order to attain high level of precision. The micrometer carriage was placed on the center portion of the beam such that the two fixed legs were on the center line of the beam. The curvature meter was mounted on the beam at a predetermined point between the legs of the carriage with its axis to be calibrated lying along the center line of the beam. More accurate displacement measurements on the measuring bridge could be obtained if the transducer probe was close to its mechanical zero position at the unloaded state. This was obtained by moving the transducer housing vertically until the measuring bridge meter needle was close to zero while all the electrical settings were at middle positions. The meter needle was brought to exact zero position electrically and the measuring bridge was then balanced for phase and amplitude. The measuring amplifier K.W. S/T-5 used could be set to various measuring range sensitivites such that even a fractional part of the nominal 1 mm range of displacement of the transducer probe indicated a full deflection on the recording meter. The measuring bridge meter was then calibrated such that the needle indicated a full deflection in the meter when the maximum displacement corresponding to the selected sensitivity range was simulated electrically. The micrometer reading was recorded at this unloaded state and then the beam was deflected by moving the two screw jacks downwards. The micrometer readings and the measuring bridge meter readings were recorded at various stages of loading. For each sensitivity range selected these measurements were carried out for two continuous cycles of beam deflection obtained by loading, unloading, reloading and re-unloading. This was to obtain an idea of the significance of the hysteresis of the total system and to check whether the meter was capable of reproducing the results faithfully. The data that were obtained from these calibration tests are discussed in the next chapter.

The question arose as to whether the calibration obtained for a particular initial balance position of the probe close to its mechanical zero position would be valid if the initial balance position of the probe during testing was not the same, although in both cases the measuring bridge could be set for "initial zero" using its electronic settings. Therefore, the calibration procedure was repeated for a number of off set positions of the probe on both sides of its mechanical zero position. For each calibration, the positions of the appropriate "coarse" electronic setting and the "fine" electronic setting of KWS/T-5 (or S A II) were recorded. However, it was not possible to record the position of the "extra fine" setting. All three meter axes were calibrated in three sensitivity ranges that showed deflections of 0.01 mm, 0.005 and 0.002 mm at full range. In calibrating the θ+45° axis of the meter, all the three transducer readings were recorded and used in Equation [C] (page 24). The three transducers used on the three curvature meter axes were marked with different numbers in order to make sure that in testing they were used on the same axes on which they were calibrated.

5.2 Procedure for Obtaining Curvature Data

The curvature meter was mounted on the model at the point under investigation such that the middle leg of the meter coincided with the reference point. The three transducer housings then were locked onto the curvature meter such that the probes were close to their mechanical "zero" positions while the measuring bridge electrical settings were at their middle positions. The purpose of this adjustment was two-fold. First, as mentioned earlier, the sensitivity of the displacement transducer was at its peak when its probe was at this middle position. Secondly, this adjustment gave a one millimetre range above and below the "zero" position, thus allowing the probe to record both positive curvature and negative curvature, (Figure 5.3, page 53). The measuring bridge meter needle was brought to the zero position for each transducer circuit. The measuring bridge was then balanced for phase and amplitude for each transducer circuit. When the bridge was balanced, it

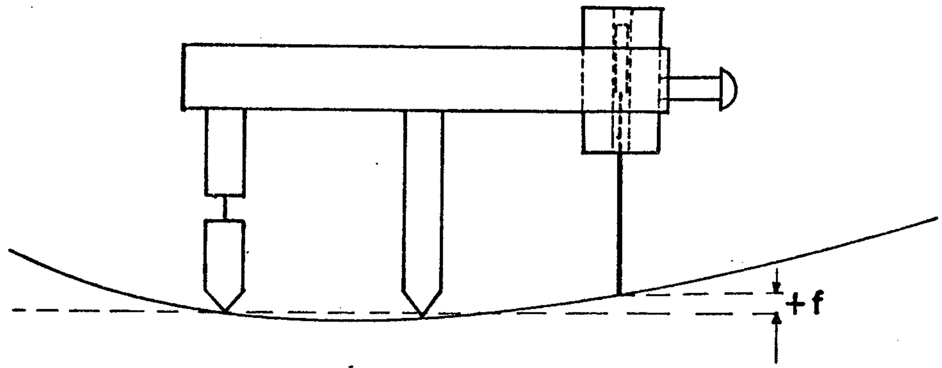

Positive Curvature

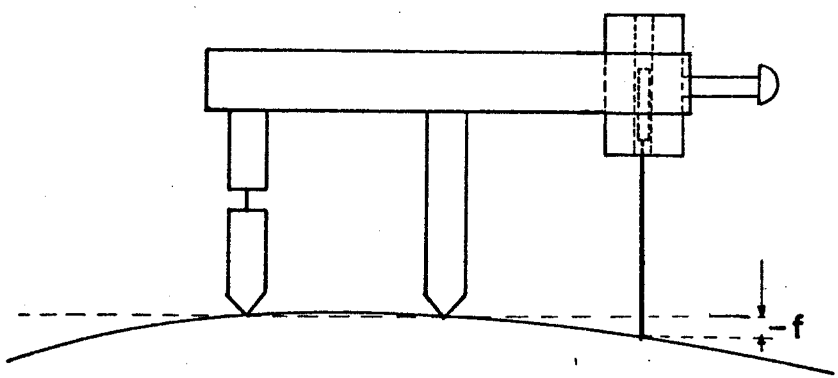

Negative Curvature

Figure 5.3

was assumed to have "zeroed" the initial conditions of the model. From then on, the meter registered the deflections corresponding to change in curvature due to any additional load applied to the slab. Therefore, the earlier mentioned initial curvatures produced by the pre-loading and the weight of the curvature device did not have any bearing on the curvature recorded due to the load. The measuring bridge was calibrated internally as described earlier in all the three selected sensitivity ranges. The model was then loaded at the required place (the "load point") and the three transducer readings were recorded. This was repeated three times, starting with a different transducer every time to ensure that the readings were not influenced by factors such as the transducer circuit transfer switch box, connecting cables, etc. After the first model was completely tested this was carried out only as an occasional check. Every time when the load was lifted it was checked to see whether the measuring bridge remained balanced for all the three circuits. The reading of the transducer type 7DCDT-100 (HEWLETT PACKARD) was also recorded to make sure that the selected load did not produce deflection large enough to violate the small deflection theory for elastic plates.

In the case of first model, the symmetry of the measured values for the three reference points on the center radial line were checked by loading the model at load points on both sides of this symmetric radial line. For the other two models this symmetry check was done occasionally. In addition, on the first model an extra symmetric reference point (Figure 4.1, page 37) was examined to check the symmetry.

In order to load the model from underneath, it is usual to change the knife edge set-up. Instead of this complicated procedure the fact that the curvature meter measures only the change in curvature was used. First, the model was loaded from above at a number of points close to both supports with reasonably heavy loads. This was to ensure that the plate was pressed against the supports when it was loaded from underneath. Then the meter was zeroed for initial conditions and the load was applied from below using the cantilever system described in Chapter IV. The same experimental procedure described in the previous paragraph was then followed.

5.3 Material Properties and Calibration of Loading Systems

A tension test was carried out to obtain the modulus of elasticity and the poisson's ratio of the model material. The loading mechanism used to load from above was calibrated using a precision balance capable of reading down to the nearest 1/100th of a gm. It was ascertained that even the small friction that existed between the shaft and the teflon bushing could be rendered negligible by tapping lightly on the shaft after loading. This procedure was followed at all times.

CHAPTER VI

OBSERVATIONS FROM CALIBRATION AND SYMMETRY TESTS

6.1 Calibration Constants for the Three Transducers

The circular curvature produced by the strain gauge testing beam apparatus was measured in two ways as described in the previous chapter. Then they were compared with each other in order to find a calibration constant "C_θ" (or C_R or $C_{\theta+45°}$). Instead of calculating a number of "C_θ" 's at different levels of loading and taking the average value, it was decided to plot the curvature measured by the testing apparatus (using Equation 2.4 on page 18) vs the curvature measured by the meter (using Equation [A] on page 24). In each case the slope of the best straight line through these calibration points was taken as the constant "C_θ" (or C_R or $C_{\theta+45°}$). The Calcomp line plotter computer programme "AVLIN" that is available at the computer center of University of Manitoba was used to plot the calibration data. The slopes of these straight lines were obtained as out puts of the programme. Excellent linearity and reproducibility of the measured values indicated the high degree of reliability of the measuring bridge apparatus and the transducers. When the data for loading, unloading, re-loading and re-unloading were plotted on the same sheet, it was obvious that the hysteresies in the system was insignificant. From these calibration graphs (Figure 6.1, page 57) the reproducible nature of the curvature meter was very evident.

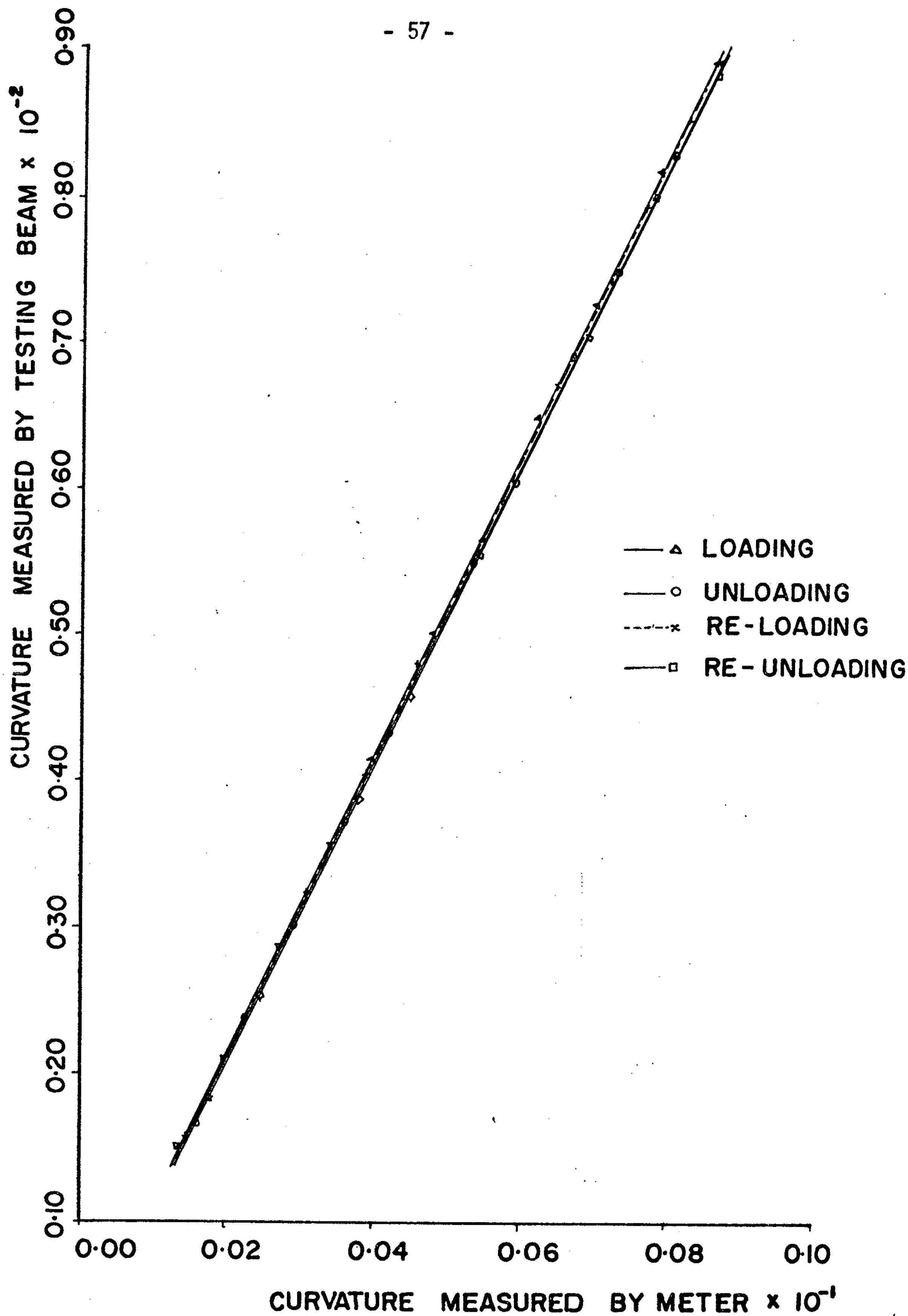

TYPICAL CALIBRATION GRAPH SHOWING INSIGNIFICANT HYSTERESIS

Fig. 6·1

Each meter axis was calibrated in three sensitivity ranges. There was a slight difference in "C" values between the three sensitivity ranges of the measuring bridge for all the three curvature meter axes. The effect of offsetting the transducer probe from its mechanical zero position was found to be insignificant on the calibration constants C_θ and $C_{\theta+45°}$ in all the three sensitivity ranges. The constant C_R was affected by offsetting the transducer probe and this was found to be very significant in the 0.002 mm (the highest) sensitivity range. In the cases of 0.01 mm and 0.005 mm sensitivity ranges this effect was found to be significant only when the probe was offset considerably from the mechanical zero position. However, this did not have any bearing on the testing since the positions of electronic balance settings of KWS/T-5 (or S A II) were recorded during each calibration.

A different procedure that was used in plotting the calibration curve for the θ+45° axis of the meter because of its complicated expression for curvature is given below.

The circular curvature calculated from the testing beam apparatus $= \frac{8F}{(L_T)^2}$ where L_T is the gauge length of the carriage meter. The same curvature calculated on θ+45° axis of the meter $= \frac{16}{(L_T)^2} [f_{\theta+45°} - \frac{3}{8}(f_\theta + f_R)]$. The readings f_θ and f_R can be corrected since C_θ and C_R are known.

$$\frac{8F}{(L_T)^2} = \frac{16}{L^2} [f_{\theta+45°} - \frac{3}{8}(C_\theta f_\theta + C_R f_R)]$$

$$f_{\theta+45°} = \frac{F}{2}\left(\frac{L}{L_T}\right)^2 + \frac{3}{8}\left(C_\theta f_\theta + C_R f_R\right)$$

Let $$F^* = \frac{F}{2}\left(\frac{L}{L_T}\right)^2 + \frac{3}{8}\left(C_\theta f_\theta + C_R f_R\right)$$

Hence F^* vs $f_{\theta+45°}$ was plotted to find $C_{\theta+45°}$. $C_{\theta+45°}$ is really a calibration for the third transducer alone. Hence, in correcting the curvature measured on the $\theta+45°$ axis, all three calibration constants C_θ, C_R and $C_{\theta+45°}$ were used in the Equation [C].

The calibration constants obtained are given below.

Full Deflection of the Sensitivity Range.	C_θ	C_R	$C_{\theta+45°}$
0.01 mm	1.002	0.992	0.995
0.005 mm	1.011	0.998	0.991
0.002 mm	1.008	0.999	0.987

6.2 Checks on Experimental Results

As mentioned in the previous chapter in the case of the first model tested, the model slab was loaded at loading grid points on both sides of the symmetric radial line in studying the three reference points A, B and C. Since these reference points were on the symmetric radial line, this provided a comprehensive check for symmetry. For all the three reference points A, B and C, the transducer values f_θ were found to be remarkably close for symmetric load points [e.g., g, g'/h, h'/ etc. (Figure 4.2a, page 38)]. The maximum difference obtained was much less than one half of the smallest readable division (0.0002 m m) of the 0.01 m m scale used. At the reference point A, the registered transducer values of f_R were small compared to the orthogonal axis values f_θ. Some discrepancy could be noted for these small values of f_R for symmetric loading. However, only in four instances these differences were more than the smallest readable divisions (0.001 m m) of the 0.005 m m scale used. The obvious solution appeared to be the use of higher loads so as to obtain higher readings for f_R that could be read on a less sensitive scale than the one already used. However, it was not possible to use higher loads since the small deflection theory of plates would have been violated. The alternate solution for the above problem are discussed in Chapter IX. The third transducer readings $f_{\theta+45°}$ obtained at reference point A were entirely different from each other for symmetric load points. However, when the twisting curvatures $K_{\theta R}$ at A were calculated using f_θ, f_R and $f_{\theta+45°}$ in Equation [C] for symmetric load points, remarkably close values were obtained with opposite signs. This was an excellent demonstration of the highly precise performance of the curvature meter. It also proved that symmetric boundary conditions had been obtained from the modelling technique employed. These transducer readings are listed in Table 6.1 on page 61. As expected zero values were obtained for $K_{\theta R}$ at reference point A when the model was loaded at points on the symmetric radial line. All the three transducer readings obtained for reference point D for all the load

Table 6.1 Some of the Symmetric Load Points for the Reference Point A.

Load Points	Transducer Readings		
	θ	R	θ+45°
a	0.00705	-0.00296	0.00152
b	0.00850	+0.00221	0.00236
c	0.00576	-0.00090	0.00250
d	0.00958	-0.00232	0.00272
e	0.00740	-0.00300	0.00165
f	0.00600	-0.00225	0.00110
f'	0.00603	-0.00225	0.00173
g	0.00683	-0.00164	0.00165
g'	0.00683	-0.00175	0.00221
h	0.00755	-0.00105	0.00239
h'	0.00755	-0.00105	0.00249
i	0.00760	-0.00178	0.00235
i'	0.00762	-0.00181	0.00198
j	0.00660	-0.00240	0.00178
j'	0.00664	-0.00232	0.00140
k	0.00603	-0.00208	0.00102
k'	0.00609	-0.00216	0.00194
l	0.00558	-0.00145	0.00123
l'	0.00560	-0.00144	0.00188
m	0.00536	-0.00111	0.00138
m'	0.00536	-0.00100	0.00183
n	0.00532	-0.00129	0.00189
n'	0.00534	-0.00130	0.00101
o	0.00535	-0.00179	0.00188
o'	0.00542	-0.00180	0.00081

Some of the Readings at Symmetric Reference Points D and D' *

Load Points	Transducer Readings at the Reference Point D			Transducer Readings at the Reference Point D'		
	θ	R	θ+45°	θ	R	θ+45°
a	0.00403	-0.00142	0.00142	0.00401	-0.00138	0.00141
b	0.00467	-0.00122	0.00152	0.00464	-0.00122	0.00154
c	0.00540	-0.00115	0.00144	0.00538	-0.00116	0.00142
d	0.00534	-0.00128	0.00104	0.00532	-0.00128	0.00104
e	0.00453	-0.00150	0.00054	0.00452	-0.00150	0.00052
f	0.00514	-0.00200	0.00155	0.00295	-0.00093	0.00118
f'	0.00295	-0.00098	0.00120	0.00511	-0.00196	0.00158
g	0.00585	-0.00136	0.00195	0.00342	-0.00095	0.00120
g'	0.00341	-0.00096	0.00120	0.00579	-0.00134	0.00200
h	0.00660	-0.00070	0.00205	0.00400	-0.00100	0.00119
h'	0.00400	-0.00100	0.00120	0.00653	-0.00070	0.00210
i	0.00648	-0.00140	0.00153	0.00328	-0.00088	0.00063
i'	0.00322	-0.00085	0.00068	0.00645	-0.00140	0.00155
j	0.00564	-0.00202	0.00076	0.00330	-0.00103	0.00041
j'	0.00330	-0.00103	0.00042	0.00564	-0.00202	0.00078

* At the reference point D' the curvature meter is located with a 90° rotation (clockwise) from that at D. The loading points a, b, c, d and e are located on the symmetrical radial line. Hence for the above mentioned loading points identical transducer readings are obtained for the reference points D and D' as shown above.

points were in good agreement with the corresponding values obtained for the symmetric reference point D' as shown in Table 6.1 on page 61 .

In the other two models tested, only occassional load symmetry tests were performed.

CHAPTER VII

PRESENTATION OF TEST RESULTS

7.1 Dimensionless Curvature Influence Coefficients

The moments M_θ, M_R and $M_{R\theta}$ could be obtained from Equation 2.1, 2.2 and 2.3 on page 9 using the curvatures calculated from test results. Influence surfaces presented in terms of these moments would not be of much direct use to the designer since they were calculated for a certain load P and for a plate material of certain Poisson's ratio μ. Therefore, it was decided to present the results in the form of non-dimensional curvature influence surfaces as shown below. This method would help in attaining a better accuracy in correlating the model results to prototype slabs made of materials of different Poisson's ratios. The method of obtaining this correction for Poisson's ratio is given below. However, some discrepancies would still be present and they are discussed later in this chapter. I_θ, I_R and $I_{\theta R}$ are the non-dimensional influence coefficients corresponding to the curvatures K_θ, K_R and $K_{\theta R}$ where

$$I_\theta = \frac{DK_\theta}{P} \qquad (7.1)$$

$$I_R = \frac{DK_R}{P} \qquad (7.2)$$

$$I_{\theta R} = (1 - \mu)D\,\frac{K_{\theta R}}{P} \qquad (7.3)$$

These curvature influence coefficients can then be used to find the moments of prototype slabs of the same shape but of different Poisson's ratios, in the following way. If the Poisson's ratio of the prototype material is μ_p and the concentrated load is P_p, then:

$$M_\theta^P = P_p \, (I_\theta^m + \mu_p \, I_R^m) \tag{7.4}$$

$$M_R^P = P_p \, [\, I_R^m + \mu_p \, I_\theta^m \,] \tag{7.5}$$

$$M_{\theta R}^P = P_p \, I_{\theta R}^m \tag{7.6}$$

where I_θ^m, I_R^m and $I_{\theta R}^m$ are the model curvature coefficients. This can be shown in the following way:

Prototype curvature/unit load $= \frac{Dm}{Dp} \cdot \frac{Km}{Pm}$

where Dm = model stiffness

Km = model curvature for a load Pm

Pm = model load

D_p = prototype stiffness

Therfore, for a prototype load P_p

$$K_p = \frac{DmKm}{Dp} \times \frac{Pp}{Pm} = \frac{Pp}{Dp} \left(\frac{DmKm}{Pm} \right)$$

But $I^m = \frac{DmKm}{Pm}$

Hence $Kp = \frac{Pp}{Dp} I^m$

Therefore $M_\theta^p = Dp\ (K_\theta^p + \mu_p\ K_R^p)$

$$= Dp\ \left(\frac{Pp}{Dp} I_\theta^m + \mu_p \frac{Pp}{Dp} I_R^m \right)$$

$$= Pp\ (I_\theta^m + \mu_p\ I_R^m)$$

Euqations 7.4 and 7.5 are simplified forms of more complex expressions that have been developed by S. Timoshenko and S. Krieger[24] to modify the bending moments in slabs for a change in Poisson's ratio from μ_m to μ_p. The expressions given by Timoshenko and Krieger are:

$$M_\theta^p = \frac{1}{1-\mu_m^2} [(1 - \mu_m\mu_p)\ M_\theta^m + (\mu_p - \mu_m)\ M_R^m]$$

$$M_R^p = \frac{1}{1-\mu_m^2} [(1 - \mu_m\mu_p)\ M_R^m + (\mu_p - \mu_m)\ M_\theta^m]$$

It can readily be shown that the above equations are not valid when applied to the slabs with boundary conditions such as free edges or cases of elastic supports--where μ is implied in those boundary conditions. For example, at a free edge, the use of the above equations for conversion of moments from μ_m to μ_p yields an expression $M_R^p = \frac{1}{1-\mu_m^2} [(\mu_p - \mu_m)\ M_\theta^m]$ for the transverse moment M_R. Clearly this expression is not zero although the transverse moments at a free edge must be zero for any Poisson's ratio. However, it has been shown that, although the use of the above equations leads to some errors near a free edge or an elastic support, it does not influence the moments elsewhere on the slab, [24, 27, 30, 31, 32]. A detailed investigation of the effect of change of Poisson's ratio is beyond the scope of this dissertation. However, the writer has carried out a survey of literature available on this subject [15, 24, 27, 30, 31, 32] and therefore with the aid of those he offers the following comments.

Robinson [31] in his investigation of centrally loaded square slabs found that a reduction of Poisson's ratio from 0.30 to 0.15 resulted in a considerable reduction in both spanwise and transverse moments under the load point. The effect of this on span-wise moment at the center of a free edge was found to be negligible. He ascertained similar results for a reduction from 0.3 to zero. In the reference (30) it is mentioned that Balas and Hanuska [32] have observed that for a uniform loading, an increase in Poisson's ratio from zero to 1/3 resulted in an increase of deflection at the center of a free edge. For a concentrated load near the free edge, an increase of both deflection and spanwise moment was observed. Yeginoboli [27] from his studies on continuous skewed plates commented that the deflections and moment increased with increase in Poisson's ratio. The above comments illustrate only a few examples of the research that has been done on this subject.

The writer concludes that in correlating the model results to the prototype, any difference in Poisson's ratio between the model and the prototype should be considered. Since the use of Equations 7.4 and 7.5 leads to some errors near a free edge or an elastic support, at those places it appears safer to use the model results directly in the design without any coversion if the model test has been carried out on a material of higher Poisson's ratio. than the prototype[21]. The reason for the above recommendation is that the model deflections and moments will be higher than those of a material of lower Poisson's ratio.

7.2 Evaluation of Influence Surfaces

(a) Uniformly Distributed Load (U.D.L.)

As mentioned earlier an influence surface drawn for a particular reference point presents the influence of a unit load anywhere on the slab at that point. Therefore, the influence of any load is measured by the product of the magnitude of the load and the corresponding ordinate of the influence surface. The distributed load can be considered as closely packed concentrated loads.

If p is the loading per unit area and i is the influence ordinate of curvature under the load p, the curvature created at the reference point by this loading is:

$$dI = (p\ i)\ Rd\theta dR \tag{7.7}$$

If one replaces arc length $R\theta$ by T, then small arc length $Rd\theta$ becomes dT. Therefore, Equation (7.7) becomes

$$dI = (p\ i)\ dT\ dR$$

The total curvature due to uniformly distributed load over the whole slab is given by the summation of each of these curvatures dI.

$$I = \int dI = \int (p\ i)\ dTd\theta \tag{7.8}$$

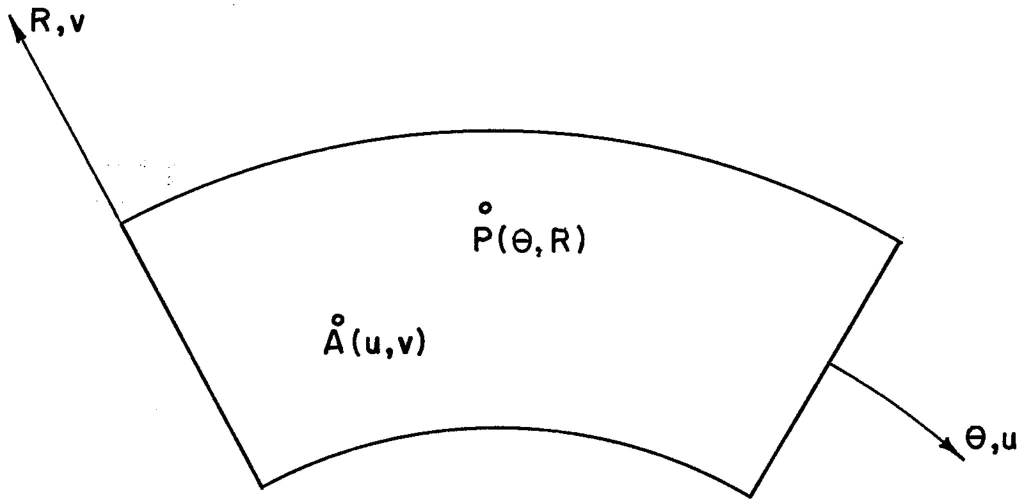

Reference point A and load point P with coordinates (u,v) and (Θ,R) respectively.

Figure 7. 1a

The influence ordinate i depends on four variables, namely u, v, θ, and R. The reference point location is denoted by u and v. The load location is given by R and θ as shown in Figure 7.1a (Page 68a). Therefore, Equation 7.8 becomes

$$I\ (u, v) = \iint (R, \theta)\ .\ i\ (u, v, \theta, R)\ dT\ dR \qquad (7.9)$$

If one replaces the acutal dimensions R and T by dimensionless coordinates

$$a = \frac{T}{l} \qquad b = \frac{R}{l} \qquad c = \frac{u}{l} \qquad d = \frac{v}{l}$$

where l is an arbitrary length:

then $dT = l da$ $\qquad$ $dR = l db$

Hence Equation 7.9 becomes

$$I\ (u, v) = l^2 \iint p\ (a, b)\ \ i\ (c, d, a, b)\ da\ db \qquad (7.10)$$

This evaluation formula shows an important general feature of influence surfaces. That is they are independent of the absolute plate dimensions and that only the shape of the plate is important.

In general, uniformly distributed loads are constant. Therefore, Equation (7.10) becomes

$$I\ (u, v) = p.l^2 \iint i\ (c, d, a, b)\ da\ db \qquad (7.11)$$

The double integral in Equation (7.11) can be interpreted geometrically as the volume of the influence surface over the loaded area. This geometric meaning is the key for the evaluation since, in general, it is not possible to determine the exact influence function i in order to perform the double integration in Equation (7.11) mathematically. When the contour plan of an influence surface is given, it is a simple problem to find the "influence volume" from plane projected areas of the contours or from the section through the contours as shown by A. Pucher (13). These calculations are made in a manner identical to earthwork volume computations, using Simpson's rule where appropriate.

Although any arbitrary value could be used for l in Equation (7.11) in this work the width of curved bridge deck is used for l.

(b) Wheel Loads

In designing highway bridges, it is essential to study the effect of a truck load when it travels across the bridge. The magnitude of the curvatures depends on the position of the truck on the bridge. The critical position of the truck is usually determined by a trial and error procedure. The wheel spacing is drawn on a piece of tracing paper to the same scale as the influence diagram and then it is moved about on the influence surface until the critical location of the truck is obtained. With a little practice, one can approximate to this position very closely by inspection, noting that in general, one wheel load should be on top of, or as close as possible to the reference point. All the wheel loads can be considered as concentrated loads except that wheel load, which is over the reference point or very close to it. In this case the load distribution should be considered, since at or close to the reference point the influence surface changes rapidly. Often a load distribution angle of 45° is used (13).

In the treatment of other wheel loads it has been assumed that they are concentrated loads. But if the contact area is large, consideration of load distribution is necessary, as discussed in greater detail in Reference (13). An example of the use of influence surfaces in truck load analysis is given in Reference (33) by A. M. Lansdown.

Influence surfaces are useful to the bridge designer not only in assessing the effect of abnormally heavy loads on ane existing bridge, but also assist in the design of bridges in many ways. The critical moment locations can be obtained quickly if a set of influence surfaces for the structure to be designed are available. They also become useful in laying out the reinforcement for the structure. When the pertinent influence surfaces for the particular structure to be designed are not available, the designer can employ a set of influence surfaces representing a structure that is closely similar to that under design. The hypothetical structure so chosen can assist him to arrive at the final structure. For example, when a bridge engineer is called upon to design a bridge, the total span and the approximate width will be the only definite properties of the bridge that he will have at hand. The plane geometry of the bridge of course depends on the traffic requirements at the particular location. If the influence surfaces are available for various shapes of structures of different span to width ratios, the engineer can select a structure that appears to be the most suitable for his problem. Then he can start to build up his particular structure using the critical moments in the selected influence surface as the primary design moments. For instance, if the designer has selected a horizontally curved bridge deck, at once he will notice from the influence surfaces that the critical locations are the mid points of the two free edges instead of the mid span. Hence, it would indicate to him that edge beams are likely called for. Similarly, in the case of a skew slab, the influence surfaces will indicate the obtuse corner as the critical location that should be considered in detail. From an inspection of influence surfaces alone, with a little experience one may be able to pick a hypothetical structure that will be close to the final structure.

7.3 Correlation of Model Results to Actual Structure

The gauge length of the curvature meter controls the accuracy of the measured values and therefore indirectly governs the choice of size of the model. This stems from the curvature meter's measuring only an average curvature over the base length L of the meter. The ratio L/L_M (where L_M is the span of the model slab) therefore becomes a prime factor for the accuracy of the model results. The assumption of constant radius of curvature within the base length L is assisted by the selection of smaller ratios of L/L_M. An analytical approximation to the effect of L/L_M on curvatures is presented in Appendix 1.2. Weigler and Weise [29] recommended that for practical purposes ratios of (L/L_M) of 1/10 to 1/8 is satisfactory. Mehmel and Weise [8] mentioned that the error that could result from a ratio of 1/6 was less than one percent in the mid span region. The ratio used in this investigation was 1/18 with respect to the center spans of the simply supported model slabs, whereas it was 1/9 with respect to the continous slab. The ratio was very close to 1/7 in the transverse direction with respect to the width of both model slabs.

Any curvature meter does not accurately measure the curvature at or in the close vicinity of a concentrated load where the curvature of the deformed plate changes rapidly. This inaccuracy in curvature measurement is due to its peak value being rounded (flattened off) as a result of the curvature meter's measuring only an average curvature over the base length.

Theoretically the curvature under a perfectly concentrated load is a singular function which reaches an infinite value directly under the load point. In reality, however, perfectly concentrated loads do not exist. As explained by Westegaard [2], the load tends to spread over a definite contact area. For analytical purposes the "concentrated load" is distributed over an even greater area than the actual contact area. The further distribution is usually considered by projecting it on to the neutral plane along 45° lines as shown in Figure 7.1 on page 74. Such a spreading of the load reduces the infinite curvature under the load to a finite value. The greater the distribution of the "concentrated load", the less sharp the maximum peak becomes at the load location. The contact area between the ball transfer of the loading shaft and the model slab is much smaller than that of a real wheel load and the actual slab.

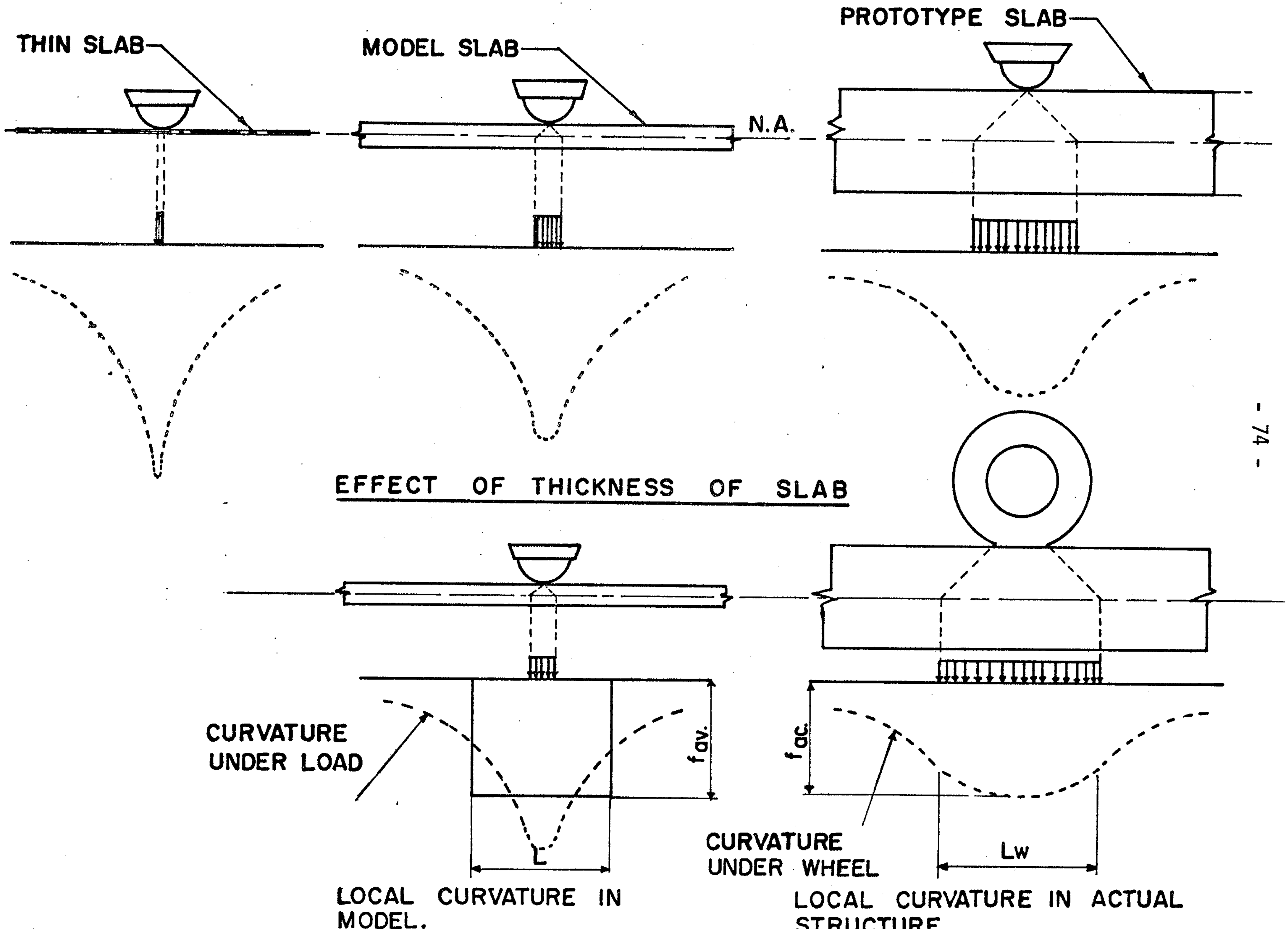
THIN SLAB
MODEL SLAB
PROTOTYPE SLAB
N.A.
EFFECT OF THICKNESS OF SLAB
CURVATURE UNDER LOAD
$f_{av.}$
L
LOCAL CURVATURE IN MODEL.
$f_{ac.}$
CURVATURE UNDER WHEEL
Lw
LOCAL CURVATURE IN ACTUAL STRUCTURE.

Fig. 7.1

Hence, the load spread area on the model is less than that on the actual slab as shown in Figure 7.1 on page 74. Therefore, the curvature due to a unit load on the model at the load point is greater than that occuring on the actual slab due to a unit wheel load. Although the curvature meter measures an average curvature, the difference between the measured curvature and the practical curvature on the actual slab tends to be negligibly small for practical purposes, with the model tending to give higher (conservative) value.

CHAPTER VIII

ANALYSIS OF RESULTS

8.1 Comparison of Influence Surfaces

In general, the contours of the influence surfaces follow a definite pattern for the corresponding reference points in all the three models (15° opening angle, 45° opening angle and continuous) except for the three reference points on the interior support of the continuous model. The spanwise θ-axis of the curvature meter was found to be more sensitive to the location of the load than the other two axes R and θ+45°. Hence, as it can be seen in Appendix II the contours of the I_θ influence surfaces are more closely spaced than those of I_R and $I_{\theta R}$. The I_θ influence coefficients are higher in magnitude compared to the corresponding I_R and $I_{\theta R}$ coefficients at all the loading grid points in all the models.

In the transverse curvature influence surfaces I_R (Figures I-2 and I-14) for the reference points A and D (Figure 4.1, page 37) of the single span models, large areas of anticlastic curvatures are noticeable unlike in the case of transverse influence surfaces for rectangular slabs and skew slabs as given by Pucher [13] and Rusch[6] respectively. This anticlastic curvature occurs because the slab behaves more like a cantilever in the transverse direction due to the fact that a considerable portion of the horizontally curved slab is unsupported outside the chord of the outer circular edge. This cantilevering effect becomes less for curved slabs of short spans and narrow opening angles that are more similar to the case of rectangular slabs. The transverse curvature influence surface I_R (Figure I-30) for the reference point D of the continuous model shows the diminution of this cantilever effect. In general, for each model the maximum ordinates of I_θ surfaces for the edge reference points B, C, E, F, G, H (Figure 4.1, page 37) are greater than those for the corresponding A and D, the center and the quarter span reference points respectively. The ratios of the corresponding I_θ values for the edge reference points and center reference points (e.g. $\frac{I^B_\theta}{I^A_\theta}$, $\frac{I^C_\theta}{I^A_\theta}$, $\frac{I^E_\theta}{I^D_\theta}$, $\frac{I^F_\theta}{I^D_\theta}$) are considerably greater than those ratios in the case of a rectangular slab (13)*. The above comparison shows that the free curved edges must be considered in detail in analysing and designing curved slabs.

(a) <u>The Center Reference Points (A) of Model 1 (15° opening angle) and Model 2 (45° opening angle)</u>

(a_1) <u>I_θ Influence Surface Figures I-1 and I-13</u>

The general shape of the influence contours and the maximum influence ordinates for both cases are practically the same, except that in model 2 the contours start to open out towards the outer

* The rectangular slabs considered for comparison were of span to width ratios of 2 and 3. The models tested had span to width ratio of 2.7.

edge. This occurs because as the opening angle is increased, the outer edge becomes more flexible and inner edge becomes more stiff even though both models have the same center span length. The above statement is clear from the fact that the influence ordinate at the mid point of the inner edge is reduced from a value of 0.605 for model 1 to a value of 0.538 for model 2 while the ordinate at the mid point of the outer edge is increased from 0.690 for model 1 to 0.804 for model 2. The influence ordinate at a similar point on a rectangular slab of 3 to 1 span/width ratio (close to that of the models) is 0.696 [13]. Although the maximum ordinates are practically the same, a close comparison reveals that the area covered by each contour of particular influence ordinate value is increased as the opening angle is increased. Therefore, the total influence volume under the influence surface for the reference point A of model 2 is greater than that of model 1. From the contour patterns it can be seen that at regions close to the inner edge the contours of particular influence values that are obtained for model 2 with a load close to the mid radial line occur for a load further away from the mid radial line in the case of model 1. The above shows that the inner edge of model 1 of smaller opening angle is less stiff than that of model 2.

When the influence surface I-1 and I-13 are compared with Pucher's influence chart 19 [13] for the center of a cantilever plate strip and with Molkenthin's influence chart 13 [14] for the center of a simply supported rectangular slab, it can be seen clearly that the inner edge becomes stiff and starts to act more like a fixed edge.

(a_2) <u>I_R Influence Surface Figures I-2 and I-14</u>

The shape of the contours for both cases appear to be similar to each other and to those that have been published for the rectangular slabs [(13)]. One striking difference between these influence surfaces and those for the rectangular slabs is that a smaller area is covered by the positive contours of these influence surfaces for the curved slabs compared to the other surfaces. The reason for the presence of more negative contours is that in the transverse direction the slab acts more like a cantilever as a result of the middle strip of the curved slab being stiffer than that of a rectangular slab. This extra stiffness is due to the supports being aligned in a radial direction instead of being parallel to each other and also due to the reason mentioned earlier in this chapter. To illustrate the above statement, an example of a plate strip having non-parallel supports is considered.

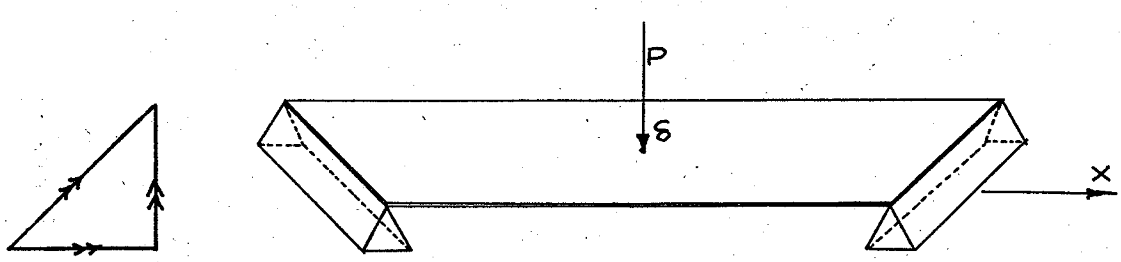

From the above shown moment vectors, it can be seen that the twisting and the bending moment at the support in the X direction are not zero unlike in the case of parallel supports. This illustrates the presence of twisting due to radially aligned supports.

If we consider a virtual displacement δ the total energy in the system can be given by the following equation.

$$P\delta = \Sigma E_B + \Sigma E_t$$

But if there is no twisting as in the case of parallel supports, the above equation will have only one term (i.e. ΣE_B) on the right hand side too. Therefore, for the above equation to be true, the magnitude of P has to be less. The above example illustrates the increase in stiffness due to radially aligned supports. Pucher's influence chart 18 (13) for the transverse curvature at the center of a clamped plate strip is useful for illustration of the above mentioned behaviour of the curved plate. This cantilevering action is also assisted by a distribution of twisting curvature across the slab especially close to the outer edge even though their influence ordinates are low. Some evidence of this cantilever effect can be seen in the influence surface Figures I-2 and I-14.

The anticlastic curvature influence ordinate at the mid point of the outer edge increases as the opening angle is increased.

(a$_3$) $I_{\theta R}$ Influence Surface Figures I-3 and I-15

The influence surface Figures I-3 and I-15 are practically the same. The low twisting influence coefficients compared to the two bending influence coefficients at the reference point A indicate that the load carrying capacity at this point relies mainly on the bending restraint of the slab. However, as mentioned earlier, a distribution of this twisting curvature can influence the stress distribution in the transverse direction. It also indicates that the principal curvatures and their directions remain close to those of I_θ and I_R as the load moves away from the symmetric radial line. From the two influence surface diagrams I-3 and I-15 it can be seen that the twisting curvature at the center point of the slab is not influenced by the opening angle unlike the bending curvatures I_θ and I_R.

(b) Reference Points (B) for Model 1 and Model 2

I_θ Influence Surface Figures I-4 and I-16

There is no considerable difference between these two influence surfaces and those that have been published for a similar point on a rectangular slab [13, 14]. However, when compared with each other, the stiffening of the inner edge as the opening angle is increased can be seen. In the case of model 2 the influence ordinate starts to change to low values rapidly as the load is moved towards the inner edge unlike in model 1. A similar effect can be observed in the rectangular plates as the span to width ratio is decreased [13, 14].

(c) Reference Points (C) for Model 1 and Model 2

I_θ Influence Surface Figures I-5 and I-17

The greater flexibility of the slab at regions close to the outer edge with increment of the opening angle is evident from these influence surfaces (I-5 and I-17) in the same way as described above but with an opposite action taking place in this case. The influence surface for model 1 is similar to that of a rectangular slab. In the case of model 2 the shape of the contours changes at regions close to the outer edge. This change in the contour patterns is due to the increased flexibility of the outer edge. Okamura and Matsui [34] obtained a similar set of contours for the mid point of an inner edge of a curved slab of 30° opening angle.

(d) Reference Points (D) for Model 1, Model 2 and the Continuous Model

(d_1) I_θ Influence Surface Figures I-6, I-18 and I-29

The surfaces I-6, I-18 and I-29 appear to be similar to I_θ influence surfaces discussed in (a_1) above except that they are not symmetrical due to the unsymmetrical location of the reference point. In all the three cases maximum ordinates are reduced, of course. When the influence surface I-29 for the continuous model is compared with the influence surfaces I-13 and I-18 for model 2, the reduction in maximum influence ordinate and the larger spacing of contours indicate that a considerable reduction in bending stresses can be obtained with the aid of an interior support. Some negative contours of low influence values are present in the adjacent panel due to continuity of the slab across the support.

(d_2) I_R Influence Surface Figures I-7, I-19 and I-30

The areas of anticlastic curvature contours are prominent in the influence surface Figures I-7 and I-19 for models 1 and 2 as in the case (a_2) above. As mentioned earlier, considerable areas of positive contours are present in the case of the continuous model as in the case of a rectangular slab. The short span length and the small opening angle permit the curved slab to behave in a manner similar to a rectangular slab. This similarity to a rectangular slab is the reason for the above behaviour.

(d_3) $I_{\theta R}$ Influence Surface Figures I-8, I-20 and I-31

The influence surface Figures I-8 and I-20 are similar to each other. The twisting curvatures at quarter points also seem to be small compared to I_θ's at those points as in the case of the center reference point. The general pattern of contours of Figure I-31 for the continuous model is similar to $I_{\theta R}$ influence surfaces I-3 and I-15 for the center point of model 1 and 2, although they are unsymmetrical due to the presence of the middle support. The contours on Figures I-8 and I-20 are also unsymmetrical as the reference points are located away from the symmetric radial line. From Figures

I-8 and I-20 it can be noticed the amount of negative twisting curvature contours for the reference point D is decreased with the increase of the opening angle.

(e) Reference Points (E) for Model 1, Model 2 and the Continuous Model I_θ Influence Figures I-9, I-21 and I-32

The Figures I-9, I-21 and I-32 appear to be similar to those discussed in (b) above except that the contours are unsymmetrical. In Figures I-9 and I-21 this again occurs because of unsymmetric reference point locations. In Figure I-32 the unsymmetry is due to the presence of a middle support. The support is also the cause for the negative contours that appear in the adjacent panel.

(f) Reference Points (F) for All Three Models I_θ Influence Surface Figures I-10, I-22 and I-33

The foregoing remarks apply equally to the comparison of all the three influence surface contours Figures I-10, I-22 and I-33. Again as in the case of the earlier discussed influence surface I-17 for the reference point C of model 2 the pattern of contours for I-22 also differs from those of I-10 and I-33.

(g) Reference Points (G) for All Three Models I_θ Influence Surface Figures I-11, I-23, and I-34

From Figures I-11, I-23 and I-34 it can be stated that the stresses at these corners are significant only when the load is near those corners. Also, it can be noticed that they are not influenced significantly by the other factors such as opening angle and number of spans.

(h) Reference Points (H) for All Three Models

I_θ Influence Figures I-12, I-24 and I-35

The foregoing remarks are true for the influence surface Figures I-12, I-24 and I-35 for the reference point H also.

(i) Reference Points (A), (B) and (C) on the Middle Support of the Continuous Model

I_θ Influence Surface Figures I-25, I-27 and I-28 and $I_{\theta R}$ Influence Surface Figure I-26

The influence surface Figures I-25, I-27, I-28 and I-26 represent the curvatures I_θ and $I_{\theta R}$ at the interior support. As one would expect, the negative contours are predominant in the case of I_θ's at A, B and C. There is no irregularity in $I_{\theta R}$ surface Figure I-26 presented. The only difference in form between these surfaces and those that have been published for moments and curvatures at supports involve a question of slab thickness. The influence surfaces presented in this work have been calculated for a slab of real thickness and hence the contours die down to a zero value at the reference point. Since the published influence surfaces are obtained for an infinitely thin slab, the contours merge in to a maximum value at the reference point. This question of infinitely thin slab in terms of real slab created an interesting problem for Kurata and

and Hatano [21]. The model results were compared with the "exact" solution results obtained from the computer programme developed along the lines of that of A. Coull and C. Das [36], and were found to be in good agreement. The differences for I_θ values at the reference points A and D were not more than 2.5 per cent. At the edge reference points B, C, E, F, G and H the differences for I_θ values were in the region of 4-5 per cent. However, these differences are acceptable since the model results were obtained for practical edge reference points close to the edges whereas the theoretical results were calculated for theoretical reference points exactly on the edges. The differences for the other curvature values I_R and $I_{\theta R}$ were in the range of 3-5 per cent. For a very few readings the differences were as high as 6-8 per cent, but these were limited to the cases where the recorded transducer readings were of small magnitudes. This consistency between the test and analytical results enhances the confidence in both the analytical and the test results.

CHAPTER IX

CONCLUSIONS AND SUGGESTIONS FOR FURTHER RESEARCH

The writer concludes that the material presented in this dissertation provides adequate evidence to show the reliability and accuracy of the prediction of structural behaviour by means of model analysis. A simple but precise experimental technique that can be used effectively in model analysis has been presented. The adapted method does not require an advanced knowledge of mathematics that is usually required in solving fourth order partial-differential plate equations nor does it require the aid of electronic computers as in the case of numerical analysis. The use of this experimental method is not limited to cases of simple (or simplified) boundary conditions as in the case considered in this work. It is more useful in analysing slabs of any shape, particularly of complex boundary conditions which defy the accurate analysis by mathematics. Versatile but unsophisticated nature of this experimental method makes it possible to be used even in a remote field design office. The simplicity of the apparatus required is the main advantage of this method. However, in using this technique one has to remember the compromises that are required to make between the gauge length of the curvature meter, the span and the thickness of the model and the magnitude of the loads so as to obtain reliable results.

The validity of the application of model results to prototype slabs has been discussed. The limits and the method of incorporating any change in Poisson's ratio between the model material and the prototype material have also been included and have been shown to pose no major difficulties. The model results have been presented in the forms of contour influence surfaces useful as a permanent record which can be used as aids in bridge designing as well as in checking existing curved slab bridges for abnormally heavy loads, that may cross the bridge from time to time.

Most of the influence surfaces prepared illustrate the substantially greater flexibility of the longer outer edge compared to that of the inner edge. It is shown that the inner edge becomes stiff and starts to act more like a fixed edge with the increase of the opening angle. The presence of large areas of anticlastic curvatures is a notable difference in behaviour of these curved slabs compared to rectangular slabs or skewed slabs. These suggest that a well distributed torsional action is present in curved slabs unlike in the case of a rectangular slab. However, this prediction could only be conformed by further detailed studies at more locations closer to the outer edge and to the inner edge. In general, the maximum curvatures occur at the free edge of the slab. The considerable reduction in maximum curvature at the center and the larger spacing of the contours due to the presence of an interior support provide some valuable data to the designer. The influence surfaces at A, B and C for the support moments indicate that there is a considerable difference among these negative moments even for a uniformly distributed load over both spans. This unevenly distributed negative moments at the interior support in turn indicate that the reactions on the supports are not evenly distributed. This leads to a bearing problem which has to be studied from the measurement of support reactions.

A highly precise experimental technique that could be used to check the reliability of various analytical approaches has been presented. This experiment also could be used to find out the limits of the approximations that has to be incorporated in using these analytical methods in order to obtain data accurate enough for practical purposes. For instance in the case of a finite element programme, the shape and the size of the mesh pattern that is required for an optimum design could be found very easily and quickly using this model technique as a basis of comparison.

A study of the influence of number of bearings and the spacing of them on the bending and torsional curvatures is recommended for further studies along with the following. It is desirable to study further the effect of change of opening angle for single span, two-span and three-span curved bridges. The influence surfaces of the above mentioned structures along with the other already published surfaces will provide invaluable design data for the bridge engineer to have in hand when he is called upon to design bridges. However, the writer recommends the following improvements to the technique used above.

(1) An automatic influence surface plotter should be employed to cut down the time required for the tedious process of plotting influence surfaces by hand. At the same time it would help in selecting better reference points (more critical) during the experiment itself since the surfaces for already considered points are in hand.

(2) A thick slab and hence a larger model that allows the use of heavier loads should be used, so as to obtain considerably high readings in all the three transducers. A material of high modulus of elasticity is suitable for larger models since in a stiffer model the deflections due to its self-weight and other dead loads are small. Hence, a greater portion of the allowable deflections could be obtained from the external loading alone. Glass, micro-concrete, sand filled epoxy are few examples of the suitable model materials.

(3) The use of spring loaded transducers are recommended since with these type of transducers the curvature meter could be attached to the underside of the model. Hence, the load could be applied from top even at locations close to the reference point.

The curvature meter so designed is a simple but precise apparatus that is most suitable for the influence surface plotting. In turn the availability of influence surfaces for variety of standard shapes of slabs is a valuable aid to the designer for preliminary design or for special load analysis.

REFERENCES

(1) Jaeger, L. G., Pergamon Press (1964), "Elementary Theory of Elastic Plates".

(2) Westergaard, H. M., "Computation of Stresses in Bridge Slabs due to Wheel Loads", Public Roads, Volume II, No. 1, March, 1930.

(3) Rowe, R. E. and Base, G. D., "Model Analysis and Testing as a Design Tool", Proc. I. C. E., V. 33, Feb., 1966.

(4) Rowe, R. E. and Best, B. C., "The Use of Model Analysis and Testing in Bridge Design", Preliminary Publication, Seventh Congress of the I. A. B. S. E., Rio de Janeiro, 1964, p. 115-121.

(5) Andrä, W., Leonhardt, F., and Krieger, R., "Vereinfachtes Verfahren zur Messung von Momenteneinflussflächen bei Platten", Der baningenieur, V. 33, n. 11. Nov. 1958. p. 407-414.

(6) Rüsch, H. and Hergenröder, A. "Einflusfelder der Momente Schiefwinkliger Platten", Third edition 1969 with an English translation, Werner-Verlag-Düsseldorf, 19 pp. and 174 charts.

(7) Mehmel, A. and Weise, H., "A Contribution on the Structural Behaviour of Skew Slabs Using a Model", English Translation, N. R. C. of Canada, Technical Translation 1128.

(8) Mehmel, A. and Weise, H., "Model Investigation of Skew Slabs on Elastically Yielding Point Supports", Cement and Concrete Association Library Translation No. 123, 1965.

(9) Andrä, W. and Leonhardt, F., "Influence of the Spacing of the Bearings on Bending Moments and Reactions in Single-Span Skew Slabs", Cement and Concrete Association Library Translation No. 99, 1960.

(10) Cheung, Y. K. "The Analysis of Cylindrical Orthotropic Curved Bridge Decks", International Association for Bridge and Structural Engineering Publications, Vol. 29, Part II, 1969, pp 41-52.

(11) Meyer, C. and Scordelis, A. C., "Analysis of Curved Folded Plate Structures", Journal of the Structural Division, ASCE, Vol 97, No. ST-10, Proc. Paper 8434, Oct, 1971, pp 2459-2480.

(12) Buragohain, D. N., "Discrete Analysis of Cylindrical Orthotropic Curved Bridge Decks", International Association for Bridge and Structural Engineering Publications, Vol 32, Part 1, 1972, pp 37-47.

(13) Pucher, Adolf, "Influence Surfaces of Orthogonal Anistropic Plates", Springer-Verlag, Vienna and New York, 1964 (3rd ed.) 35 pp. and 93 charts.

(14) Molkenthin, A., "Influence Surfaces of Two-Span Continuous Plates with Free Longitudinal Edges", Springer-Verlag, Heidelberg and New York 1971, 44 pp. and 165 charts.

(15) Olsen, H. and Reinitzhuber, F. "Die Zweiseitig Gelagerte Platte", Verlag W. Erust & Sohn, Berlin, 1959, (3rd ed.) 113 pp.

(16) Krug, S. and Stein, P., "Influence Surfaces of Orthogonal Anisotropic Plates". Springer-Verlag, Berlin, 1963, 33 pp. and 193 charts.

(17) Homberg, H. and Marx, W. R., "Schiefe Stäbe und Platten", Werner Verlag, Düsseldorf, 1958, 324 pp.

(18) Aneja, I. K. and Roll, F., "Experimental and Analytical Investigation of a Horizontally Curved Box-Beam Highway Bridge Model", Second International Symposium on Concrete Bridge Design, ACI Publication SP-26.

(19) Knowles, W. L. C. and Huggins, M. W., "Model Study of a 60-Degree Three-Span Skewed Bridge", Department of Civil Engineering, University of Toronto, March 1965, (O. J. H. R. P. Rep 35).

(20) Aneja, I. K. and Roll, F., "Model Tests of Box-Beam Highway Bridge with Cantilevered Deck Slabs", Conference Preprint No. 395 A S C E, Transportation Engineering Conference, Philadelphia, Pa., Oct. 17-21, 1966.

(21) Kurata, M. and Hatano, S. "The Influence Surface for the Indeterminate Clamping Moment of Slab-Bridge-Type Skewed Plates", I. A. B. S. E. Publications, Vol. 24, 1964, p. 101-112.

(22) Chen, T. Y., Siess, C. P. and Newmark, N. M., "Studies in Slab and Beam Highway Bridges, Part VI. Moments in Simply Supported Skew I-Beam Bridges", University of Illinois Engineering, Exp. Sta., Bull, 439, Jan. 1957, 72 pp.

(23) Kawai, T. and Thürlimann, B., "Influence Surfaces for Moments in Slabs Continuous over Flexible Cross Beams", I. A. B. S. E. Publications, Vol. 17, 1957, p 117-138.

(24) Timoshenko, S. and Woinowsky-Krieger, S., "Theory of Plates and Shells", McGraw-Hill, New York, 1959.

(25) Ligtenberg, F. K., "The Moire Method", Proceedings of the S. E. S. A., Vol. 12 No. 2, 1955, p. 83-98.

(26) Holister, G. S., "Experimental Stress Analysis", Cambridge, University Press 1967, 322 pp.

(27) Yeginobali, A., "Continuous Skewed Slabs", Ohio State Univ. Eng'g. Exp. Sta., Bul. 178, Nov. 1959.

(28) Schmidt, E., "Modellversuche zur Bemessung von Baukonstrucktioneu", Schweizerische Banzeitung, 1949.

(29) Weigler, H. and Weise, H., "Modellstatisches Verfahren zur Aufuahine von Einflussflachen von Platten", Beton und Stahlbetoubau, May, 1959.

(30) Kennedy, J. B. and Tamberg, K. G., "Problems of Skew in Concrete Bridge Design", Dept. of Highways, Ontario, Report No. RR 144, March 1969.

(31) Robinson, K. E., "The Effect of Skew on the Behaviour of Simply Supported Bridge Slabs", Cement and Concrete Assoc., Tech, Rep. TRB/271, July, 1957.

(32) Balas, J. and Hanuska, A., "Der Einfluss der Querdehuungszahl auf den Spannungszustand einer 45° schiefen Platte".

(33) Lansdown, A. M., "The Use of Influence Surfaces in Assessing Moments and Stresses in Short Span Bridges Subjected to Abnormally Heavy Loads", Trans. E. I. C. V., May, 1966.

(34) Okamura, H. and Matsui, K., "Automatic Recording Equipments for the Model Analysis of the Influence Surfaces of Plate", Proc. of the Symp. on the New Ideas in Structural Design, J. S. C. E., Dec., 1963.

(35) Engineering Digest, Vol. 20, No. 5, May 1974, p. 7.

(36) Coull, A. and Das, P. C., "Analysis of Curved Bridge Decks", Proc. I. C. E., Vol. 37, May 1967, p. 75-85.

APPENDIX I

1.1 The Writer's Inverse Approach

A qualitative idea of each individual error, that the writer feels could be present in the actual testing, is obtained by checking the curvature meter analytically on an assumed worst case as mentioned in Chapter I. This so called "inverse approach" is given below.

A deflection equal to the half the thickness of the plate is considered as the worst case. The required relative deflection f is also assumed to be equal to the maximum allowable deflection although for the considered worst case, a relative deflection between any two points within the plate will always be much less.

(a) Error Due to Tilt of the Meter

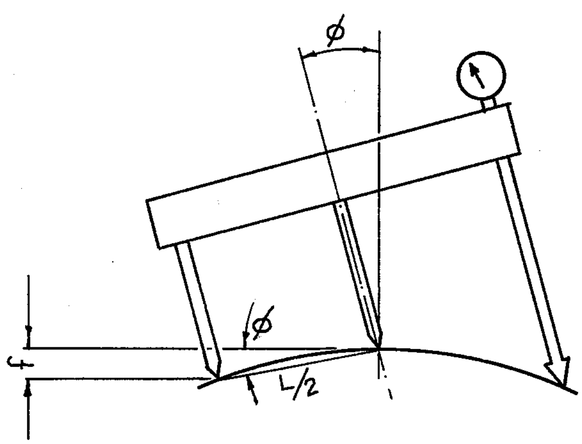

Fig. A

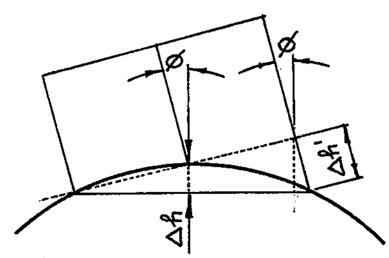

Fig. B

From the above Figure A, it can be seen that

$$\sin \phi = \frac{f}{L/2} \quad . \quad \text{For the "worst case" conditions } L=1.5'', \ f=0.0625''$$

and hence, $\sin \phi = \dfrac{0.0625}{1.5} \times 2 = 0.0833$

or,

$$\phi = 4° \ 48'$$

If the additional rotation due to the movement of the outer leg (that is shown in the next paragraph to be equal to second order quantity of θ) is neglected, as shown in Figure B above the transducer will register a reading $\Delta h'$ instead of the true reading $2\Delta h$ due to the rotation ϕ.

$$\Delta h' = \frac{2\Delta h}{\cos \phi}$$

$$= \frac{2\Delta h}{\cos 4° \ 48'}$$

$$= \frac{2\Delta h}{(0.99649)}$$

$$= 2\Delta h \ (1.00352)$$

Therefore, maximum possible error due to tilt of the meter is 0.35 per cent.

(b) <u>Error Due to the Additional Rotation of the Meter</u>

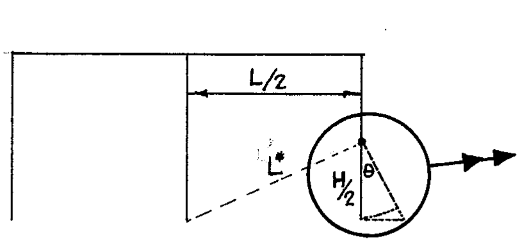

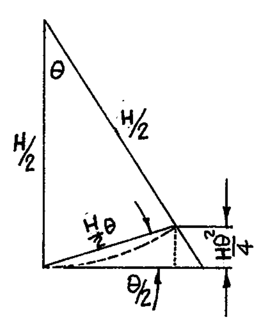

Let α be the additional rotation of the meter due to the movement of the leg as a result of elongation (or contraction) of the surface of the plate.

$$\alpha L^* = \frac{H\theta^2}{4}$$

but

$$L^* = \frac{1}{2}\sqrt{H^2 + L^2}$$

Hence, $$\alpha\sqrt{H^2 + L^2} = \frac{H\theta^2}{2}$$

Since $\sqrt{H^2 + L^2} > H$, it follows that

$$\alpha \ll \theta^2 .$$

It is shown that the additional rotation α is a second order quantity of θ. θ can be calculated as follows,

$$\text{elongation} \quad e = \epsilon \frac{L}{2}$$

$$\text{and} \quad \epsilon = K\, h/2$$

$$\text{where,} \quad K = \frac{8f}{L^2} \qquad f = 0.0625'', \; L = 1.5''$$

and $h = 0.125''$

$$\text{hence} \quad \epsilon = \frac{8 \times 0.0625}{(1.5)^2} \times \frac{0.125}{2}$$

$$= 0.0139$$

$$\text{and} \quad e = 0.0139 \times \frac{1.5}{2}$$

$$= 0.0104$$

$$e = \frac{H\theta}{2}$$

Since $H = 1.0''$

and $\theta = 0.0208$ radians

Therefore, $\alpha < \theta^2 < 0.000433$ radians

or, $< 0.025°$

It can be seen that α is insignificant compared to ϕ.

(c) <u>Error Due to Shifting of Outer Leg</u>

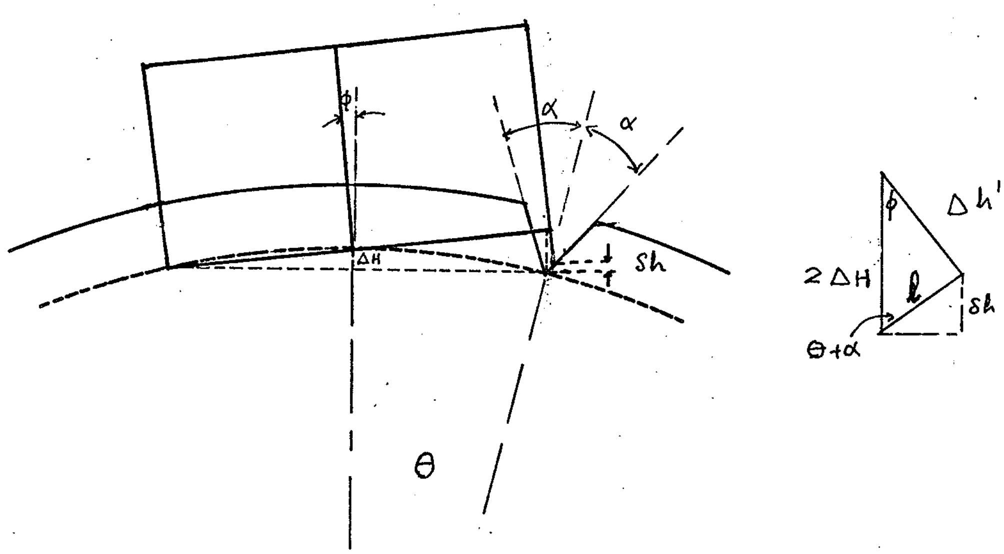

If the bottom tip of the outer leg sits on the wall of the conical shaped punch mark instead of being at the vertex as shown in the above figure, it will affect the transducer reading. The magnitude of the error and the correct size of the punch mark can be obtained as follows. For convenience the outer leg is considered as made of one solid piece. The angle subtended by the chord length at the center of radiai is assumed to be 2θ and the angle of the conical shaped punch mark is taken as 2α.

Therefore,

$$\sin\theta = \frac{L/2 \cos\phi}{R}$$

$$\delta h = 1 \sin[90 - (\theta + \alpha)]$$

$$= 1 \cos(\theta + \alpha)$$

From the above figure,

$$\frac{1}{\sin\phi} = \frac{2\Delta H}{\sin[180 - (\phi + \theta + \alpha)]}$$

or, $$1 = \frac{2\Delta H \sin\phi}{\sin(\phi + \theta + \alpha)}$$

hence, $$\delta h = \frac{2\Delta H \sin\phi \cos(\theta + \alpha)}{\sin(\phi + \theta + \alpha)}$$ For the worst case condition

$$R = \frac{L^2}{8f}, \quad f = 0.0625, \quad L = 1.5, \quad \phi = 4° \, 48'$$

giving $$\sin\theta = L/2 \cos\phi \times \frac{8f}{L^2}$$

$$= \frac{\cos 4° \, 48'}{2} \times \frac{8 \times 0.0625}{1.5}$$

$$= 0.1661$$

or,

$$\theta = 9° \, 36'$$

If $\alpha = 45°$

$$\delta h = 2\Delta H \frac{\sin 4° \, 48' \cos(9° \, 36' + 45°)}{\sin(4° \, 48' + 9° \, 36' + 45°)}$$

$$= 2\Delta H \frac{\sin 4° \, 48' \cos 54° \, 36'}{\sin 59° \, 24'}$$

$$= 2\Delta H \, . \, 0.051$$

It can be seen that δh is significant compared to the transducer reading $2\Delta H$. Therefore, it is necessary to take precautions to see that the bottom tip of the outer leg does not get shifted on to the wall of the conical shaped punch mark. However, this occurs very rarely since both outer legs have flexible bottom parts.

1.2 The Effect of the Gauge Length

An analytical approximation to the effect of gauge length on the curvatures is obtained as follows. Let us assume that the curvature meter is used to measure the curvature on a simple beam subjected to a load P at the center.

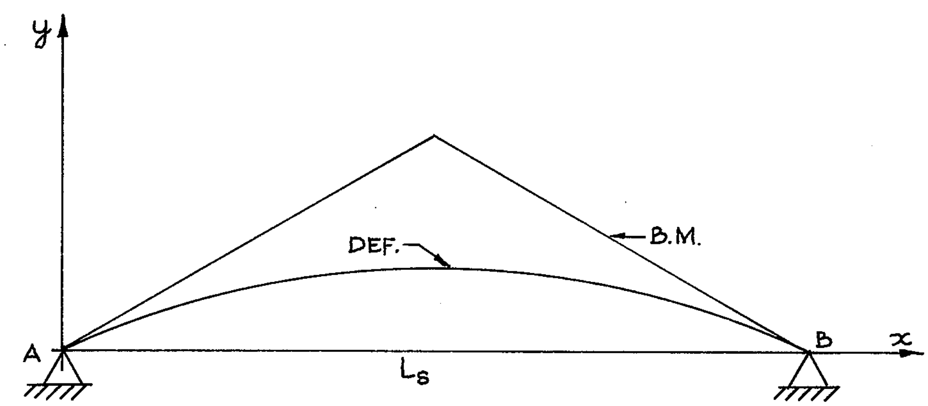

The deflection profile of a simply supported beam loaded at center is represented by:

$$Y = -\frac{P}{EI}\left\{\frac{x^3}{12} - \frac{1}{2}\left[x - \frac{L_s}{2}\right]^3 - \frac{1}{16}L_s^2\, x\right\} \qquad [D]$$

Then let the curvature meter be positioned on the beam and let

Y_c = beam deflection at the center leg = $\frac{PL_s^3}{48EI}$

Y_o = beam deflection at the outer leg

Y_t = beam deflection at the transducer

(A) Suppose the curvature meter is used to measure the curvature at the center of the beam. In this case to employ the curvature meter principle, only Y_c and Y_o are required.

<u>For a gauge length of $L_s/20$</u>

Distance to the outer leg from end A $= \frac{L_s}{2} - \frac{L_s}{40} = \frac{19\,L_s}{40}$

$$Y_o = -\frac{P}{EI}\left[\frac{1}{12}\left(\frac{19L_s}{40}\right)^3 - \frac{L_s^2}{16} \times \frac{19L_s}{40}\right]$$

since
$$f = Y_c - Y_o$$
$$= \frac{P}{EI}\left[\frac{L_s^3}{48} + \frac{1}{12}\left(\frac{19}{40}L_s\right)^3 - \frac{19L_s^3}{640}\right]$$
$$= \frac{PL_s^3}{EI}[0.00007682]$$

Hence,
$$K_c = \frac{8f}{L^2} = \frac{8}{\left(\frac{L_s}{20}\right)^2}\frac{PL_s^3}{EI}[0.00007682]$$
$$= 0.2458\frac{PL_s}{EI}$$

But the true curvature at the center from beam theory $= 0.25\frac{PL_s}{EI}$.

The difference between the two curvature values is -1.67 per cent. Similarly for gauge lengths of $\frac{L_s}{10}$ and $\frac{L_s}{5}$, differences of -3.33 per cent and -6.66 per cent are obtained respectively.

---

* The square bracket term in the Equation D is neglected when $x < L_s/2$.

(B) Suppose the curvature meter is used to measure the curvature at the quarter point.

<u>For a gauge length of $\frac{L_s}{20}$</u>

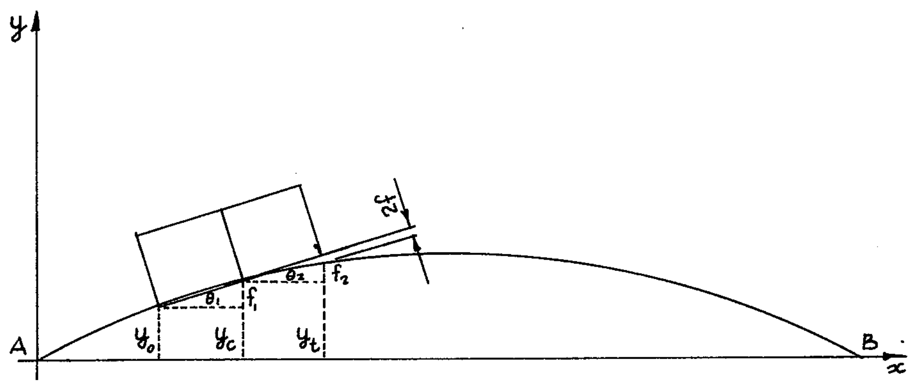

Distance to the outer leg from end A $= \frac{L_s}{4} - \frac{L_s}{40} = \frac{9L_s}{40}$

$$Y_c = -\frac{P}{EI}\left[\frac{L_s^2}{12 \times 64} - \frac{L_s^2}{16} \times \frac{L_s}{4}\right]$$

$$= \frac{11}{768}\frac{PL_s^3}{EI}$$

and

$$f_1 = Y_c - Y_o = \frac{P}{EI}\left[\frac{11L_s^3}{768} + \frac{1}{12}\left(\frac{9L_s}{40}\right)^3 - \frac{L_s^2}{16} \times \frac{9L_s}{40}\right]$$

$$= \frac{PL_s^3}{EI}[0.00121]$$

Distance to the transducer from end A $= \frac{L_s}{4} + \frac{L_s}{40} = \frac{11L_s}{40}$

similarly, $f_2 = Y_t - Y_c$

$$= -\frac{P}{EI}\left[\frac{1}{12}\left(\frac{11L_s}{40}\right)^3 - \frac{L_s^2}{16} \times \frac{11L_s}{40} + \frac{11}{768} L_s^3\right]$$

$$= \frac{PL_s^{\,3}}{EI}[0.0011317]$$

hence, $$\theta_1 = \frac{0.00121\ PL_s^{\,3}}{EI} \Big/ \frac{L_s}{40}$$

$$= \frac{0.0484\ PL_s^{\,2}}{EI}$$

and

$$\theta_2 = \frac{0.0011317\ PL_s^{\,3}}{EI} \Big/ \frac{L_s}{40}$$

$$= \frac{0.045268\ PL_s^{\,2}}{EI}$$

therefore, $$2f = (\theta_1 - \theta_2)\ L_s/40 = \frac{0.003132\ PL_s^{\,2}}{EI} \times \frac{L_s}{40}$$

giving $$K = \frac{8f}{l^2} = 4 \times \frac{0.003132}{(L_s/20)^2} \times \frac{PL_s^{\,2}}{EI} \times \frac{L_s}{40}$$

$$= 0.12528\ \frac{PL_s}{EI}$$

But the true curvature at the quarter point from beam theory = $0.125\ \frac{PL_s}{EI}$

Therefore, the difference is 0.24 per cent for a gauge length of $\frac{L_s}{20}$.

Similarly, differences of 0.0032 per cent and zero per cent are obtained for gauge lengths of $\frac{L_s}{10}$ and $\frac{L_s}{5}$ respectively.

APPENDIX II

2.1 Tables of Influence Coefficients.

(a) Influence Coefficients I_θ - Model 1 (15° Opening Angle)

Load Points	Reference Points On 15° Opening Angle Model							
	A	B	C	D	E	F	G	H
a	0.690	1.555	0.553	0.383	0.387	0.356	0.087	0.094
a_1	-	1.186	-	-	-	-	-	-
a_2	-	1.017	-	-	-	-	-	-
a_3	-	1.085	-	-	-	-	-	-
a_4	-	0.861	-	-	-	-	-	-
a_5	-	0.819	-	-	-	-	-	-
a_6	0.643	0.747	-	-	-	-	-	-
a_7	-	0.630	-	-	0.541	-	-	-
b	0.675	0.839	0.598	0.361	0.379	0.357	0.081	0.091
c	0.814	0.643	0.670	0.350	0.359	0.361	0.080	0.086
c_1	0.730	-	-	-	-	-	-	-
c_2	0.764	-	-	-	-	-	-	-
c_3	0.750	-	-	-	-	-	-	-
c_4	0.695	-	-	-	-	-	-	-
c_5	0.670	-	-	-	-	-	-	-
c_6	0.627	-	-	-	-	-	-	-
c_7	0.608	-	-	-	-	-	-	-
c_8	0.610	-	-	-	-	-	-	-
c_9	0.608	-	0.754	-	-	-	-	-
c_{10}	0.517	-	-	0.431	-	-	-	-
c_{11}	0.492	-	-	0.418	-	-	-	-
d	0.639	0.534	0.834	0.346	0.333	0.365	0.077	0.075
e	0.605	0.471	1.475	0.352	0.304	0.359	0.074	0.069
e_1	-	-	1.193	-	-	-	-	-
e_2	-	-	1.030	-	-	-	-	-
e_3	-	-	1.088	-	-	-	-	-
e_4	-	-	0.841	-	-	-	-	-
e_5	-	-	0.821	-	-	-	-	-
e_6	-	-	0.629	-	-	0.523	-	-

(Continued)

Load Points	Reference Points On 15° Opening Angle Model							
	A	B	C	D	E	F	G	H
f	0.584	0.641	0.499	0.489	0.549	0.396	0.114	0.114
g	0.542	0.614	0.529	0.453	0.522	0.407	0.112	0.113
h	0.498	0.539	0.567	0.428	0.453	0.451	0.106	0.110
i	0.503	0.469	0.621	0.433	0.387	0.511	0.095	0.098
j	0.517	0.426	0.630	0.436	0.337	0.526	0.086	0.087
k	0.393	0.384	0.365	0.493	1.327	0.358	0.156	0.122
k_1	-	-	-	-	0.712	-	-	-
k_2	-	-	-	-	0.679	-	-	-
k_3	-	-	-	0.4942	0.608	-	-	-
k_4	-	-	-	-	-	-	-	-
k_5	-	-	-	-	1.000	-	-	-
k_6	-	-	-	-	0.863	-	-	-
k_7	-	-	-	-	-	-	-	-
k_8	-	-	-	-	0.600	-	-	-
k_9	-	-	-	-	0.588	-	-	-
k_{10}	-	-	-	0.398	0.511	-	-	-
k_{11}	-	-	-	-	0.354	-	-	-
l	0.364	0.382	0.372	0.4944	0.679	0.398	0.152	0.124
m	0.347	0.364	0.383	0.610	0.461	0.477	0.130	0.138
m_1	-	-	-	0.481	-	-	-	-
m_2	-	-	-	0.460	-	-	-	-
m_3	-	-	-	0.463	-	-	-	-
m_4	-	-	-	0.459	-	0.585	-	-
m_5	-	-	-	0.508	-	-	-	-
m_6	-	-	-	0.533	-	-	-	-
m_7	-	-	-	0.558	-	-	-	-
m_8	-	-	-	0.555	-	-	-	-
m_9	-	-	-	0.523	-	-	-	-
m_{10}	-	-	-	0.472	-	-	-	-

(Continued)

Load Points	Reference Points On 15° Opening Angle Model							
	A	B	C	D	E	F	G	H
m_{11}	-	-	-	0.388	-	-	-	-
m_{12}	-	-	-	0.371	-	-	-	-
m_{13}	-	-	-	0.378	-	-	-	-
m_{14}	-	-	-	0.372	-	0.487	-	-
m_{15}	-	-	-	0.246	-	-	-	-
m_{16}	-	-	-	0.240	-	-	-	-
n	0.344	0.334	0.384	0.476	0.361	0.652	0.107	0.139
o	0.351	0.304	0.379	0.439	0.305	1.235	0.091	0.130
o_1	-	-	-	-	-	0.656	-	-
o_2	-	-	-	-	-	0.659	-	-
o_3	-	-	-	-	-	0.876	-	-
o_4	-	-	-	-	-	0.781	-	-
o_5	-	-	-	-	-	0.925	-	-
o_6	-	-	-	-	-	0.841	-	-
o_7	-	-	-	--	-	0.621	-	-
o_8	-	-	-	-	-	0.558	-	-
o_9	-	-	-	-	-	0.344	-	-
p	0.195	0.185	0.189	0.294	0.361	0.207	0.320	0.085
q	0.183	0.184	0.189	0.270	0.338	0.232	0.232	0.096
r	0.176	0.174	0.190	0.244	0.277	0.272	0.131	0.139
s	0.173	0.168	0.188	0.251	0.220	0.325	0.082	0.221
t	0.174	0.158	0.180	0.263	0.183	0.349	0.063	0.297
u	-	-	-	0.150	0.166	0.105	0.926	0.045
v	-	-	-	0.132	0.159	0.116	0.205	0.054
w	-	-	-	0.116	0.134	0.131	0.087	0.087
x	-	-	-	0.123	0.109	0.154	0.049	0.193
y	-	-	-	0.132	0.094	0.158	0.035	0.922
f'	-	-	-	0.281	0.272	0.266	0.050	0.075
g'	-	-	-	0.264	0.268	0.265	0.062	0.069

(Continued)

Load Points	Reference Points On 15° Opening Angle Model							
	A	B	C	D	E	F	G	H
h'	-	-	-	0.259	0.262	0.263	0.062	0.060
i'	-	-	-	0.254	0.252	0.260	0.059	0.057
j'	-	-	-	0.255	0.237	0.249	0.056	0.052
k'	-	-	-	0.1826	0.185	0.178	0.043	0.049
l'	-	-	-	0.177	0.179	0.173	0.042	0.046
m'	-	-	-	0.170	0.174	0.170	0.040	0.043
n'	-	-	-	0.169	0.067	0.168	0.0393	0.036
o'	-	-	-	0.168	0.162	0.165	0.0386	0.032
p'	-	-	-	0.094	0.088	0.091	-	-
q'	-	-	-	0.0884	0.087	0.089	-	-
r'	-	-	-	0.0852	0.086	0.084	-	-
s'	-	-	-	0.0852	0.083	0.082	-	-
t'	-	-	-	0.0848	0.081	0.080	-	-

(b) Influence Coefficients I_R - Model 1 (15° Opening Angle)

Load Points	Reference Points A	Reference Points D
a	-0.293	-0.129
a_6	-0.162	-
b	-0.182	-0.090
c	+0.158	-0.071
c_1	-0.110	-
c_2	-0.047	-
c_3	-0.041	-
c_4	-0.099	-
c_5	0.0	-
c_6	-0.094	-
c_7	-0.031	-
c_8	-0.082	-
c_9	-0.141	-
c_{10}	-0.097	-0.077
c_{11}	-0.089	-0.067
d	-0.157	-0.079
e	-0.243	-0.111
f	-0.231	-0.182
g	-0.142	-0.101
h	-0.075	-0.043
i	-0.123	-0.087
j	-0.200	-0.150
k	-0.145	-0.211
k_3	-	-0.128
k_{10}	-	-0.093
l	-0.100	-0.113
m	-0.079	+0.101
m_1	-	-0.058
m_2	-	-0.011
m_3	-	-0.048
m_4	-	-0.102
m_5	-	+0.033
m_6	-	-0.054
m_7	-	+0.009
m_8	-	+0.013
m_9	-	-0.041
m_{10}	-	-0.049
m_{11}	-	-0.035
m_{12}	-	+0.017
m_{13}	-	-0.022
m_{14}	-	-0.076
m_{15}	-	-0.026
m_{16}	-	-0.021
n	-0.090	-0.095
o	-0.122	-0.172
p	-0.069	-0.119
q	-0.052	-0.052
r	-0.044	-0.006
s	-0.046	-0.044
t	-0.060	-0.100
u	-	-0.059
v	-	-0.026
w	-	-0.007
x	-	-0.021
y	-	-0.049
f'	-	-0.089
g'	-	-0.071
h'	-	-0.062
i'	-	-0.063
j'	-	-0.076
k'	-	-0.055
l'	-	-0.049
m'	-	-0.043
n'	-	-0.046
o'	-	-0.049
p'	-	-0.026
q'	-	-0.025
r'	-	-0.024
s'	-	-0.0247
t'	-	-0.0251

(c) Influence Coefficients I_θ - Model 2 (45° Opening Angle)

Load Points	Reference Points	
	A	D
a	0.0	-0.139
a_6	+0.0344	-
b	0.0	-0.082
c	0.0	-0.020
c_1	0.0	-
c_2	0.0	-
c_3	0.0	-
c_4	0.0	-
c_5	+0.001	-
c_6	+0.032	-
c_7	+0.002	-
c_8	-0.026	-
c_9	-0.028	-
c_{10}	+0.027	-0.059
c_{11}	-0.021	+0.020
d	0.0	+0.040
e	0.0	+0.092
f	+0.060	-0.140
g	+0.042	-0.090
h	+0.003	-0.019
i	-0.033	+0.049
j	-0.048	+0.095
k	+0.059	-0.077
k_3	-	-0.081
k_{10}	-	-0.008
l	+0.034	-0.045
m	+0.004	-0.014
m_1	-	-0.062
m_2	-	-0.018

Load Points	Reference Points	
	A	D
m_3	-	+0.028
m_4	-	+0.046
m_5	-	-0.015
m_6	-	-0.029
m_7	-	-0.021
m_8	-	-0.006
m_9	-	+0.002
m_{10}	-	-0.012
m_{11}	-	+0.004
m_{12}	-	-0.010
m_{13}	-	-0.023
m_{14}	-	+0.010
m_{15}	-	+0.002
m_{16}	-	-0.014
n	-0.025	+0.018
o	-0.047	+0.048
p	+0.033	-0.011
q	+0.018	+0.001
r	+0.003	-0.007
s	-0.012	-0.013
t	-0.026	+0.002
u	-	-0.001
v	-	+0.002
w	-	-0.003
x	-	-0.007
y	-	-0.002
f'	-0.060	-0.112
g'	-0.042	-0.065
h'	-0.003	-0.018

Load Points	Reference Points	
	A	D
i'	+0.033	+0.028
j'	+0.048	+0.072
k'	-0.059	-0.077
l'	-0.034	-0.045
m'	-0.004	-0.014
n'	+0.025	+0.018
o'	+0.047	+0.048
p'	-0.033	-0.039
q'	-0.018	-0.023
r'	-0.003	-0.007
s'	+0.012	+0.009
t'	+0.026	+0.024

(d) Influence Coefficients I_θ - Model 2 (45° Opening Angle)

Load Points	Reference Points							
	A	B	C	D	E	F	G	H
a	0.804	1.593	0.671	0.453	0.420	0.420	0.105	0.084
a_1	-	1.260	-	-	-	-	-	-
a_2	-	1.087	-	-	-	-	-	-
a_3	-	1.085	-	-	-	-	-	-
a_4	-	0.853	-	-	-	-	-	-
a_5	-	0.824	-	-	-	-	-	-
a_6	0.698	0.747	-	-	-	-	-	-
a_7	-	0.624	-	-	0.568	-	-	-
b	0.769	0.854	0.666	0.409	0.404	0.405	0.100	0.085
c	0.842	0.640	0.722	0.371	0.372	0.399	0.095	0.082
c_1	0.773	-	-	-	-	-	-	-
c_2	0.795	-	-	-	-	-	-	-
c_3	0.767	-	-	-	-	-	-	-
c_4	0.709	-	-	-	-	-	-	-
c_5	0.706	-	-	-	-	-	-	-
c_6	0.667	-	-	-	-	-	-	-
c_7	0.626	-	-	-	-	-	-	-
c_8	0.614	-	-	-	-	-	-	-
c_9	0.581	-	0.761	-	-	-	-	-
c_{10}	0.563	-	-	0.468	-	-	-	-
c_{11}	0.515	-	-	0.429	-	-	-	-
d	0.634	0.504	0.834	0.347	0.327	0.384	0.084	0.078
e	0.538	0.399	1.481	0.332	0.268	0.371	0.071	0.077
e_1	-	-	1.151	-	-	-	-	-
e_2	-	-	0.995	-	-	-	-	-
e_3	-	-	1.076	-	-	-	-	-
e_4	-	-	0.864	-	-	-	-	-
e_5	-	-	0.815	-	-	-	-	-
e_6	-	-	0.637	-	-	0.513	-	-

(Continued)

Load Points	Reference Points							
	A	B	C	D	E	F	G	H
f	0.659	0.637	0.600	0.569	0.582	0.468	0.133	0.108
g	0.599	0.615	0.592	0.507	0.545	0.467	0.127	0.106
h	0.536	0.526	0.611	0.446	0.463	0.476	0.116	0.105
i	0.500	0.438	0.634	0.428	0.378	0.508	0.103	0.104
j	0.466	0.361	0.622	0.399	0.302	0.511	0.085	0.102
k	0.446	0.387	0.437	0.578	1.383	0.422	0.173	0.114
k_1	-	-	-	-	0.740	-	-	-
k_2	-	-	-	-	0.703	-	-	-
k_3	-	-	-	0.552	0.631	-	-	-
k_4	-	-	-	-	0.876	-	-	-
k_5	-	-	-	-	1.021	-	-	-
k_6	-	-	-	-	0.854	-	-	-
k_7	-	-	-	-	0.820	-	-	-
k_8	-	-	-	-	0.631	-	-	-
k_9	-	-	-	-	0.609	-	-	-
k_{10}	-	-	-	0.445	0.542	-	-	-
k_{11}	-	-	-	-	0.353	-	-	-
l	0.397	0.379	0.420	0.545	0.684	0.435	0.164	0.119
m	0.365	0.346	0.409	0.683	0.473	0.475	0.142	0.131
m_1	-	-	-	0.524	-	-	-	-
m_2	-	-	-	0.483	-	-	-	-
m_3	-	-	-	0.473	-	-	-	-
m_4	-	-	-	0.455	-	0.582	-	-
m_5	-	-	-	0.522	-	-	-	-
m_6	-	-	-	0.582	-	-	-	-
m_7	-	-	-	0.613	-	-	-	-
m_8	-	-	-	0.598	-	-	-	-
m_9	-	-	-	0.532	-	-	-	-
m_{10}	-	-	-	0.468	-	-	-	-

(Continued)

Load Points	Reference Points							
	A	B	C	D	E	F	G	H
m_{11}	-	-	-	0.418	-	-	-	-
m_{12}	-	-	-	0.391	-	-	-	-
m_{13}	-	-	-	0.382	-	-	-	-
m_{14}	-	-	-	0.367	-	0.507	-	-
m_{15}	-	-	-	0.277	-	-	-	-
m_{16}	-	-	-	0.250	-	-	-	-
n	0.330	0.304	0.399	0.454	0.352	0.614	0.112	0.143
o	0.310	0.254	0.366	0.381	0.270	1.242	0.082	0.145
o_1	-	-	-	-	-	0.644	-	-
o_2	-	-	-	-	-	0.680	-	-
o_3	-	-	-	-	-	0.887	-	-
o_4	-	-	-	-	-	0.782	-	-
o_5	-	-	-	-	-	0.949	-	-
o_6	-	-	-	-	-	0.837	-	-
o_7	-	-	-	-	-	0.612	-	-
o_8	-	-	-	-	-	0.572	-	-
o_9	-	-	-	-	-	0.345	-	-
p	0.228	0.201	0.228	0.341	0.360	0.255	0.321	0.085
q	0.202	0.187	0.217	0.297	0.334	0.262	0.237	0.094
r	0.186	0.171	0.207	0.257	0.273	0.288	0.134	0.130
s	0.170	0.154	0.197	0.246	0.202	0.327	0.081	0.215
t	0.156	0.133	0.175	0.226	0.155	0.342	0.052	0.302
u	-	-	-	0.170	0.161	0.129	0.932	0.046
v	-	-	-	0.144	0.159	0.135	0.218	0.054
w	-	-	-	0.124	0.135	0.147	0.087	0.083
x	-	-	-	0.121	0.105	0.156	0.047	0.172
y	-	-	-	0.113	0.078	0.155	0.025	0.908
f'	-	-	-	0.333	0.306	0.323	0.075	0.062
g'	-	-	-	0.307	0.287	0.309	0.076	0.062

(Continued)

Load Points	Reference Points							
	A	B	C	D	E	F	G	H
h'	-	-	-	0.283	0.267	0.301	0.069	0.059
i'	-	-	-	0.264	0.238	0.283	0.064	0.056
j'	-	-	-	0.247	0.211	0.266	0.056	0.055
k'	-	-	-	0.221	0.202	0.220	0.048	0.036
l'	-	-	-	0.208	0.191	0.209	0.048	0.037
m'	-	-	-	0.192	0.173	0.198	0.047	0.038
n'	-	-	-	0.178	0.154	0.183	0.043	0.038
o'	-	-	-	0.165	0.143	0.173	0.037	0.040
p'	-	-	-	0.109	0.097	0.111	0.024	0.0204
q'	-	-	-	0.101	0.090	0.103	0.0232	0.020
r'	-	-	-	0.093	0.084	0.098	0.0225	0.0173
s'	-	-	-	0.086	0.078	0.092	0.017	0.0170
t'	-	-	-	0.079	0.071	0.085	0.016	0.0166

(e) Influence Coefficients I_R Model 2 (45° Opening Angle)

Load Points	Reference Points A	Reference Points D
a	-0.362	-0.180
a_6	-0.203	-
b	-0.225	-0.126
c	+0.142	-0.0908
c_1	-0.141	-
c_2	-0.072	-
c_3	-0.052	-
c_4	-0.102	-
c_5	-0.019	-
c_6	-0.123	-
c_7	-0.046	-
c_8	-0.090	-
c_9	-0.138	-
c_{10}	-0.113	-0.094
c_{11}	-0.096	-0.070
d	-0.151	-0.0914
e	-0.210	-0.114
f	-0.287	-0.250
g	-0.178	-0.144
h	-0.092	-0.063
i	-0.121	-0.094
j	-0.175	-0.149
k	-0.179	-0.283
k_3	-	-0.154
k_{10}	-	-0.120
l	-0.123	-0.158
m	-0.0886	+0.099
m_1	-	-0.075
m_2	-	-0.003

Load Points	Reference Points A	Reference Points D
m_3	-	-0.048
m_4	-	-0.096
m_5	-	+0.036
m_6	-	-0.080
m_7	-	-0.012
m_8	-	+0.003
m_9	-	-0.0491
m_{10}	-	+0.0485
m_{11}	-	-0.046
m_{12}	-	+0.026
m_{13}	-	-0.023
m_{14}	-	-0.071
m_{15}	-	-0.036
m_{16}	-	-0.020
n	-0.0891	-0.097
o	-0.112	-0.156
p	-0.085	-0.163
q	-0.062	-0.078
r	-0.049	-0.012
s	-0.047	-0.044
t	-0.053	-0.091
u	-	-0.081
v	-	-0.038
w	-	-0.015
x	-	-0.021
y	-	-0.045
f'	-	-0.125
g'	-	-0.100
h'	-	-0.081

Load Points	Reference Points A	Reference Points D
i'	-	-0.077
j'	-	-0.084
k'	-	-0.080
l'	-	-0.068
m'	-	-0.058
n'	-	-0.054
o'	-	-0.055
p'	-	-0.040
q'	-	-0.034
r'	-	-0.030
s'	-	-0.028
t'	-	-0.027

(f) Influence Coefficients $I_{\theta R}$ - Model 2 (45° Opening Angle)

Load Points	Reference Points A	Reference Points D
a	0.0	-0.193
a_6	+0.041	-
b	0.0	-0.129
c	0.0	-0.062
c_6	+0.036	-
c_7	+0.005	-
c_8	-0.023	-
c_9	-0.024	-
c_{10}	-	-0.100
c_{11}	-	-0.018
d	0.0	-0.002
e	0.0	+0.051
f	+0.076	-0.193
g	+0.051	-0.134
h	+0.009	-0.058
i	-0.026	-0.011
j	-0.036	+0.054
k	+0.073	-0.110
k_3	-	-0.121
k_{10}	-	-0.029
l	+0.044	-0.076
m	+0.012	-0.042
m_1	-	-0.099
m_2	-	-0.051
m_3	-	-0.006
m_4	-	+0.011
m_5	-	-0.047
m_6	-	-0.059
m_7	-	-0.050

Load Points	Reference Points A	Reference Points D
m_8	-	-0.034
m_9	-	-0.025
m_{10}	-	-0.037
m_{11}	-	-0.017
m_{12}	-	-0.031
m_{13}	-	-0.043
m_{14}	-	-0.028
m_{15}	-	-0.0121
m_{16}	-	-0.027
n	-0.016	-0.009
o	-0.035	+0.022
p	+0.041	-0.021
q	+0.024	-0.0118
r	+0.008	-0.020
s	-0.007	-0.025
t	-0.019	-0.007
u	-	-0.006
v	-	-0.005
w	-	-0.010
x	-	-0.013
y	-	-0.006
f'	-	-0.158
g'	-	-0.107
h'	-	-0.057
i'	-	-0.008
j'	-	+0.037
k'	-	-0.110
l'	-	-0.076
m'	-	-0.042

Load Points	Reference Points A	Reference Points D
n'	-	-0.009
o'	-	+0.022
p'	-	-0.056
q'	-	-0.039
r'	-	-0.022
s'	-	-0.006
t'	-	+0.011

(g) Influence Coefficients I_θ - Continuous Model

Load Points	Reference Points							
	A	B	C	D	E	F	G	H
a	-0.048	-0.086	-0.0008	+0.082	+0.095	+0.048	+0.814	+0.026
b	-0.044	-0.053	-0.016	+0.064	+0.079	+0.054	+0.205	+0.039
c	-0.039	-0.025	-0.032	+0.054	+0.063	+0.071	+0.072	+0.063
d	-0.031	-0.008	-0.061	+0.054	+0.042	+0.084	+0.030	+0.157
e	-0.024	+0.001	-0.098	+0.053	+0.025	+0.089	+0.013	+0.799
f	-0.093	-0.169	-0.0009	+0.164	+0.187	+0.084	+0.287	+0.048
g	-0.0854	-0.105	-0.027	+0.136	+0.177	+0.101	+0.200	+0.064
h	-0.076	-0.049	-0.063	+0.109	+0.128	+0.148	+0.102	+0.096
i	-0.060	-0.017	-0.117	+0.109	+0.082	+0.188	+0.048	+0.177
j	-0.046	+0.002	-0.192	+0.104	+0.048	+0.205	+0.027	+0.257
k	-0.123	-0.249	0.0	+0.231	+0.374	+0.109	+0.154	+0.056
l	-0.116	-0.145	-0.033	+0.212	+0.303	+0.133	+0.135	+0.069
m	-0.106	-0.067	-0.083	+0.183	+0.183	+0.195	+0.095	+0.097
n	-0.0848	-0.019	-0.163	+0.173	+0.108	+0.300	+0.058	+0.145
o	-0.058	+0.0047	-0.285	+0.144	+0.063	+0.380	+0.131	+0.143
p	-0.131	-0.326	+0.006	+0.256	+1.042	+0.113	+0.092	+0.055
q	-0.135	-0.178	-0.029	+0.258	+0.380	+0.150	+0.087	+0.064
r	-0.127	-0.076	-0.087	+0.391	+0.204	+0.211	+0.068	+0.076
s	-0.096	-0.018	-0.193	+0.209	+0.116	+0.370	+0.048	+0.085
t	-0.063	+0.0066	-0.352	+0.158	+0.065	+0.964	+0.029	+0.095
u	-0.116	-0.387	+0.009	+0.221	+0.356	+0.098	+0.0556	+0.046
v	-0.132	-0.185	-0.020	+0.202	+0.288	+0.125	+0.0559	+0.057
w	-0.139	-0.066	-0.077	+0.171	+0.178	+0.183	+0.048	+0.056
x	-0.098	-0.012	-0.201	+0.163	+0.102	+0.295	+0.037	+0.058
y	-0.054	+0.009	-0.406	+0.133	+0.058	+0.355	+0.022	+0.063
z	-0.073	-0.432	+0.011	+0.121	+0.162	+0.070	+0.029	+0.027
a'	-0.107	-0.157	-0.010	+0.0997	+0.157	+0.088	+0.032	+0.029
b'	-0.136	-0.042	-0.048	+0.0959	+0.114	+0.124	+0.030	+0.030
c'	-0.078	-0.007	-0.164	+0.097	+0.071	+0.170	+0.022	+0.029

(Continued)

Load Points	Reference Points							
	A	B	C	D	E	F	G	H
d'	-0.029	+0.008	-0.425	+0.087	+0.041	+0.188	+0.016	+0.029
e'	-0.022	-0.411	+0.006	-0.068	+0.059	+0.035	+0.010	+0.0132
f'	-0.049	-0.077	-0.001	-0.059	+0.065	+0.038	+0.016	+0.014
g'	-0.118	-0.012	-0.016	-0.048	+0.050	+0.056	+0.013	+0.011
h'	-0.039	-0.003	-0.092	-0.044	+0.031	+0.068	+0.010	+0.0123
i'	-0.008	+0.004	-0.369	-0.045	+0.020	+0.076	+0.007	+0.0119
j'	-	-	-	-0.079	-0.079	-0.066	-0.018	-0.016
k'	-	-	-	-0.066	-0.062	-0.060	-0.015	-0.0164
l'	-	-	-	-0.058	-0.051	-0.060	-0.015	-0.015
m'	-	-	-	-0.052	-0.041	-0.063	-0.012	-0.012
n'	-	-	-	-0.049	-0.032	-0.069	-0.011	-0.011
o'	-	-	-	-0.0494	-0.092	-0.082	-0.020	-0.019
p'	-	-	-	-0.041	-0.076	-0.072	-0.018	-0.018
q'	-	-	-	-0.037	-0.060	-0.070	-0.015	-0.016
r'	-	-	-	-0.0317	-0.049	-0.075	-0.014	-0.016
s'	-	-	-	-0.0305	-0.042	-0.077	-0.012	-0.013
t'	-	-	-	-	-0.056	-0.052	+0.013	-0.0149
u'	-	-	-	-	-0.047	-0.048	+0.0098	-0.0128
v'	-	-	-	-	-0.039	-0.0458	+0.008	-0.009
w'	-	-	-	-	-0.031	-0.0462	+0.008	-0.008
x'	-	-	-	-	-0.029	-0.0481	-0.0077	-0.009

(h) Influence Coefficients I_R - Continuous Model

Load Point	Reference Point D
a	-0.048
b	-0.014
c	+0.008
d	-0.002
e	-0.024
f	-0.095
g	-0.024
h	+0.026
i	-0.004
j	-0.048
k	-0.140
l	-0.045
m	+0.066
n	-0.015
o	-0.069
p	-0.159
q	-0.059
r	+0.176
s	-0.024
t	-0.075
u	-0.137
v	-0.039
w	+0.066
x	-0.012
y	-0.065
z	-0.086

Load Point	Reference Point D
a'	-0.020
b'	+0.026
c'	-0.005
d'	-0.041
e'	-0.036
f'	-0.009
g'	+0.008
h'	0.0
i'	-0.019
j'	+0.020
k'	+0.010
l'	+0.0066
m'	+0.007
n'	+0.008
o'	+0.014
p'	+0.011
q'	+0.009
r'	+0.007
s'	+0.009
t'	+0.0083
u'	+0.0075
v'	+0.004
w'	+0.005
x'	+0.006

(i) Influence Coefficients $I_{\theta R}$ - Continuous Model

Load Points	Reference Points A	Reference Points D
a	-0.015	+0.016
b	-0.010	+0.009
c	-0.003	+0.002
d	+0.004	-0.009
e	+0.003	-0.014
f	-0.035	+0.039
g	-0.017	+0.025
h	-0.005	+0.003
i	+0.008	-0.022
j	+0.020	-0.022
k	-0.038	+0.035
l	-0.018	+0.020
m	+0.001	-0.004
n	+0.015	-0.028
o	+0.031	-0.028
p	-0.048	+0.017
q	-0.034	+0.003
r	-0.004	-0.009
s	+0.019	-0.008
t	+0.037	-0.014
u	-0.059	-0.002
v	-0.035	-0.015
w	-0.003	-0.010
x	+0.023	+0.019
y	+0.041	+0.001
z	-0.053	-0.018

Load Points	Reference Points A	Reference Points D
a'	-0.029	-0.018
b'	-0.007	-0.005
c'	+0.0234	+0.014
d'	+0.029	+0.006
e'	-0.027	-0.009
f'	-0.019	-0.011
g'	-0.008	-0.002
h'	+0.021	+0.011
i'	+0.026	+0.002
j'	-	+0.008
k'	-	+0.004
l'	-	+0.010
m'	-	+0.002
n'	-	-0.002
o'	-	+0.015
p'	-	+0.002
q'	-	+0.003
r'	-	+0.002
s'	-	-0.0004
t'	-	+0.005
u'	-	+0.009
v'	-	+0.003
w'	-	-0.0006
x'	-	-0.0008

2.2 INFLUENCE SURFACES

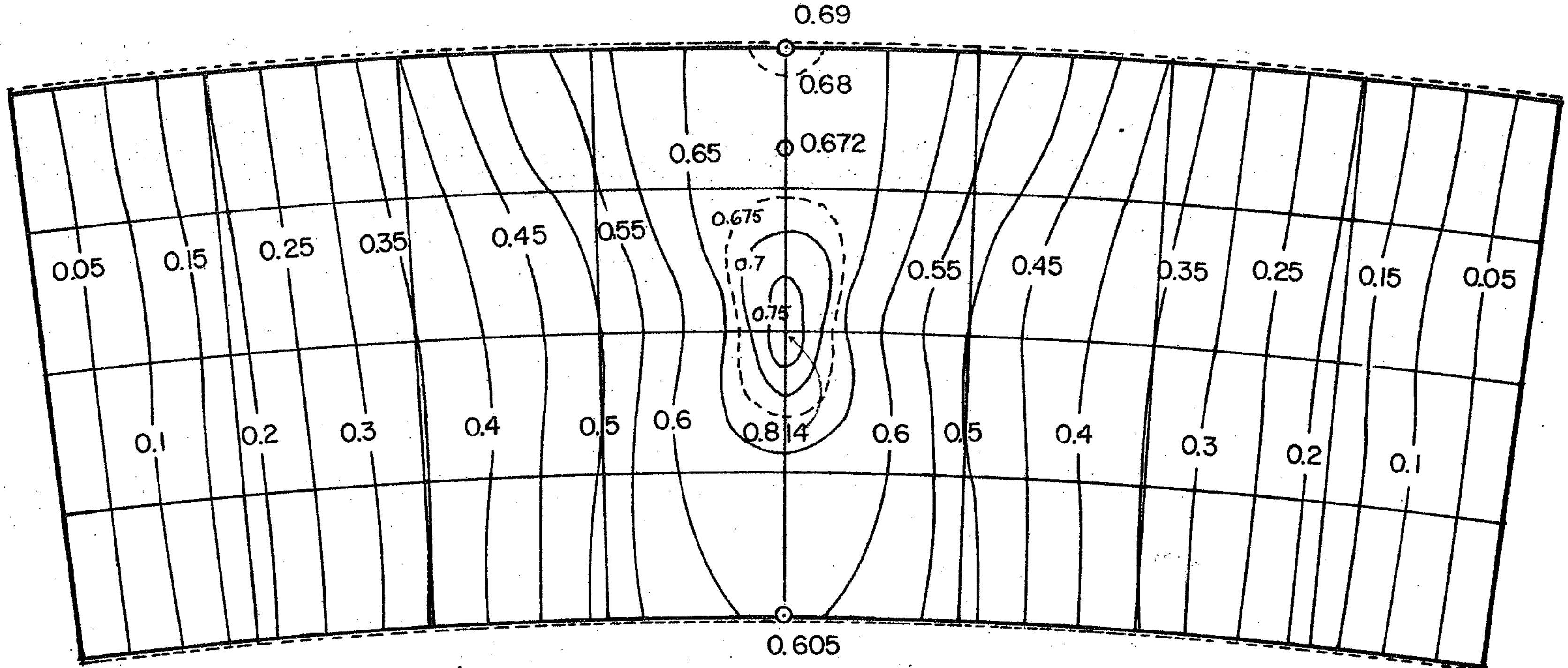

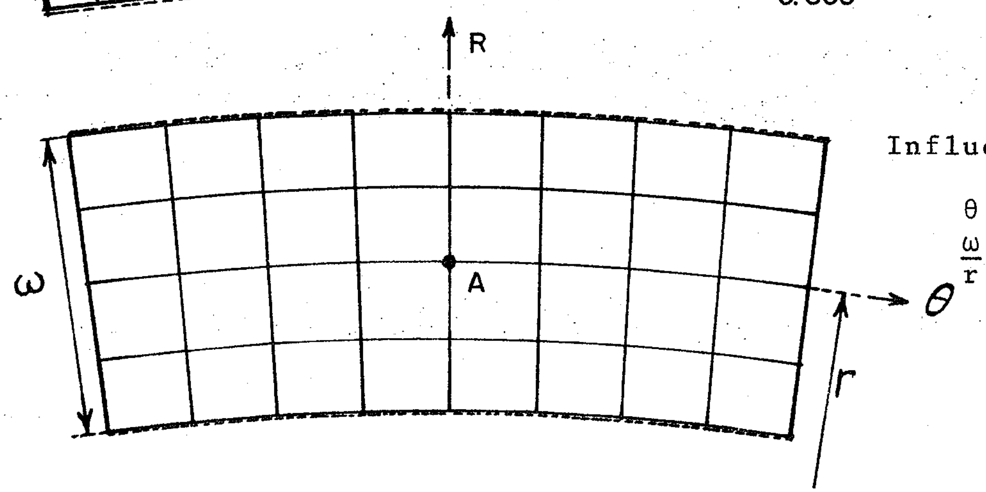

FIGURE I - 1

Influence Surface I_θ for the Reference Point A

$\theta = 15°$

$\frac{\omega}{r} = 0.1$

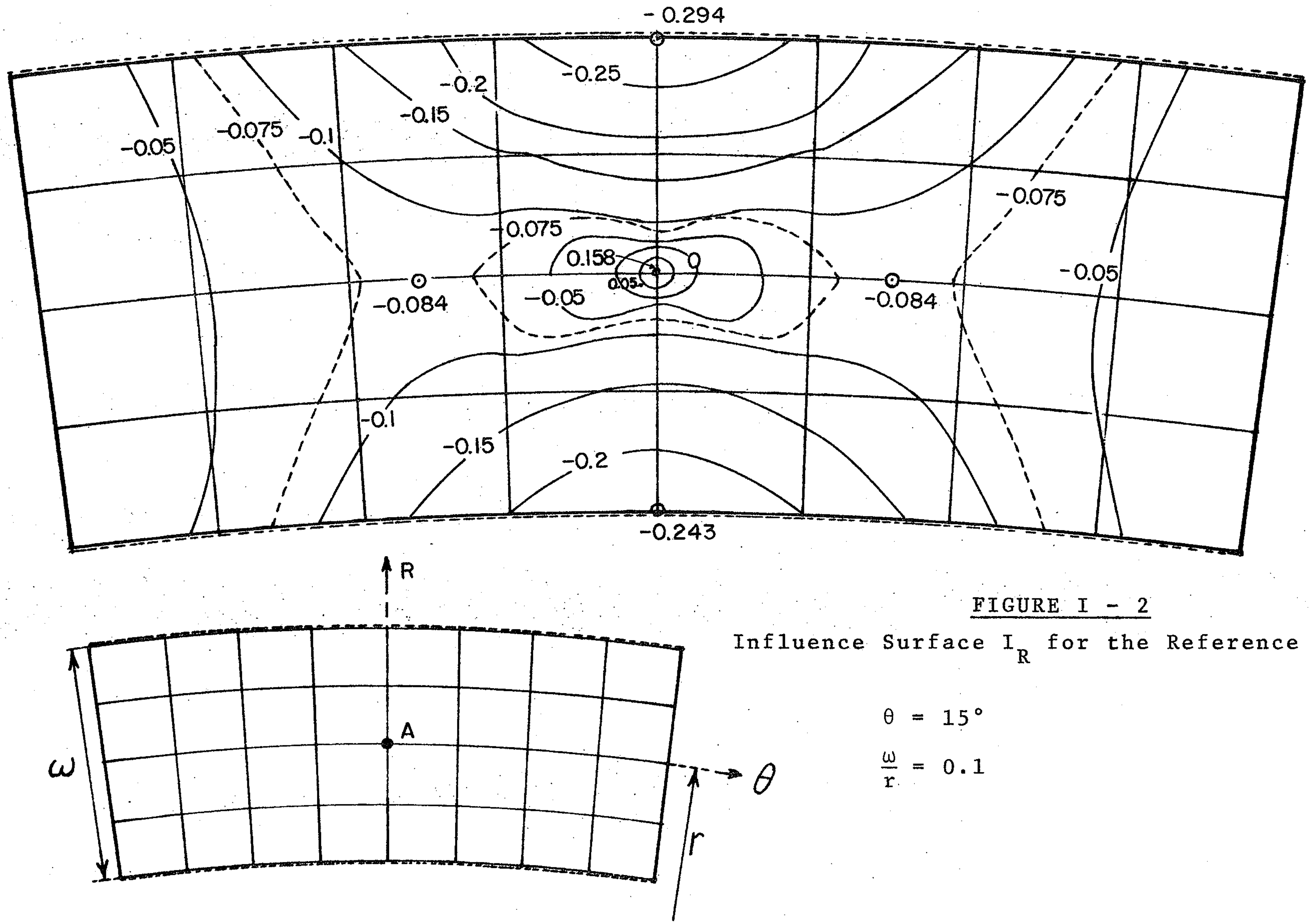

FIGURE I - 2

Influence Surface I_R for the Reference Point A

$\theta = 15°$

$\frac{\omega}{r} = 0.1$

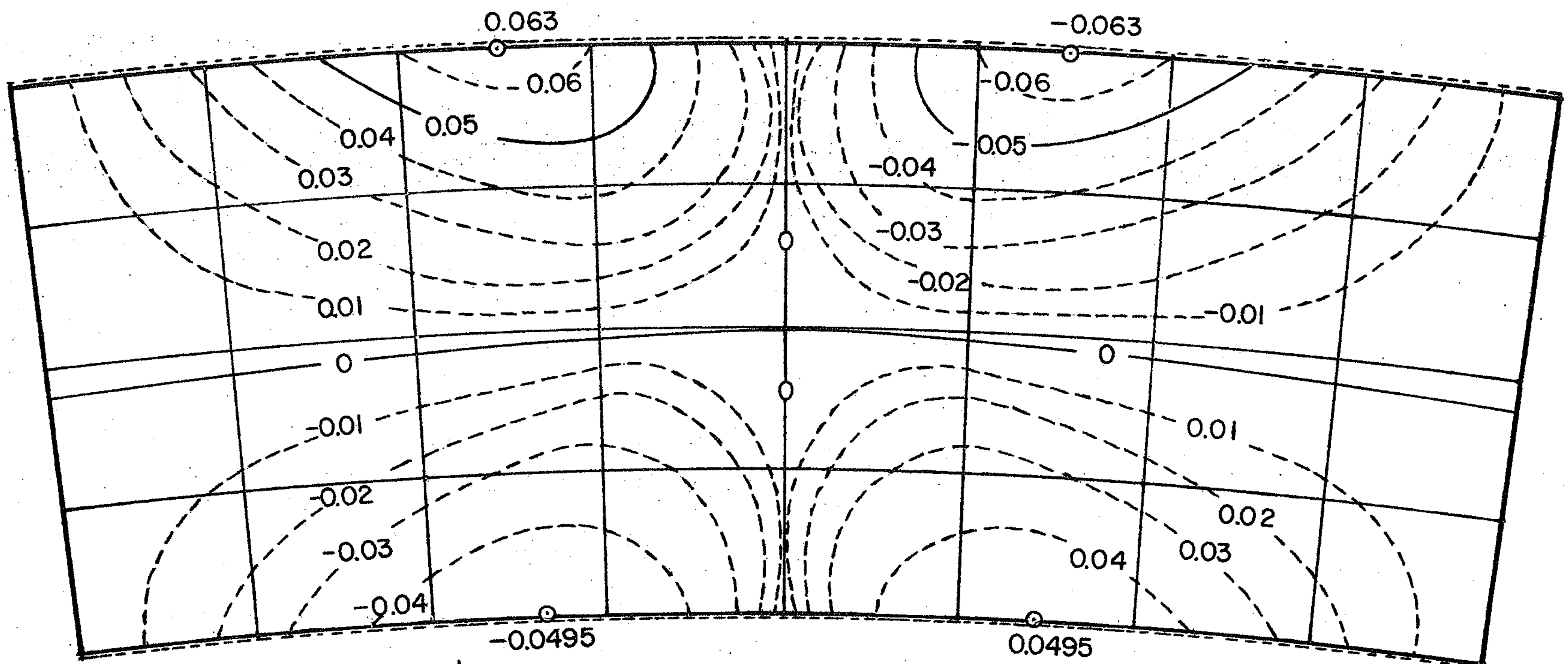

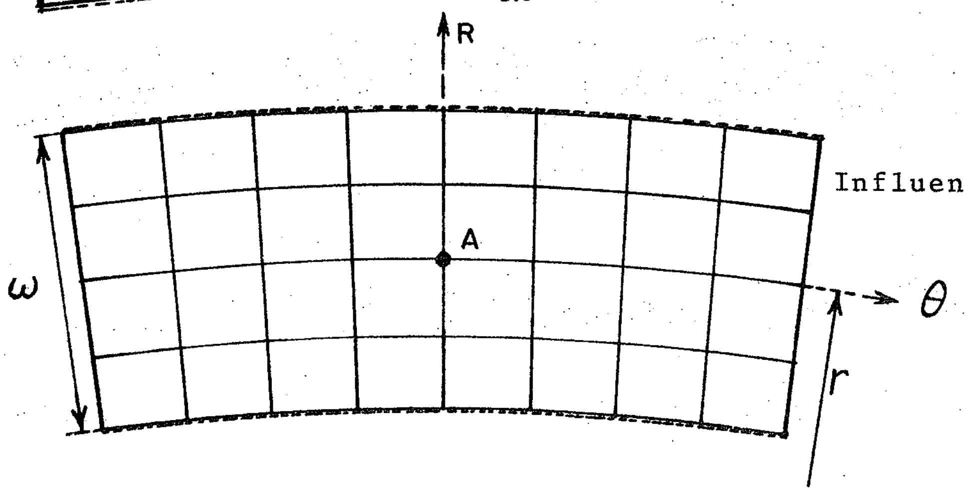

FIGURE I - 3

Influence Surface $I_{\theta R}$ for the Reference Point A

$\theta = 15°$

$\frac{\omega}{r} = 0.1$

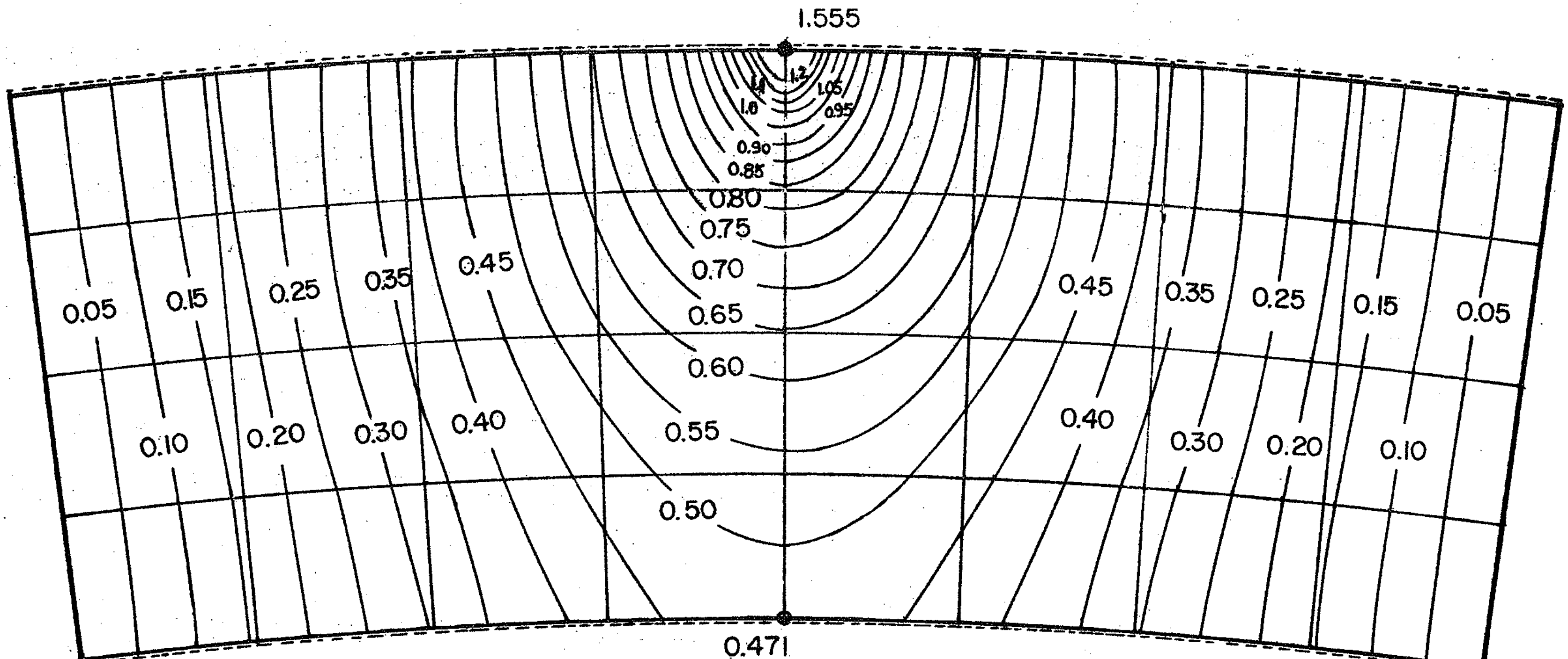

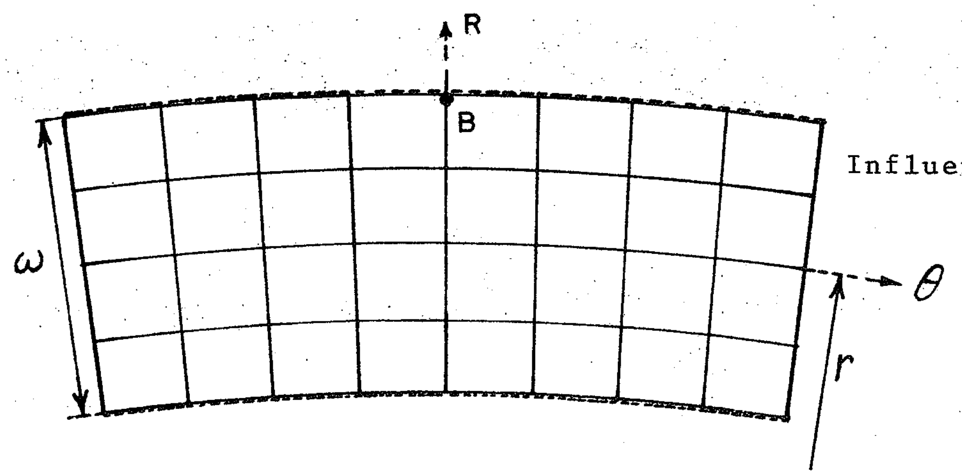

FIGURE I - 4

Influence Surface I_θ for the Reference Point B

$\theta = 15°$

$\frac{\omega}{r} = 0.1$

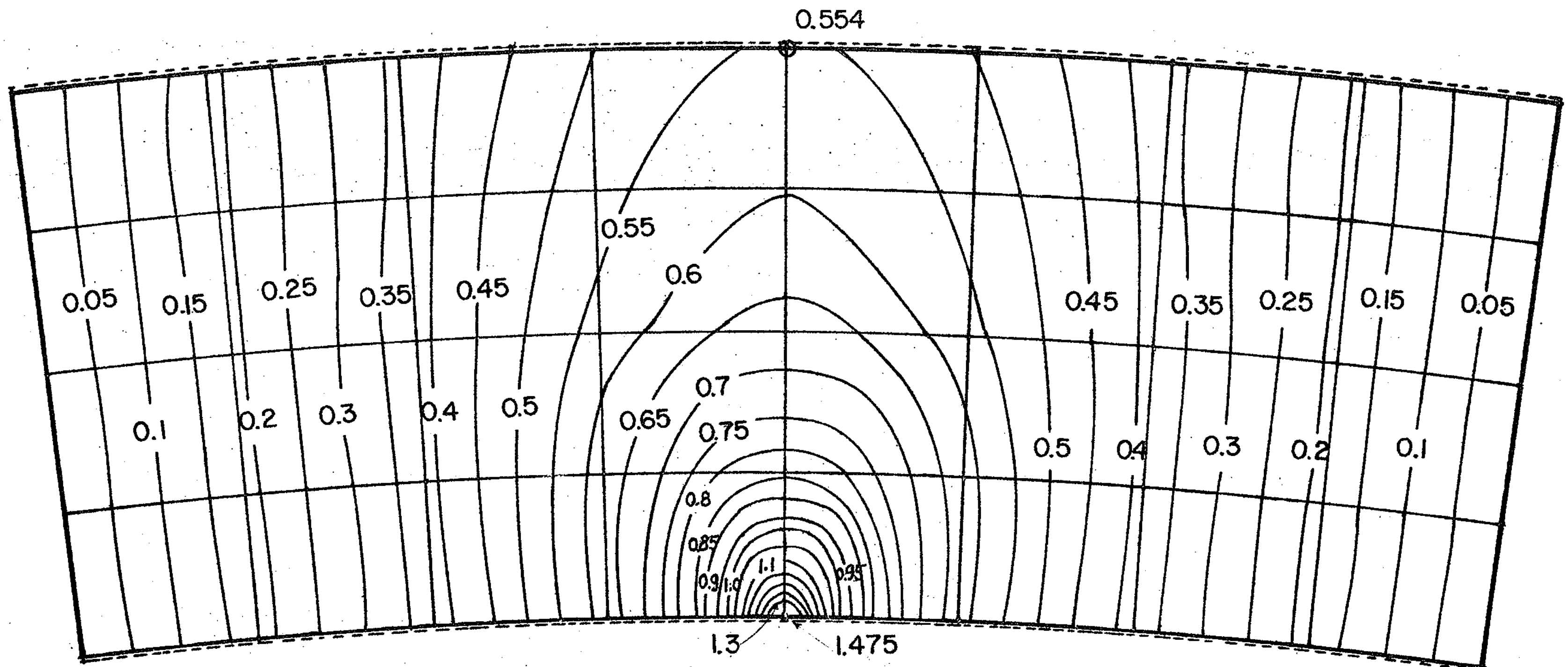

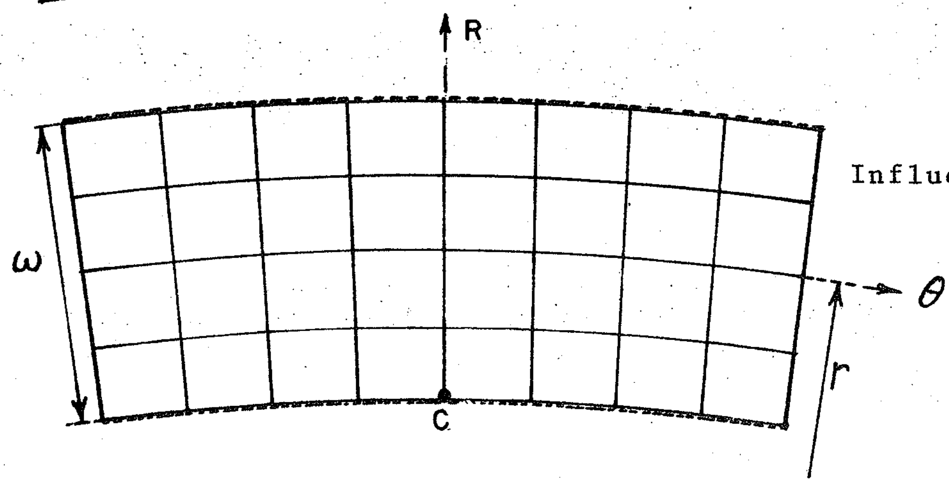

FIGURE I - 5

Influence Surface I_θ for the Reference Point C

$\theta = 15°$

$\frac{\omega}{r} = 0.1$

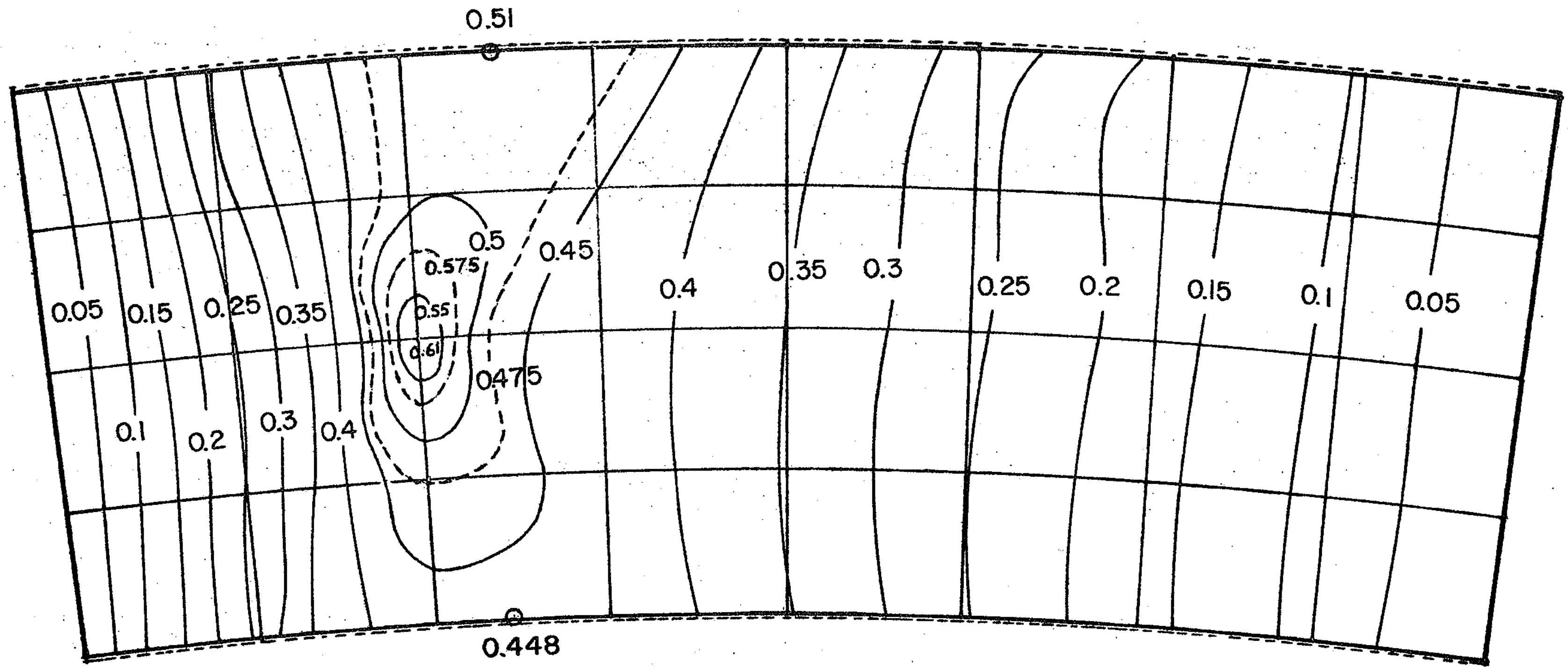

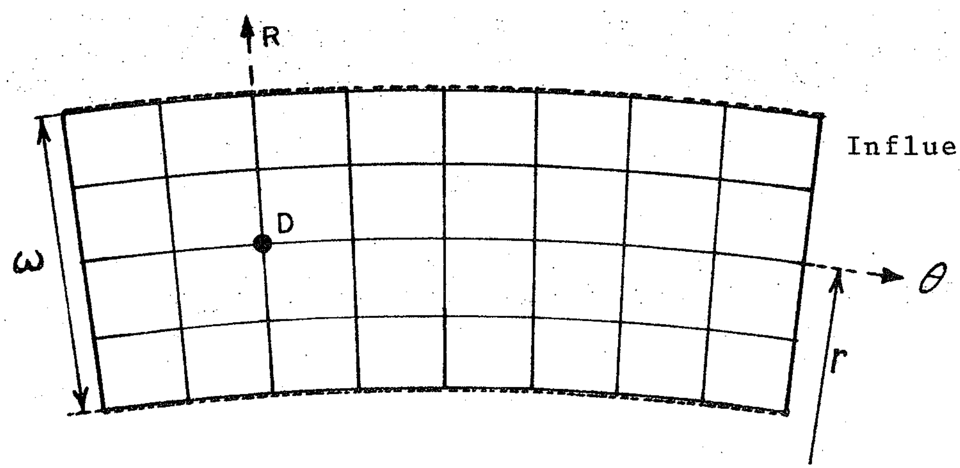

FIGURE I - 6

Influence Surface I_θ for the Reference Point D

$\theta = 15°$

$\frac{\omega}{r} = 0.1$

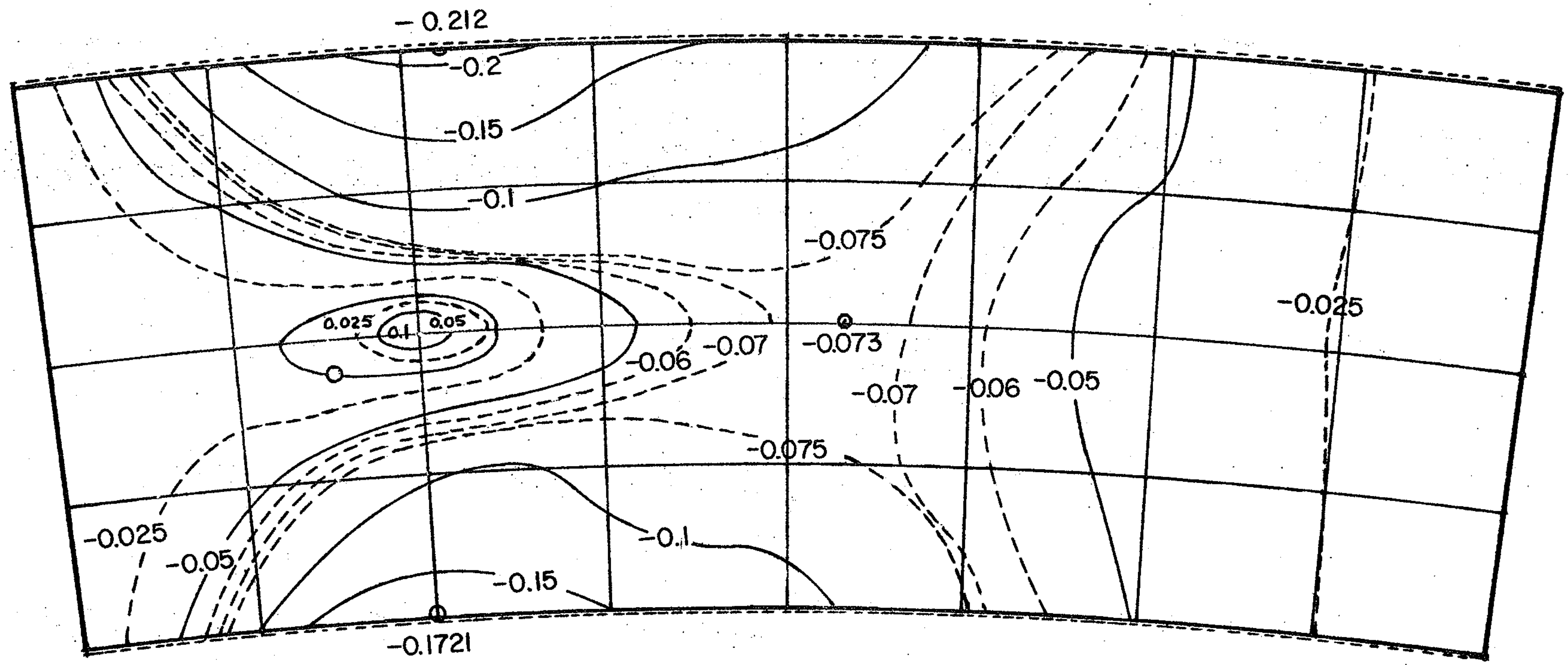

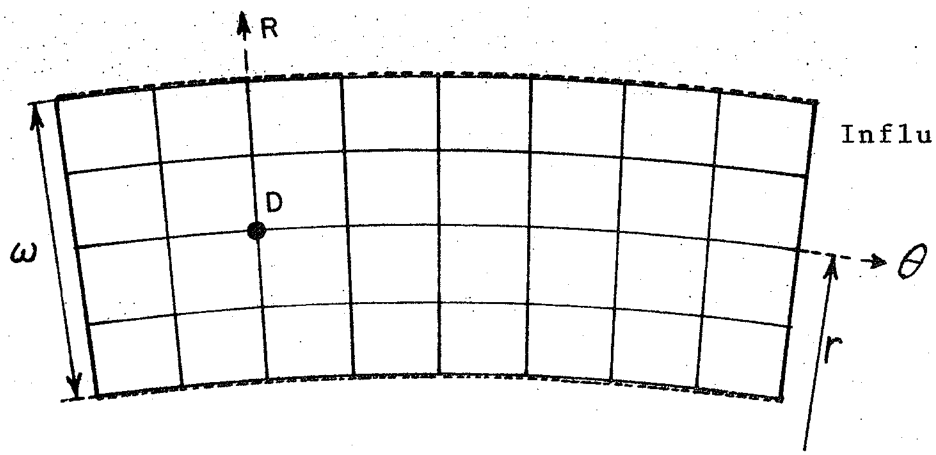

FIGURE I - 7

Influence Surface I_R for the Reference Point D

$\theta = 15°$

$\frac{\omega}{r} = 0.1$

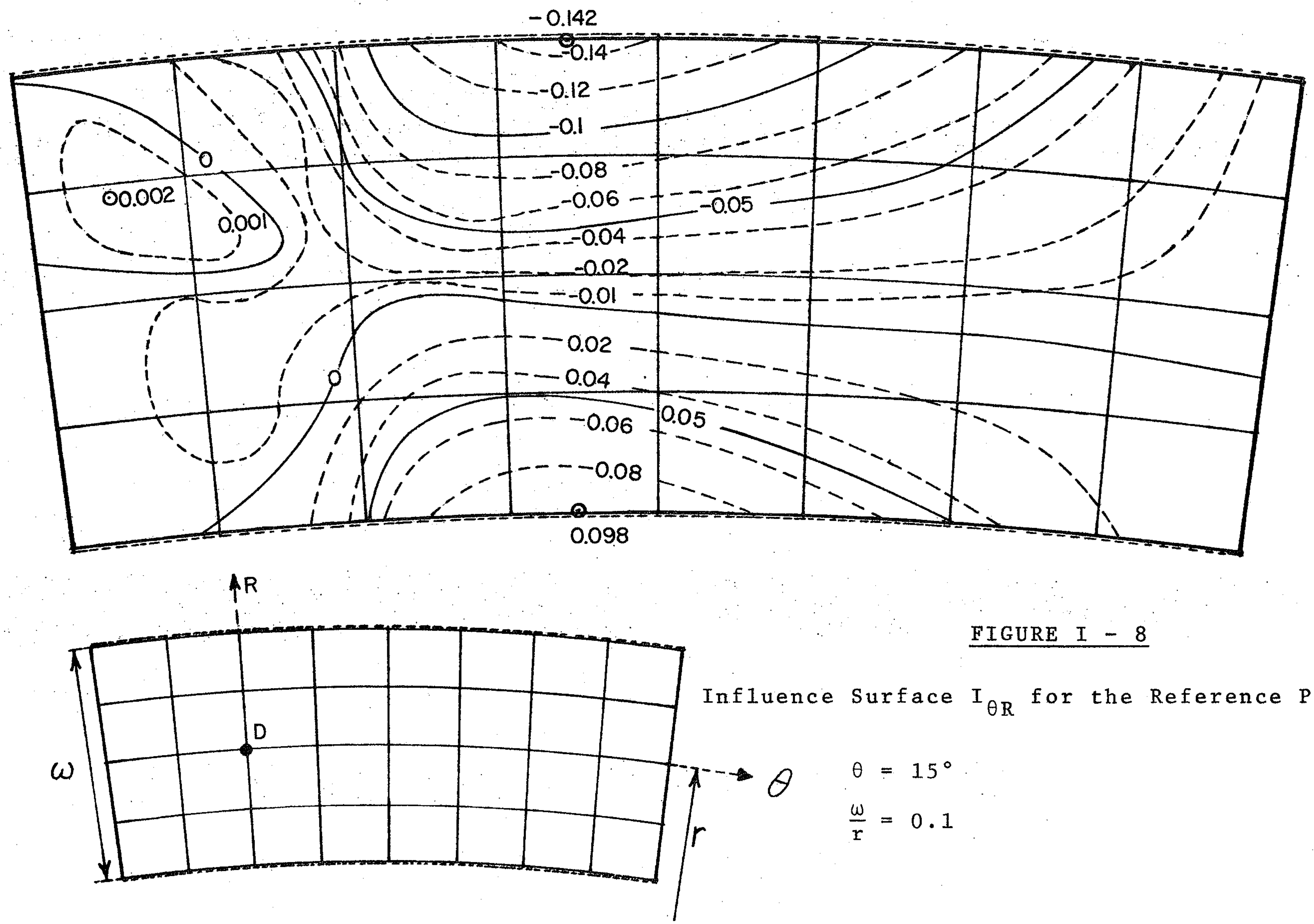

FIGURE I - 8

Influence Surface $I_{\theta R}$ for the Reference Point D

$\theta = 15°$

$\frac{\omega}{r} = 0.1$

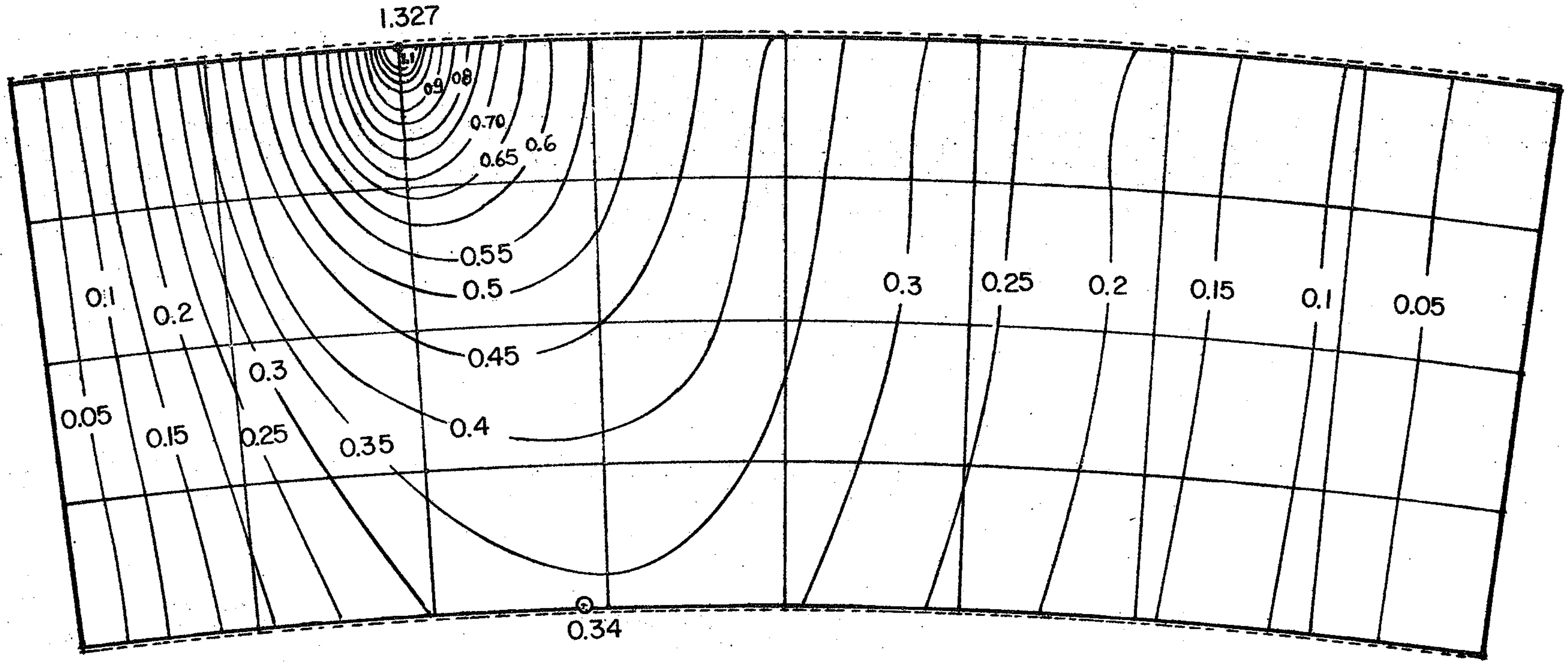

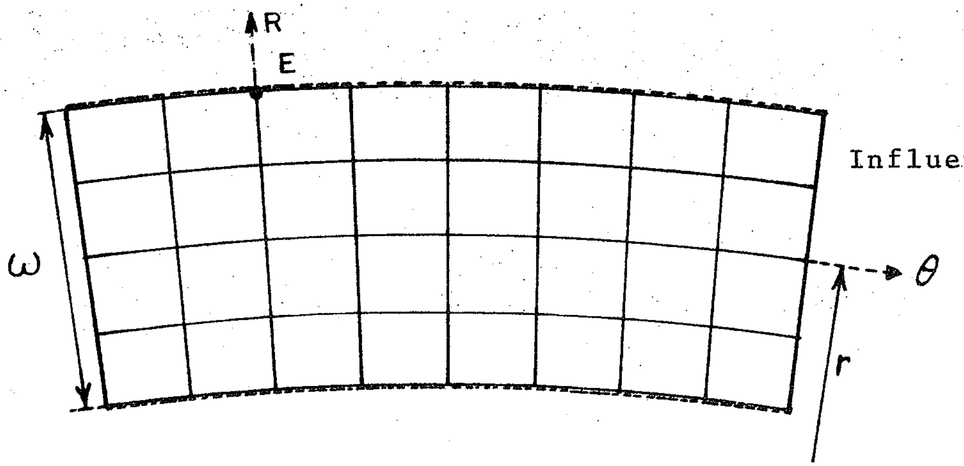

FIGURE I - 9

Influence Surface I_θ for the Reference Point E

$\theta = 15°$

$\frac{\omega}{r} = 0.1$

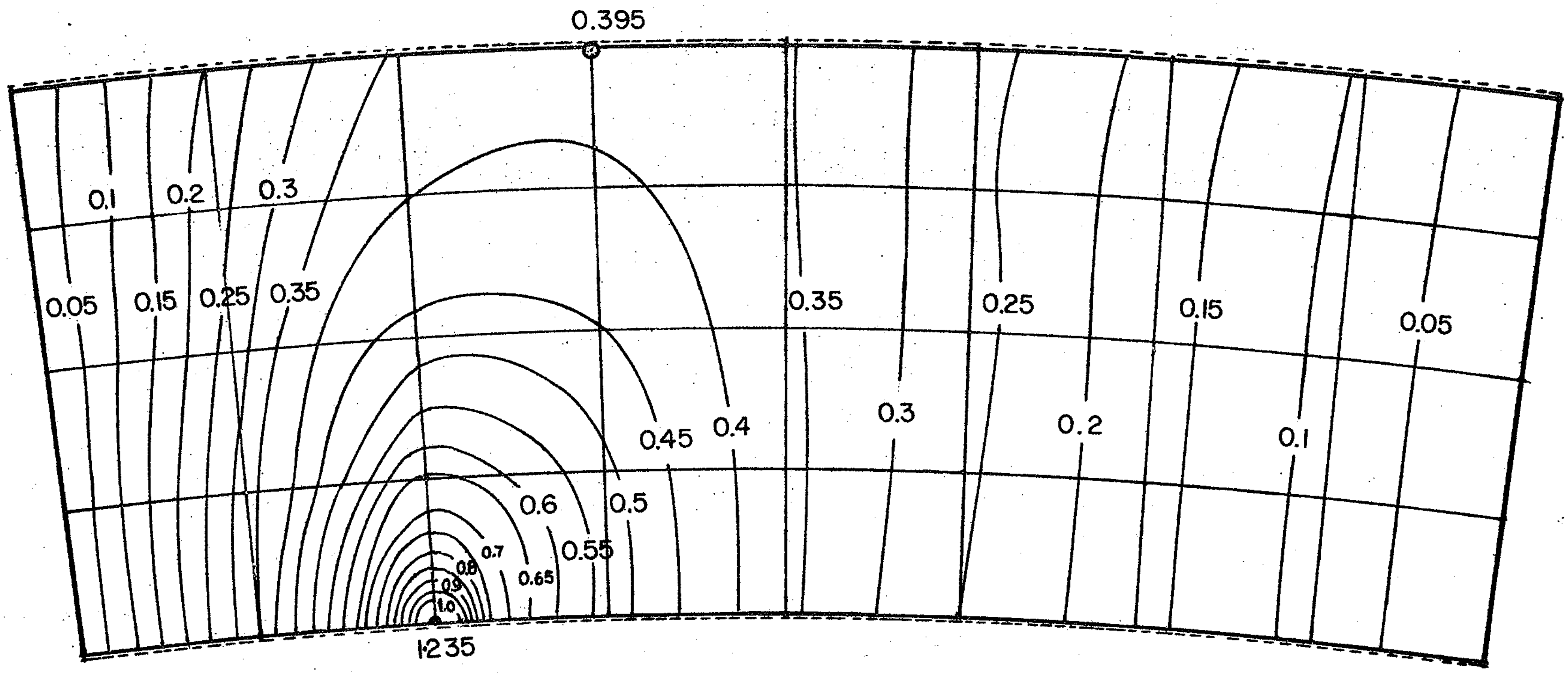

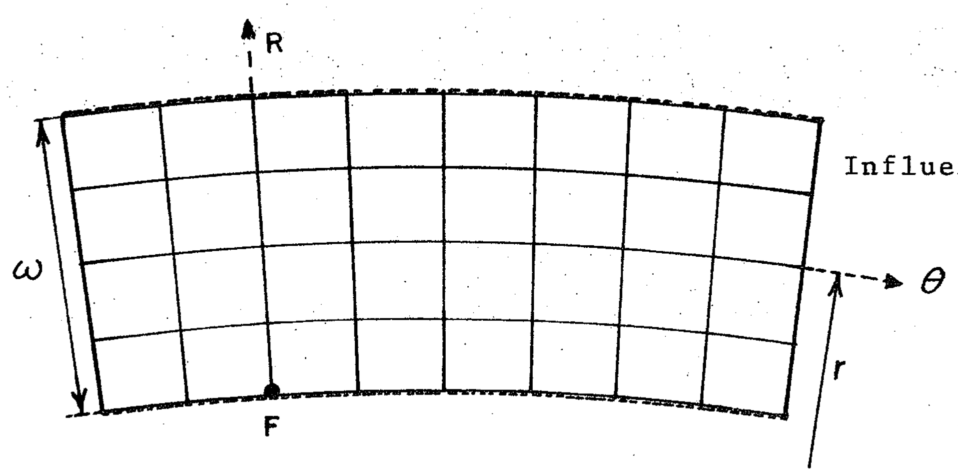

FIGURE I - 10

Influence Surface I_θ for the Reference Point F

$\theta = 15°$

$\frac{\omega}{r} = 0.1$

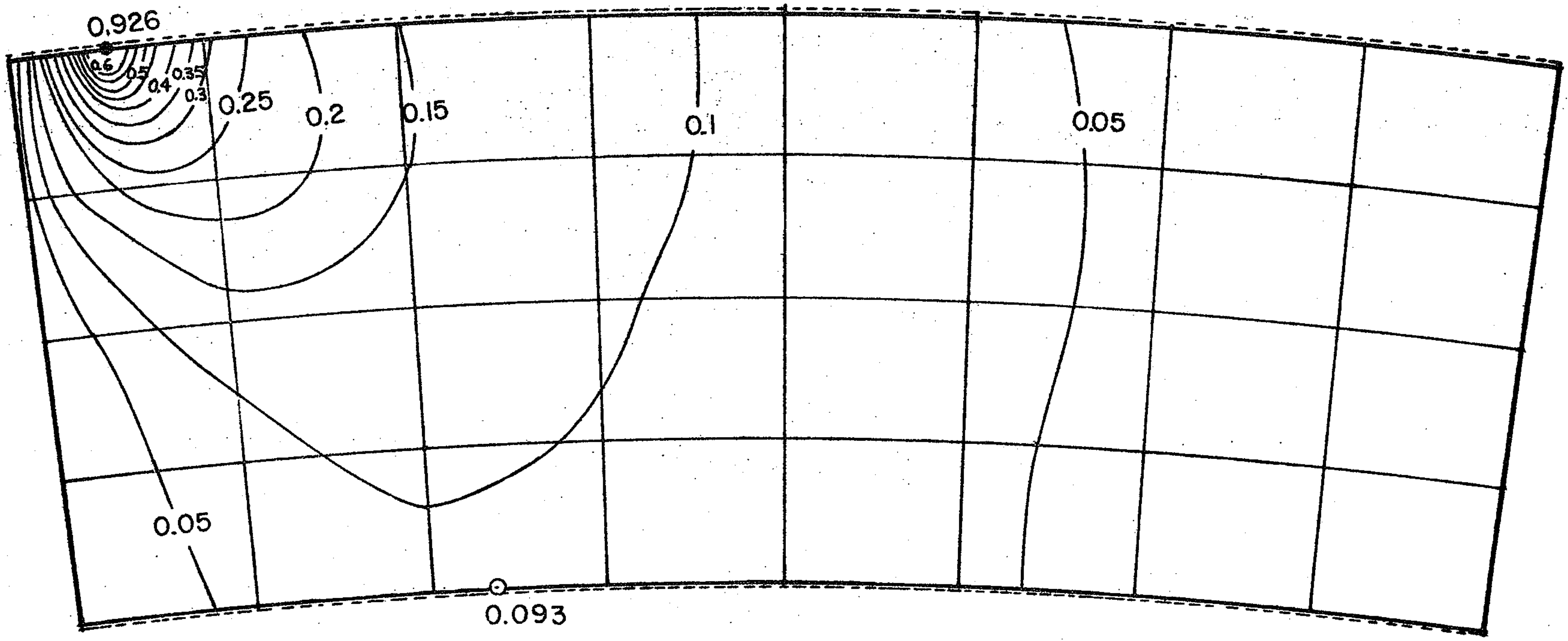

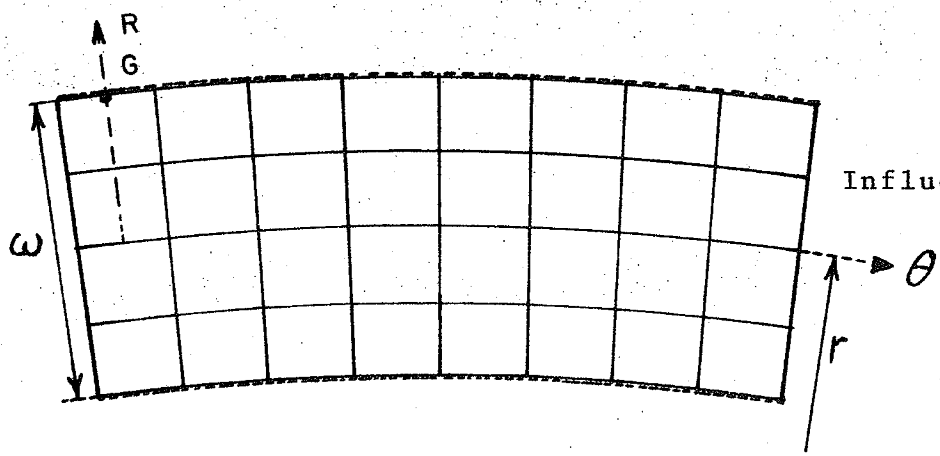

FIGURE I - 11

Influence Surface I_θ for the Reference Point G

$\theta = 15°$

$\frac{\omega}{r} = 0.1$

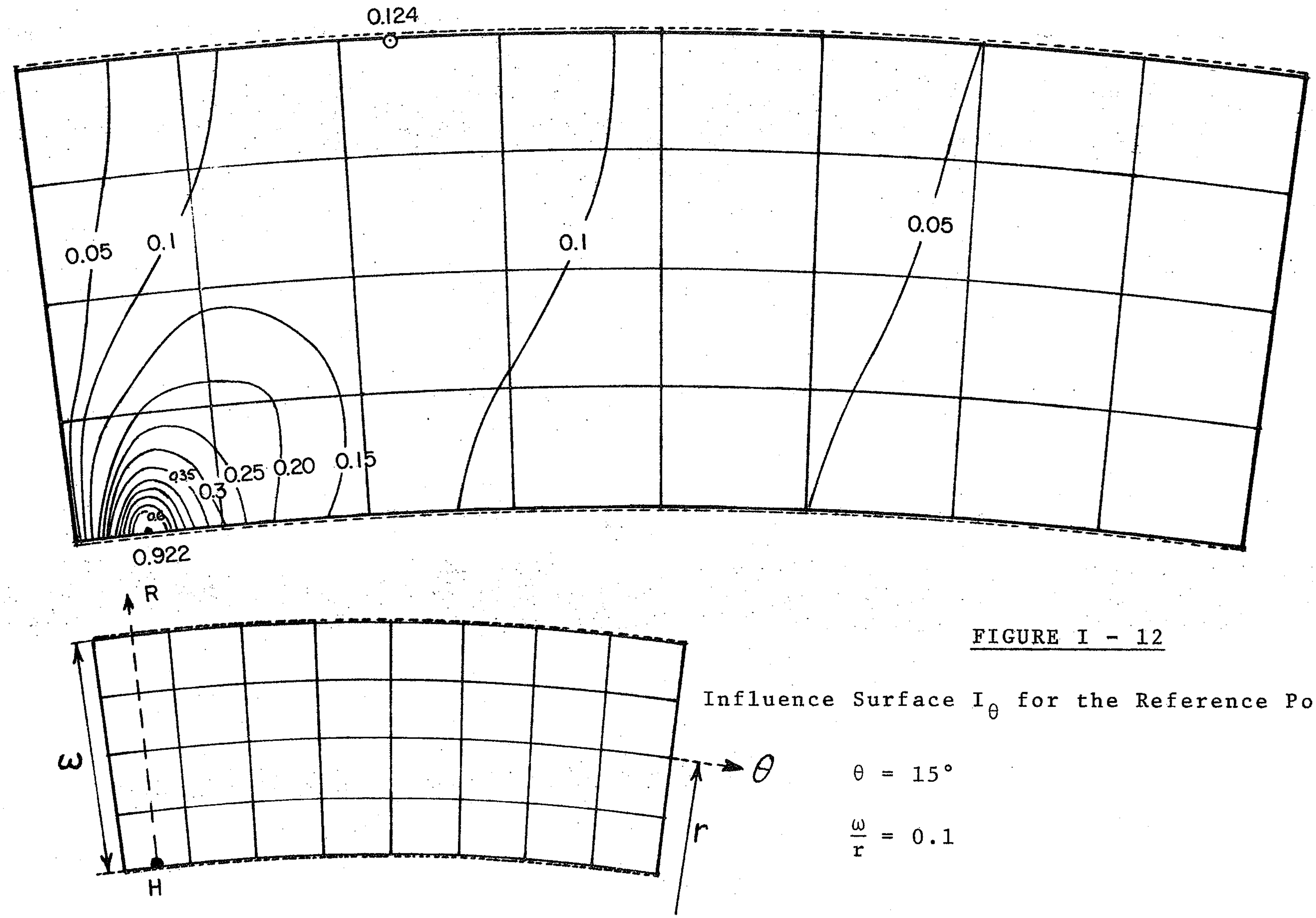

FIGURE I - 12

Influence Surface I_θ for the Reference Point H

$\theta = 15°$

$\frac{\omega}{r} = 0.1$

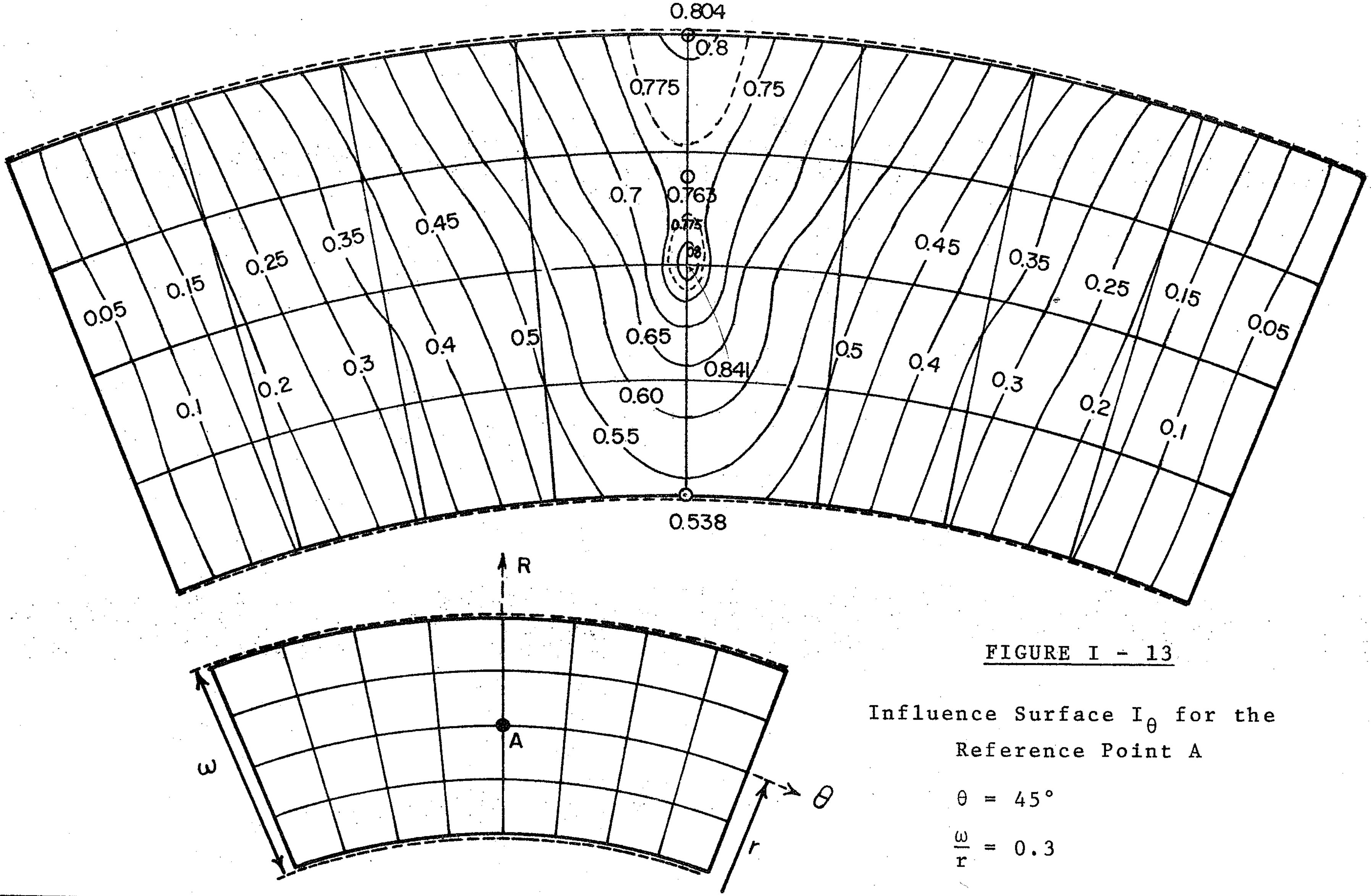

FIGURE I - 13

Influence Surface I_θ for the Reference Point A

$\theta = 45°$

$\frac{\omega}{r} = 0.3$

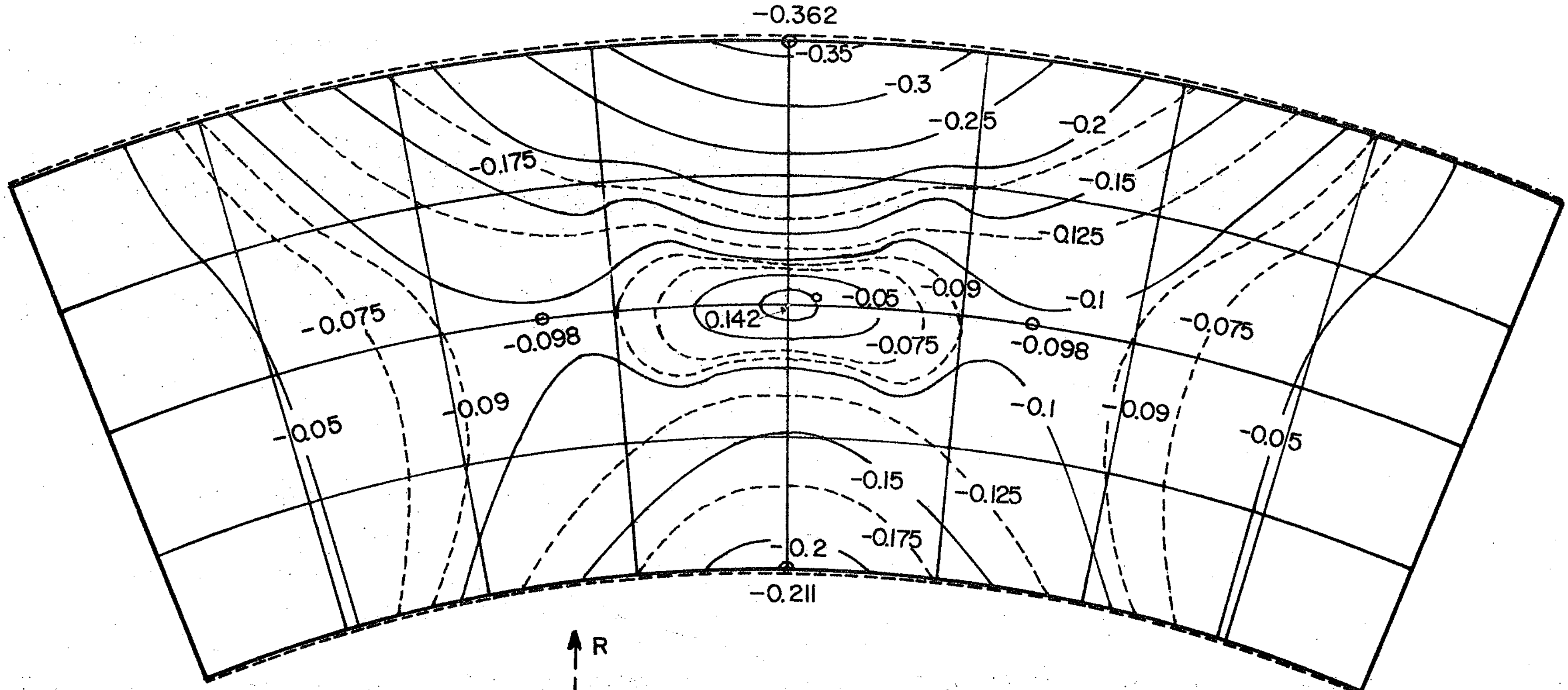

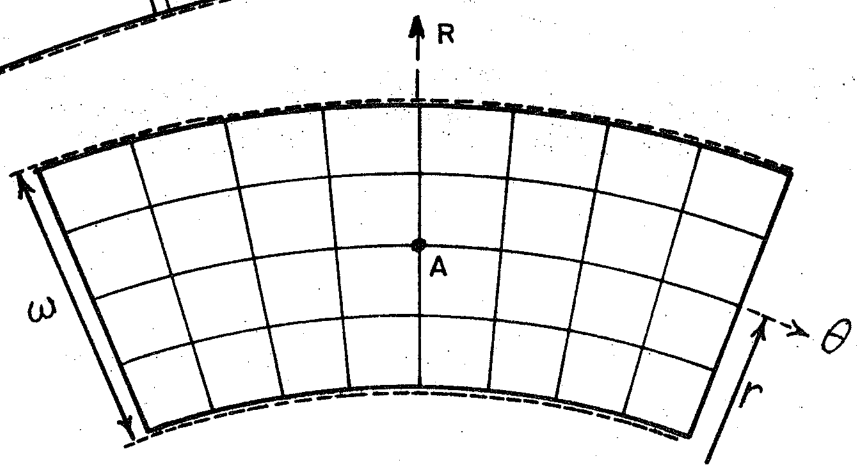

FIGURE I - 14

Influence Surface I_R for the Reference Point A

$\theta = 45°$

$\frac{\omega}{r} = 0.3$

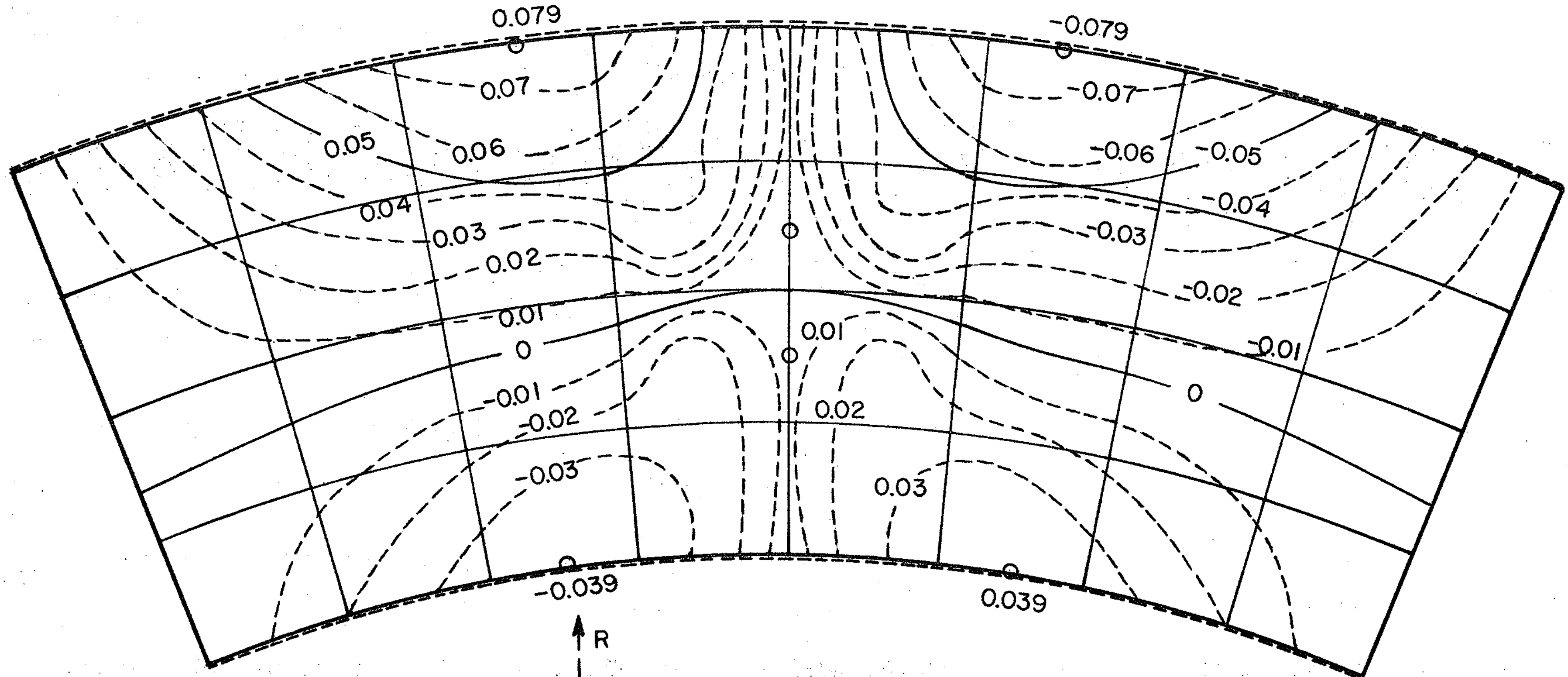

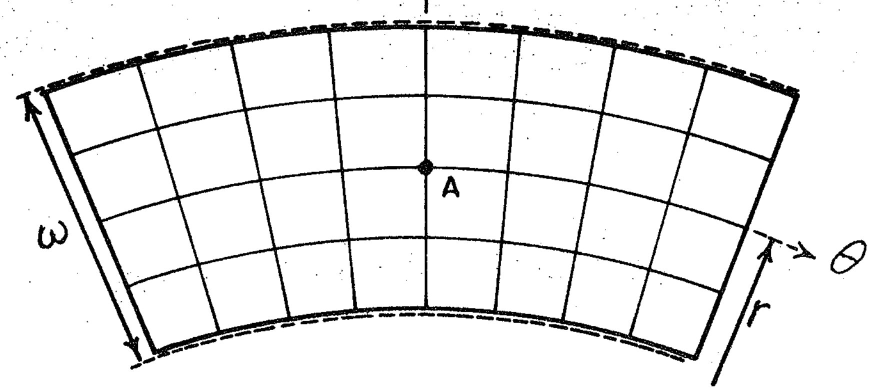

FIGURE I - 15

Influence Surface $I_{\theta R}$ for the Reference Point A

$\theta = 45°$

$\frac{\omega}{r} = 0.3$

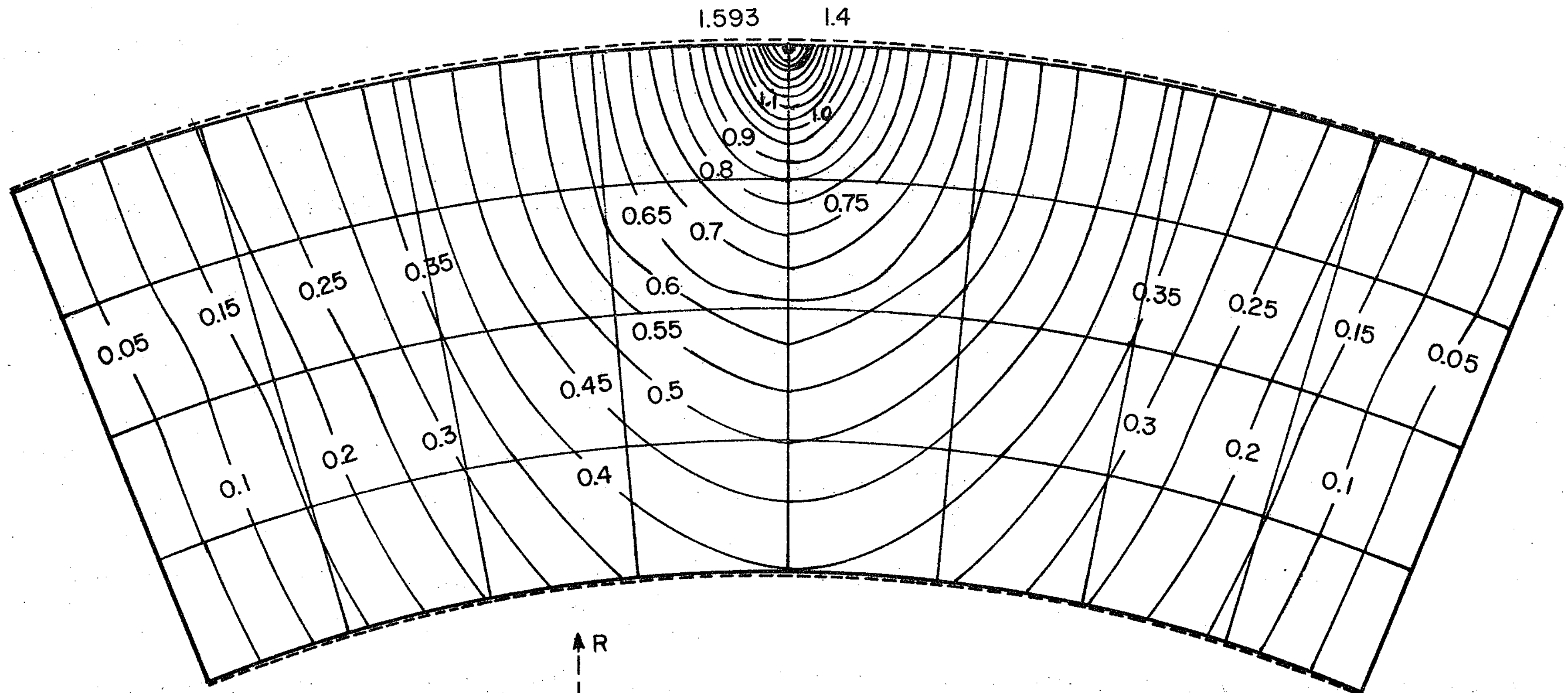

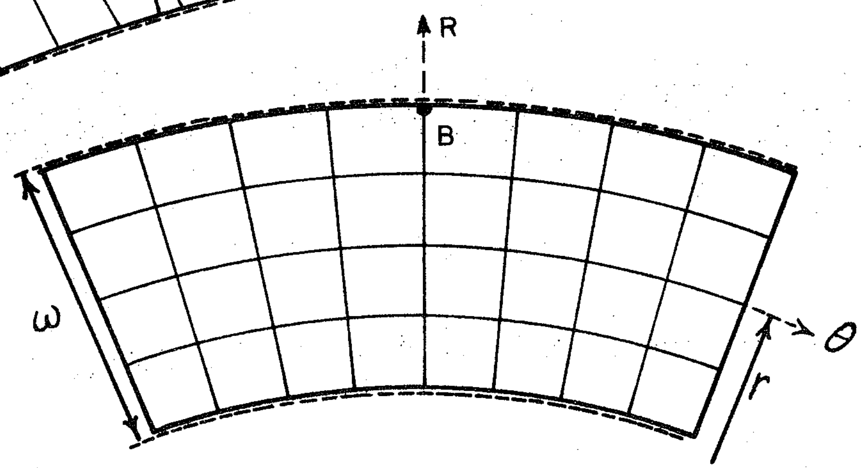

FIGURE I - 16

Influence Surface I_θ for the Reference Point B

$\theta = 45°$

$\frac{\omega}{r} = 0.3$

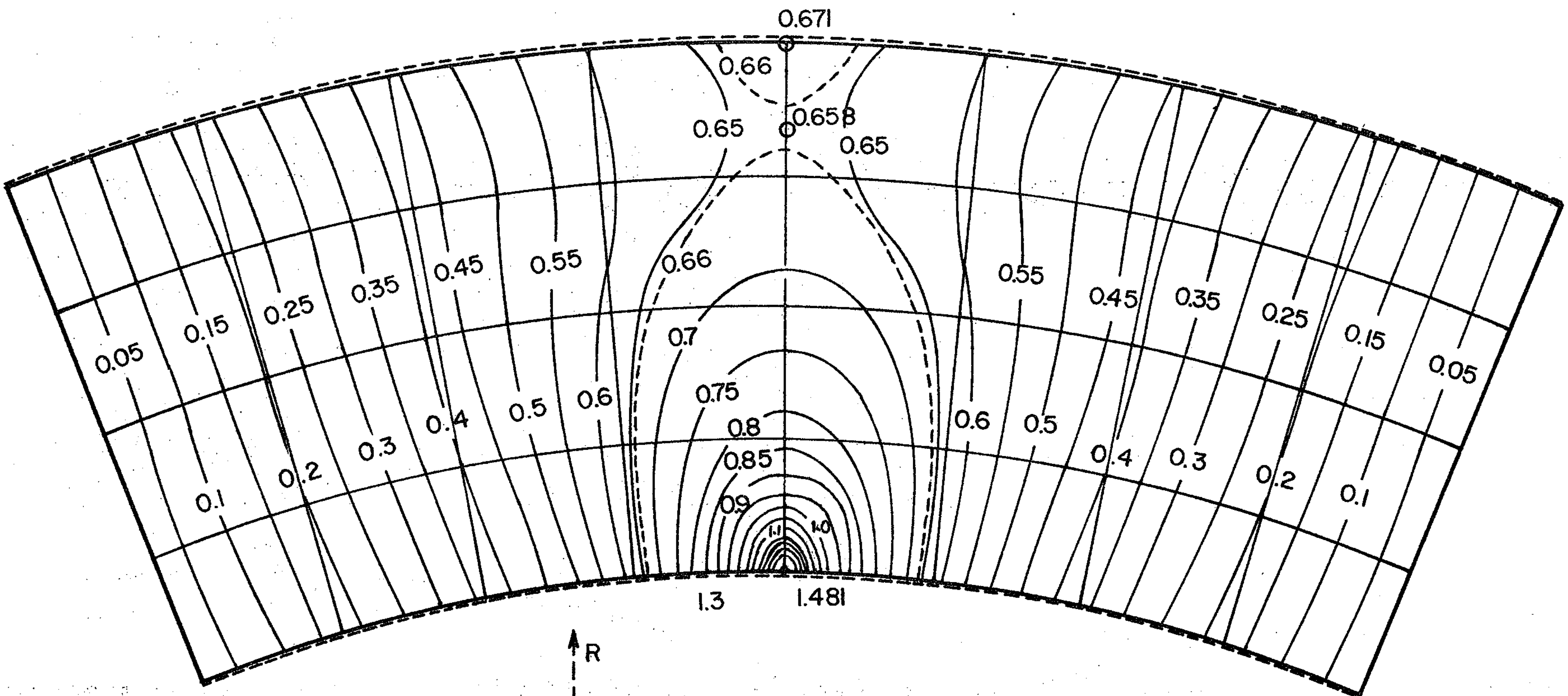

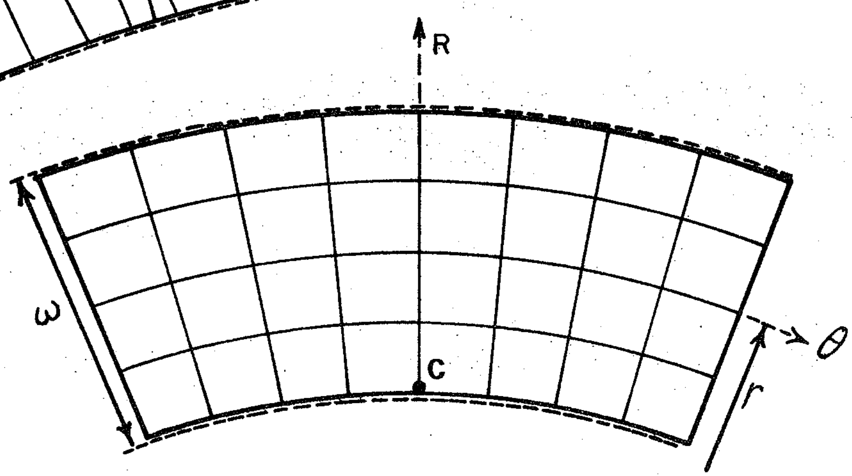

FIGURE I - 17

Influence Surface I_θ for the Reference Point C

$\theta = 45°$

$\frac{\omega}{r} = 0.3$

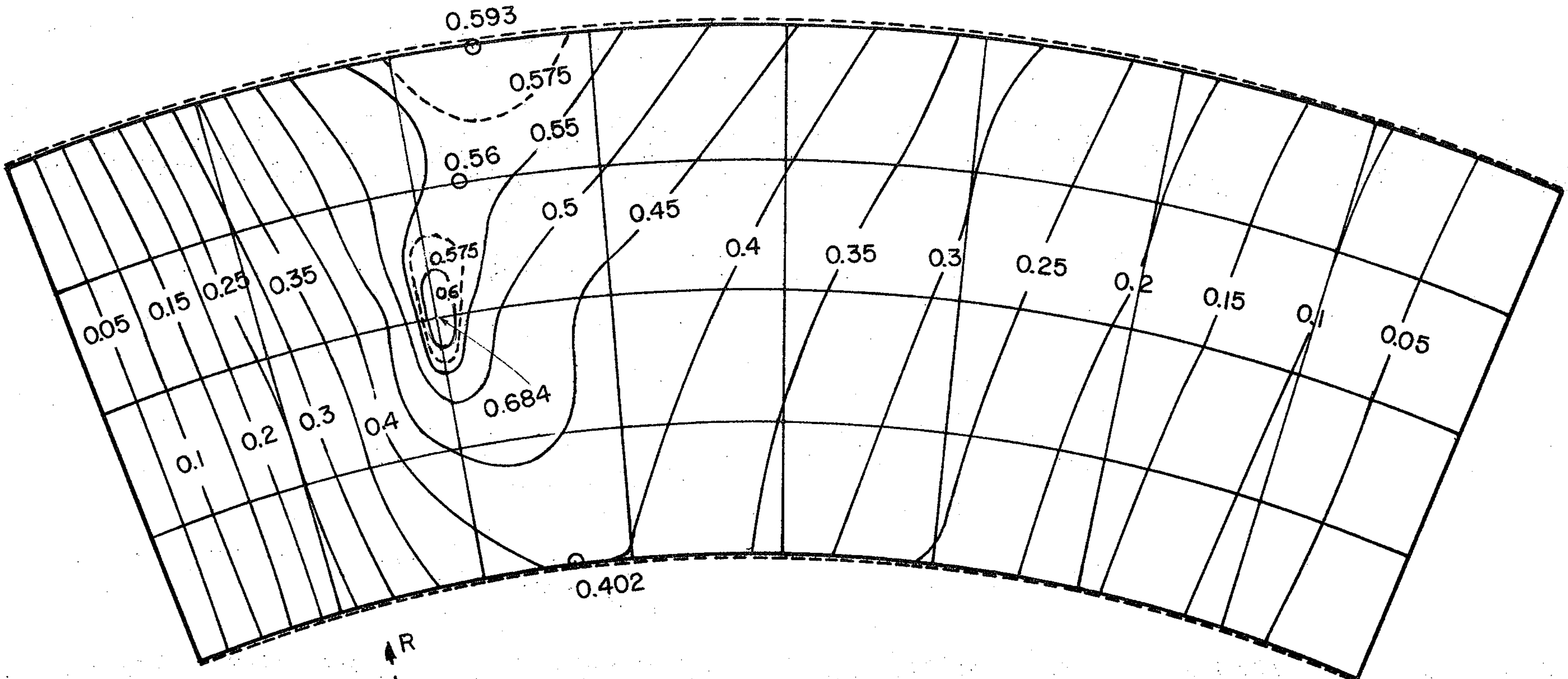

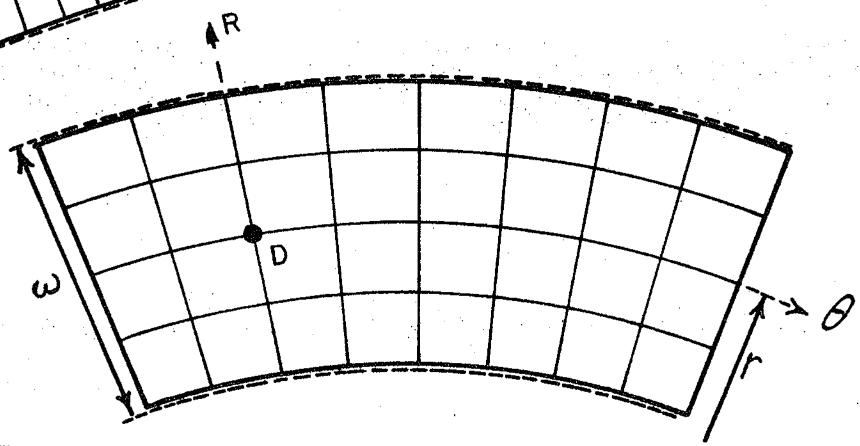

FIGURE I - 18

Influence Surface I_θ for the Reference Point D

$\theta = 45°$

$\frac{\omega}{r} = 0.3$

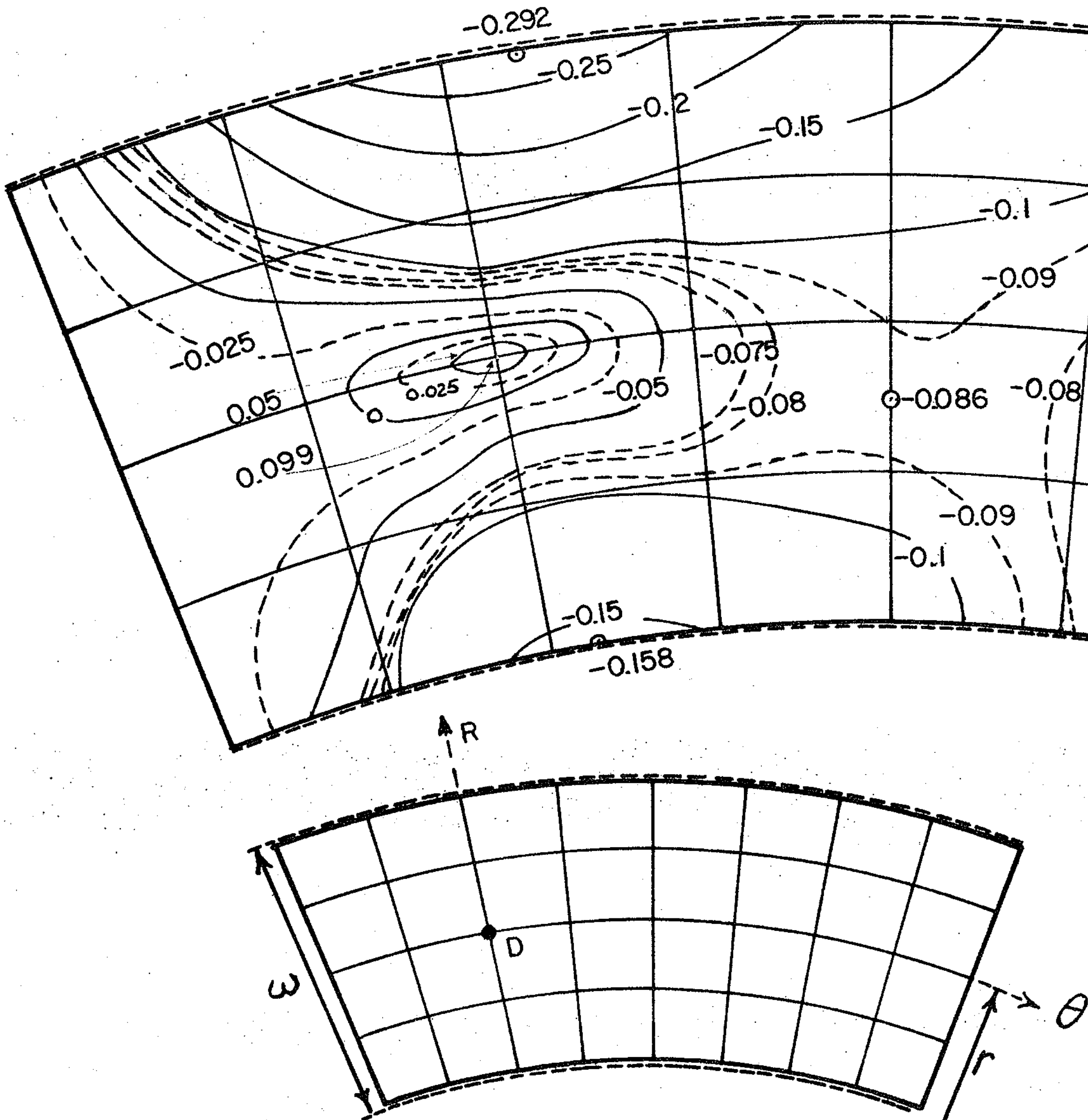

FIGURE I - 19

Influence Surface I_R for the Reference Point D

$\theta = 45°$

$\frac{\omega}{r} = 0.3$

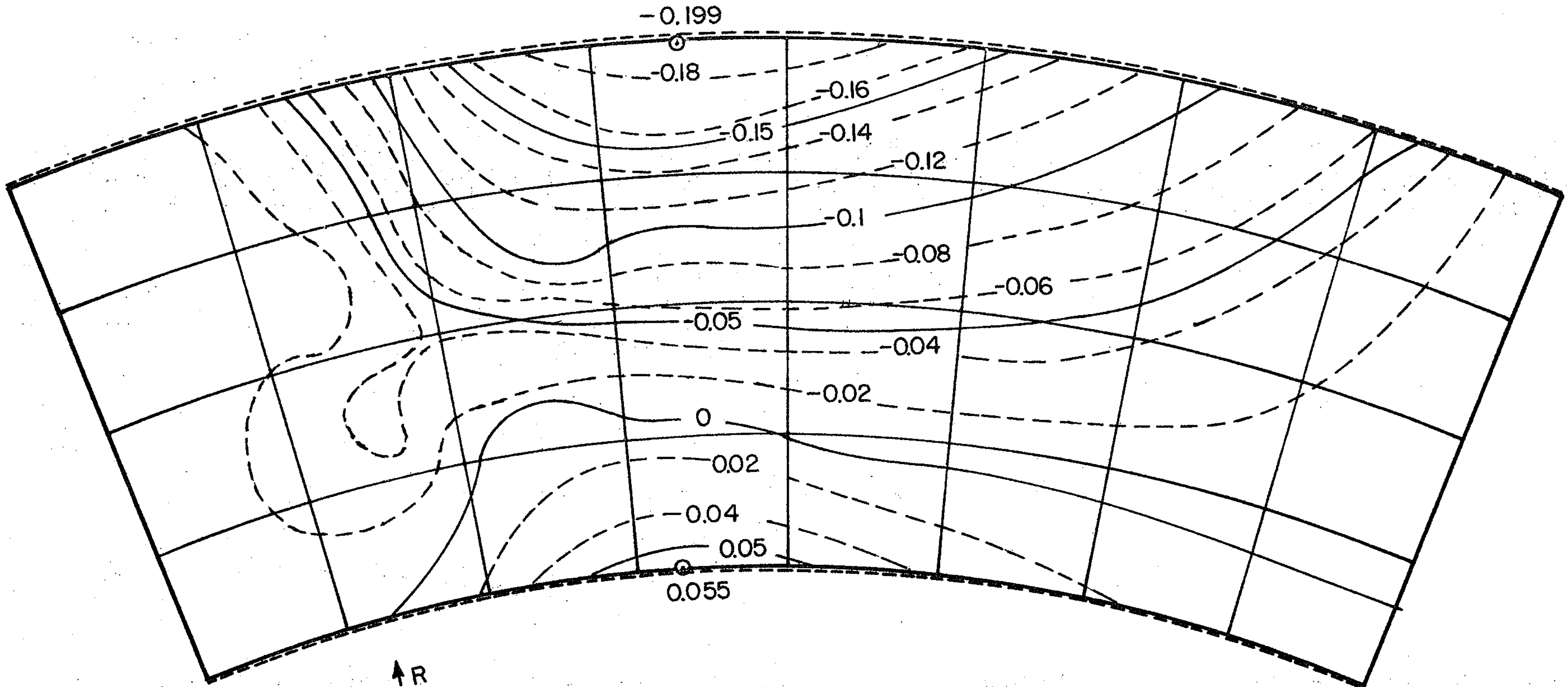

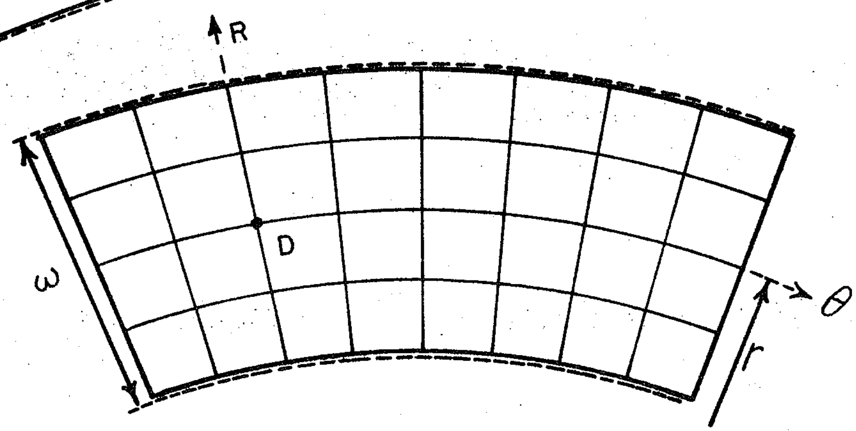

FIGURE I - 20

Influence Surface $I_{\theta R}$ for the

Reference Point D

$\theta = 45°$

$\frac{\omega}{r} = 0.3$

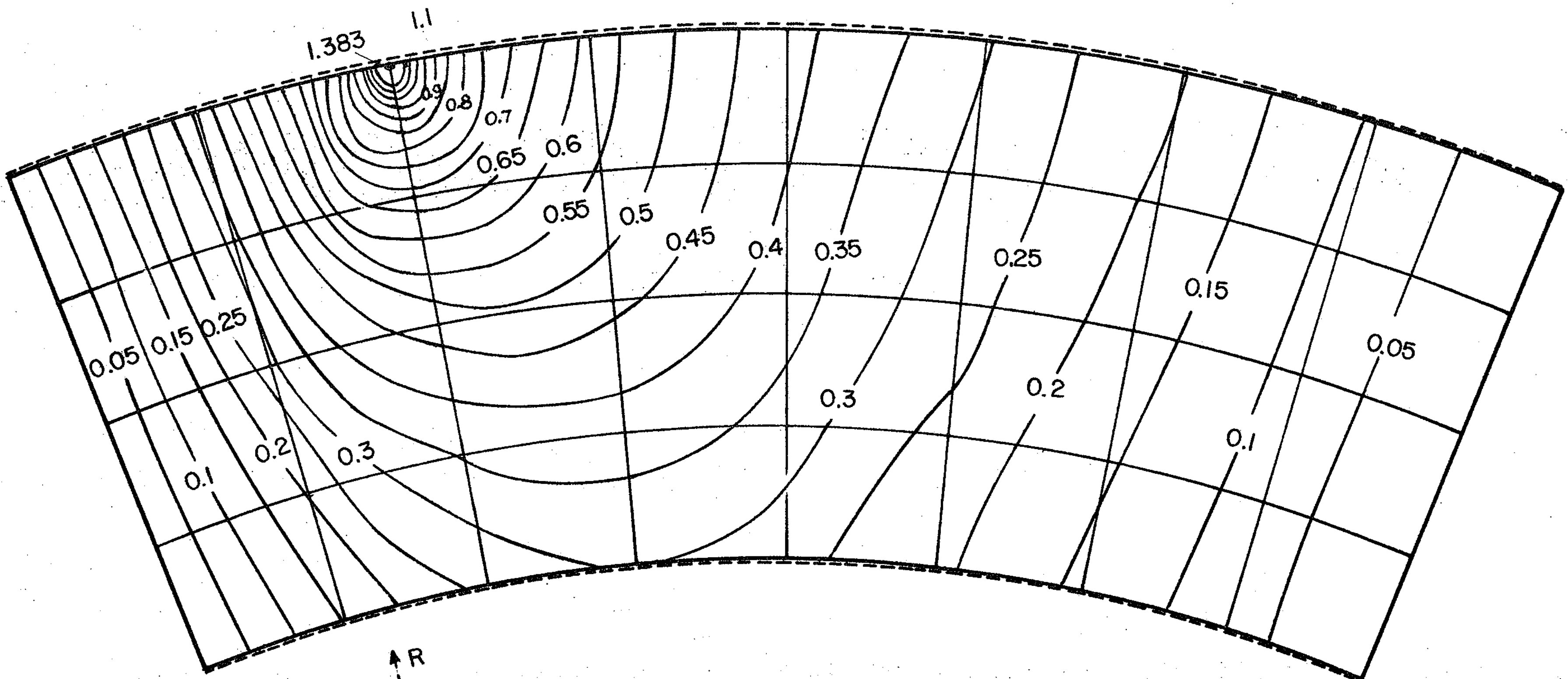

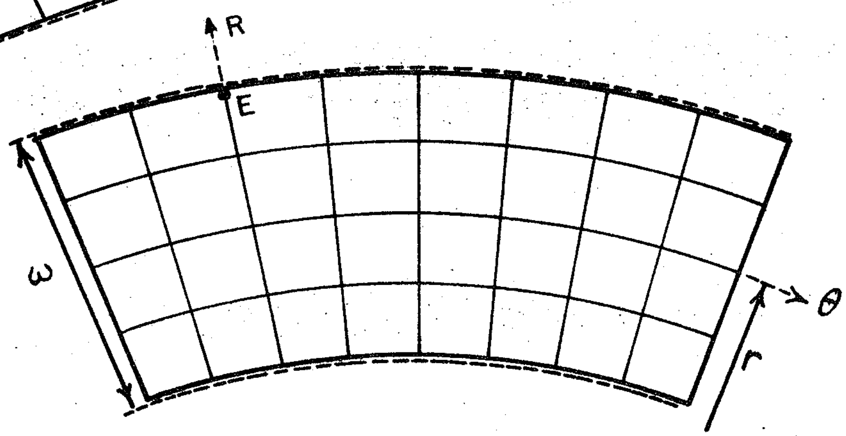

FIGURE I - 21

Influence Surface I_θ for the Reference Point E

$\theta = 45°$

$\frac{\omega}{r} = 0.3$

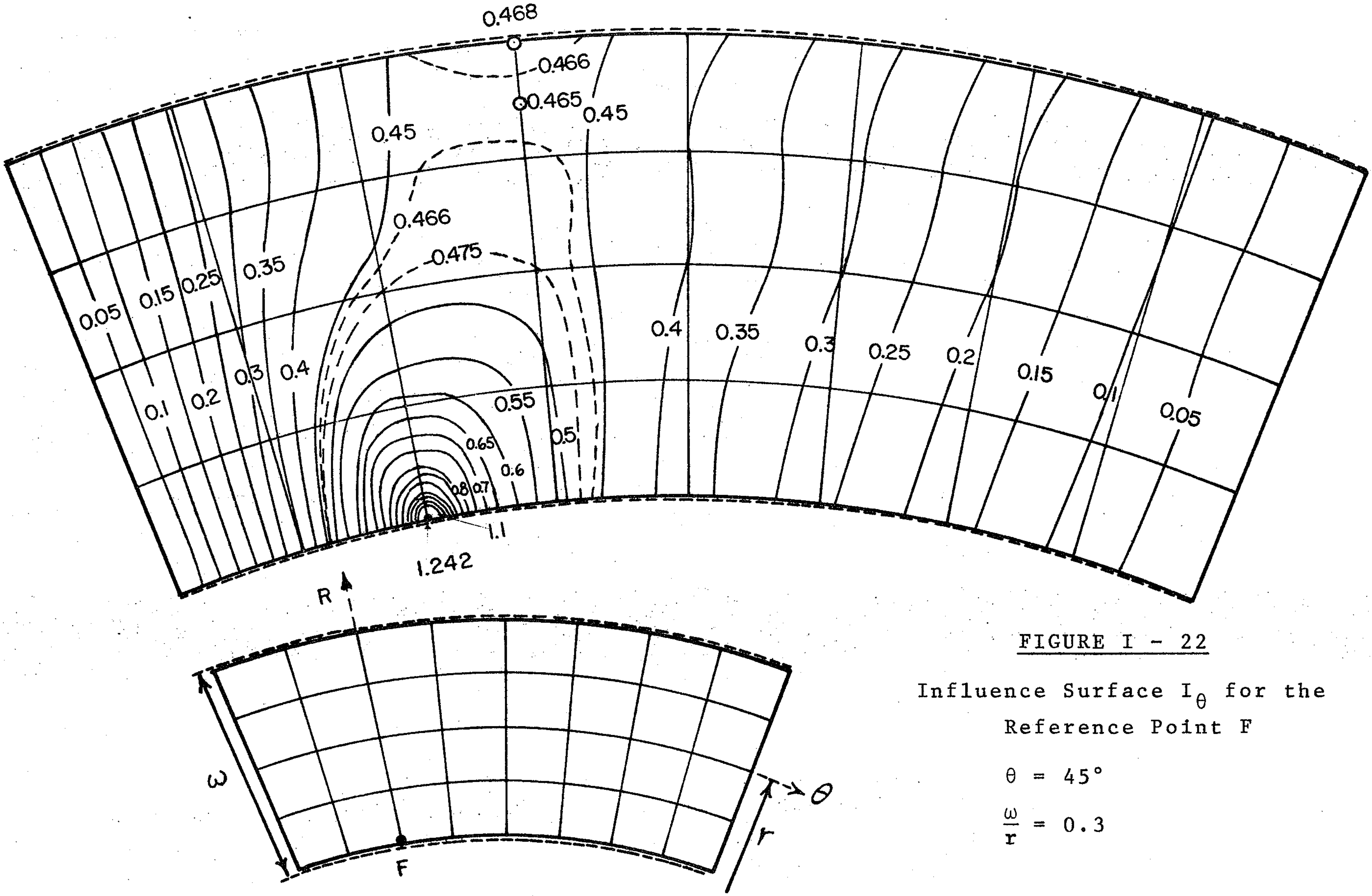

FIGURE I - 22

Influence Surface I_θ for the Reference Point F

$\theta = 45°$

$\frac{\omega}{r} = 0.3$

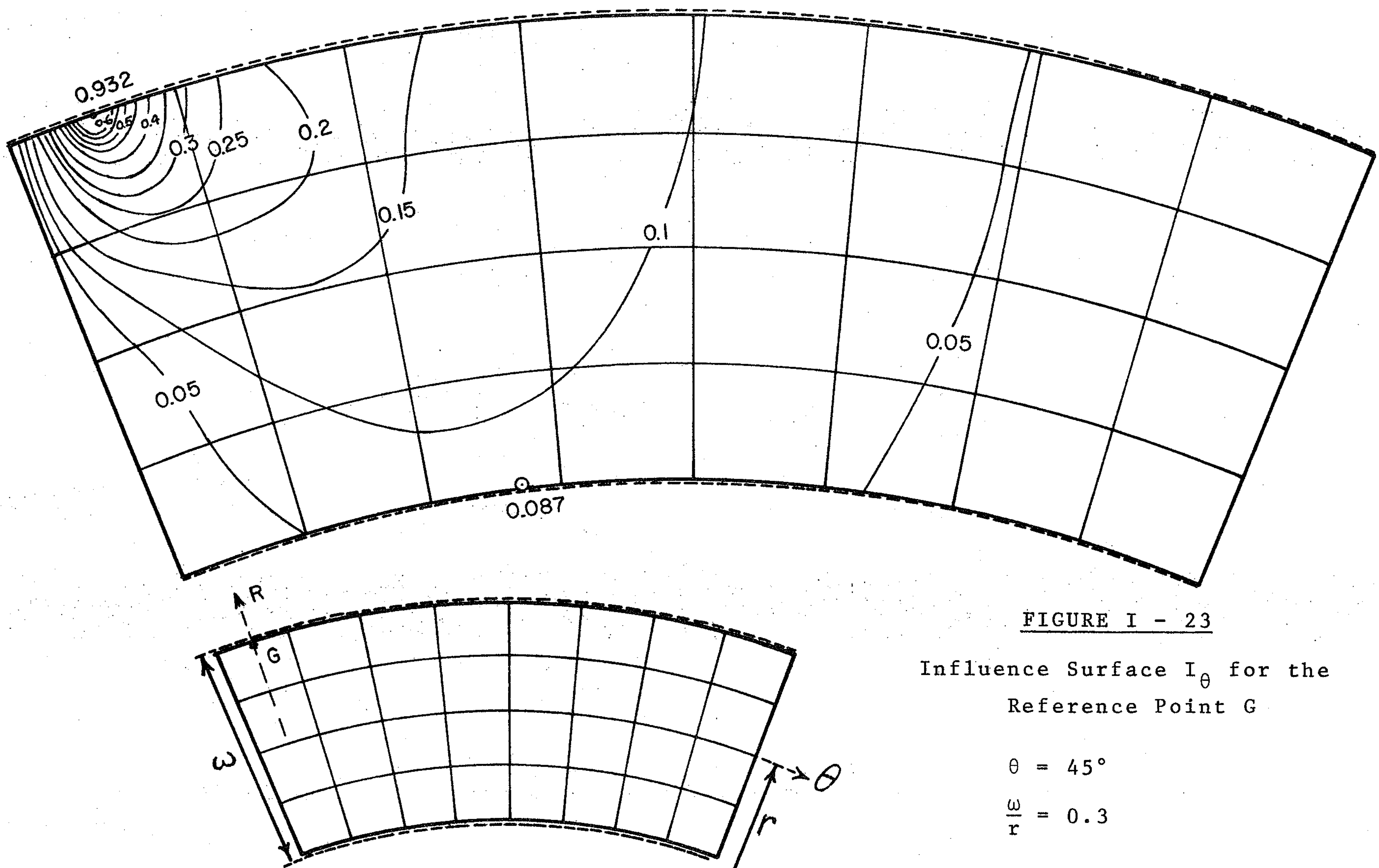

FIGURE I - 23

Influence Surface I_θ for the Reference Point G

$\theta = 45°$

$\frac{\omega}{r} = 0.3$

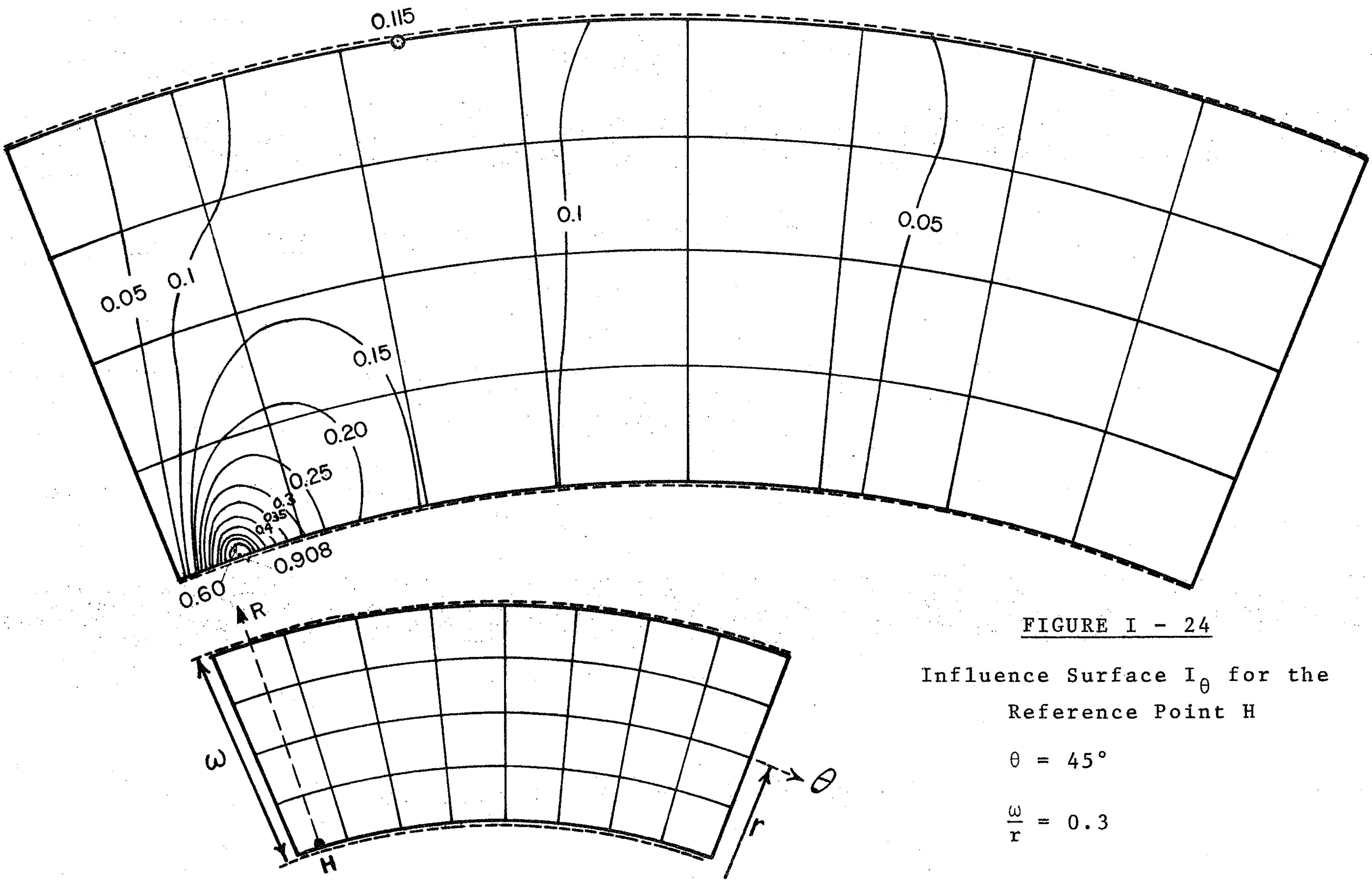

FIGURE I - 24

Influence Surface I_θ for the Reference Point H

$\theta = 45°$

$\frac{\omega}{r} = 0.3$

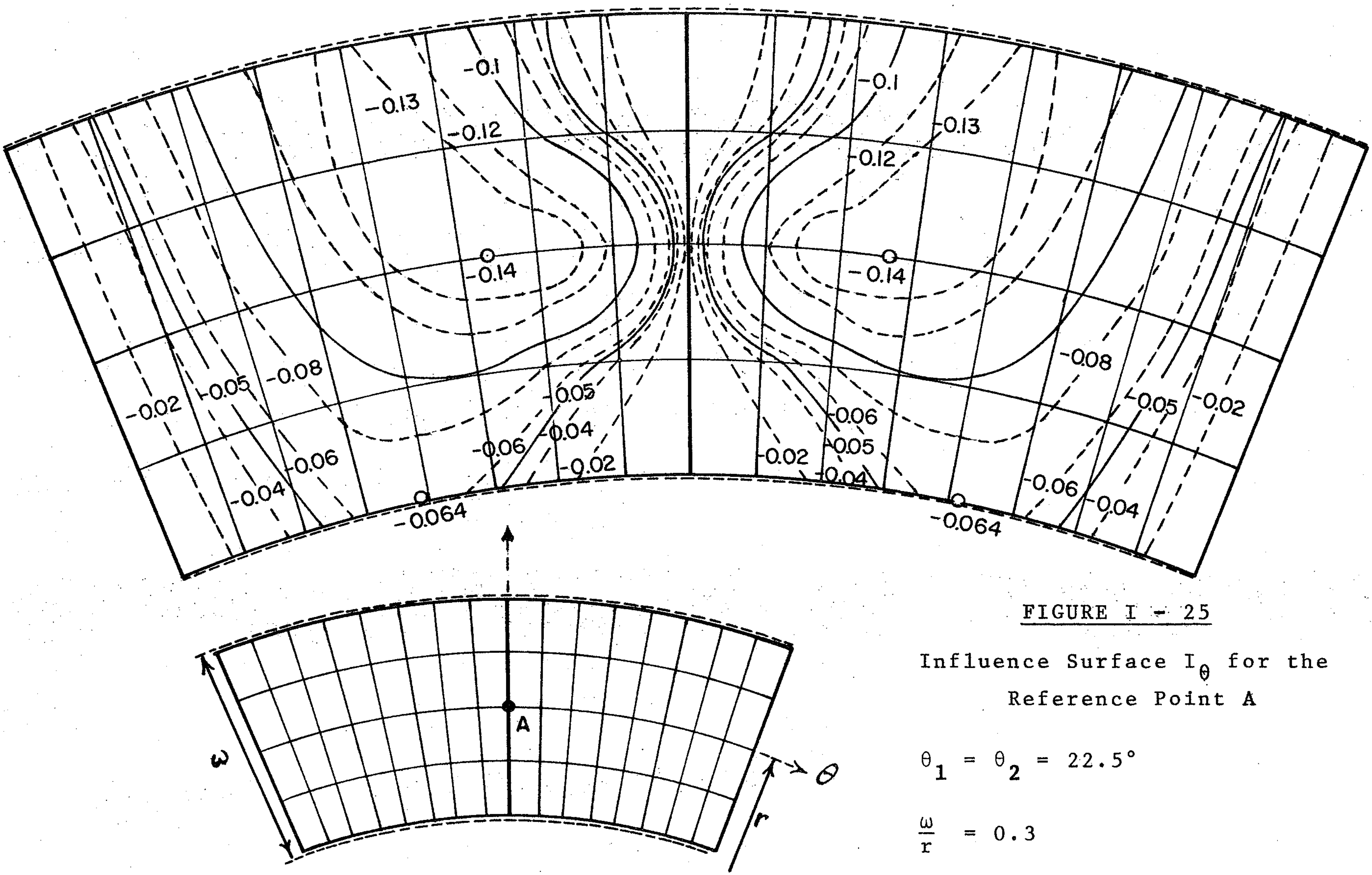

FIGURE I - 25

Influence Surface I_θ for the Reference Point A

$\theta_1 = \theta_2 = 22.5°$

$\frac{\omega}{r} = 0.3$

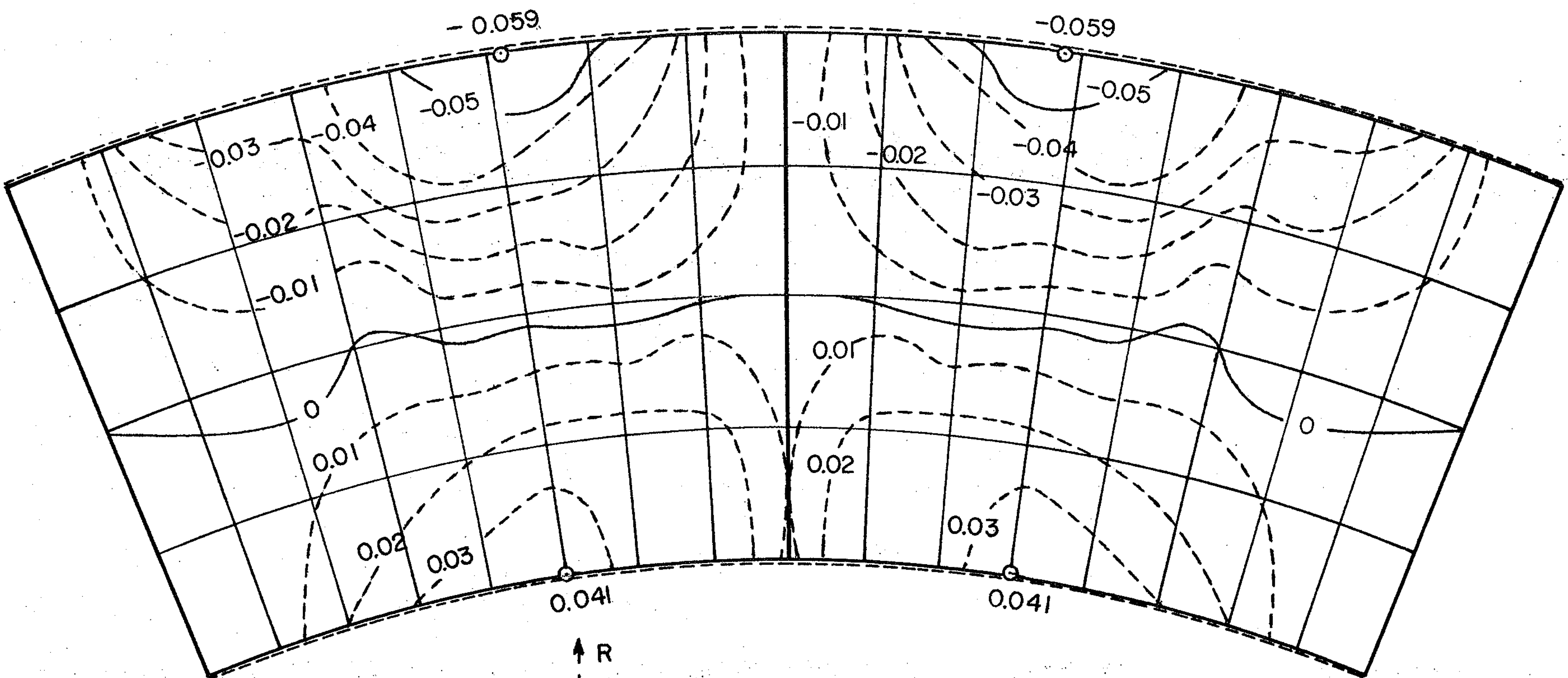

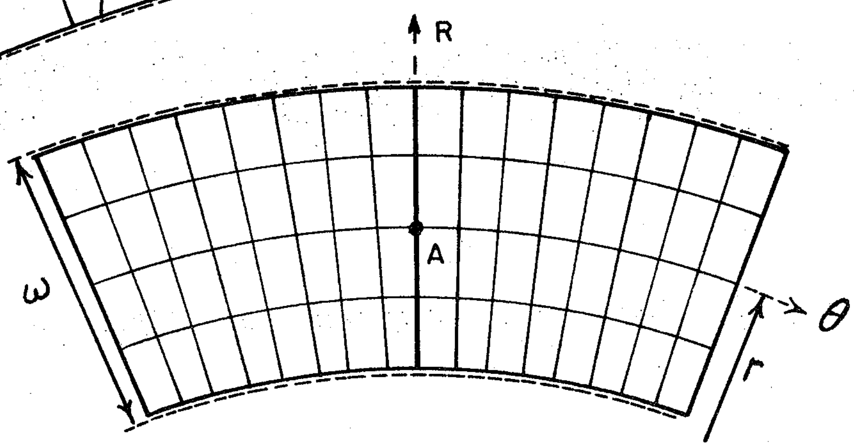

FIGURE I - 26

Influence Surface $I_{\theta R}$ for the Reference Point A

$\theta_1 = \theta_2 = 22.5°$

$\frac{\omega}{r} = 0.3$

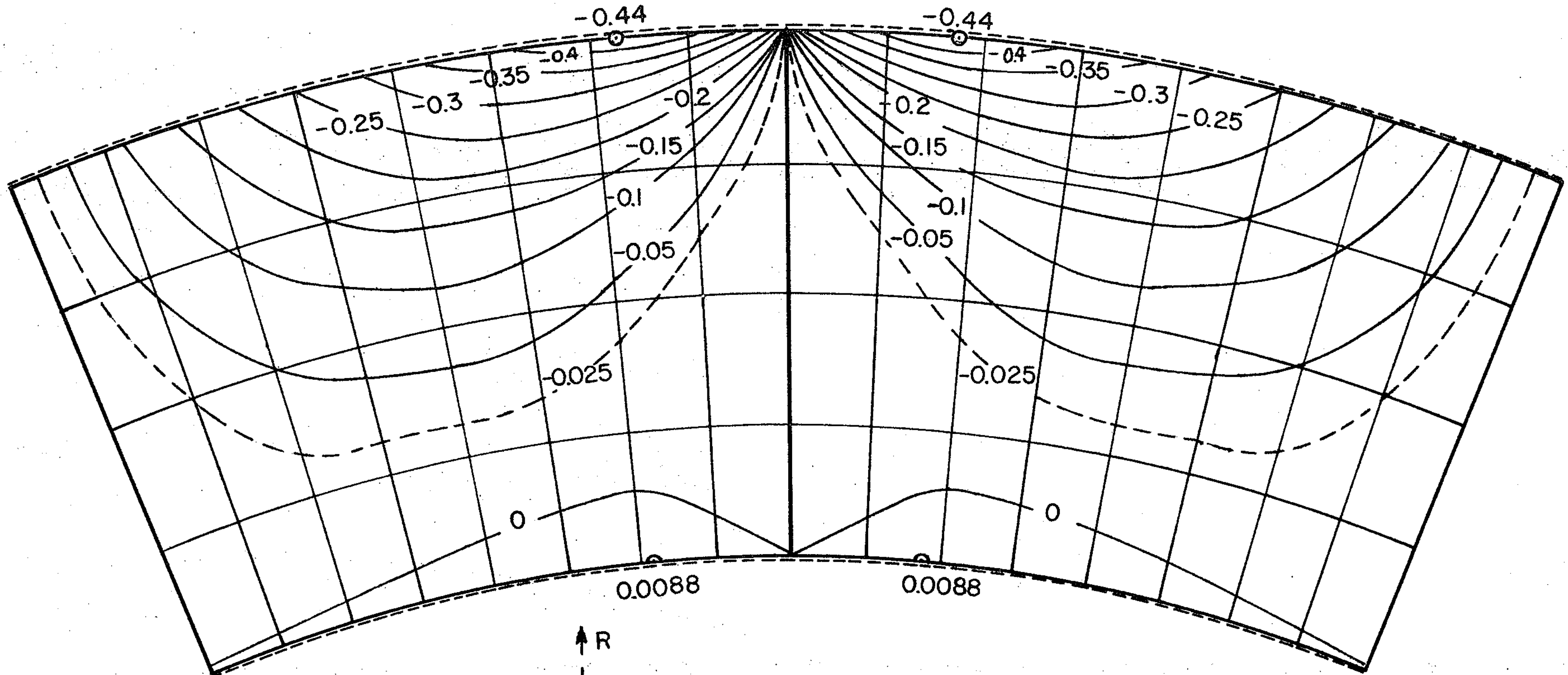

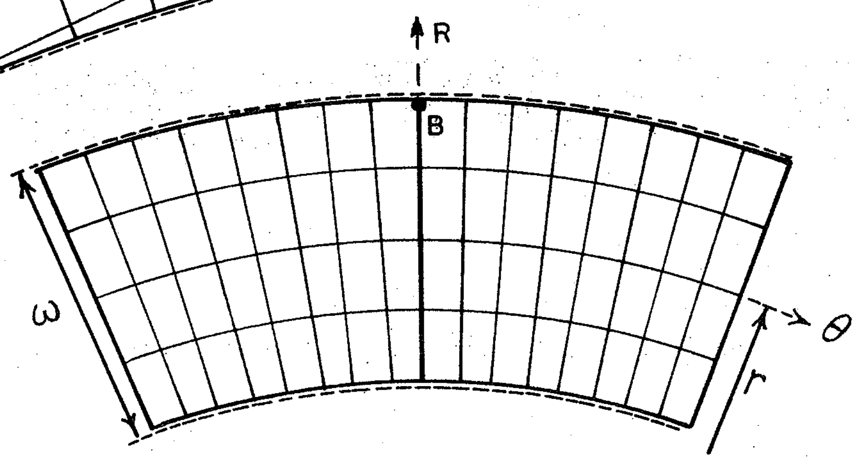

FIGURE I - 27

Influence Surface I_θ for the Reference Point B

$\theta_1 = \theta_2 = 22.5°$

$\frac{\omega}{r} = 0.3$

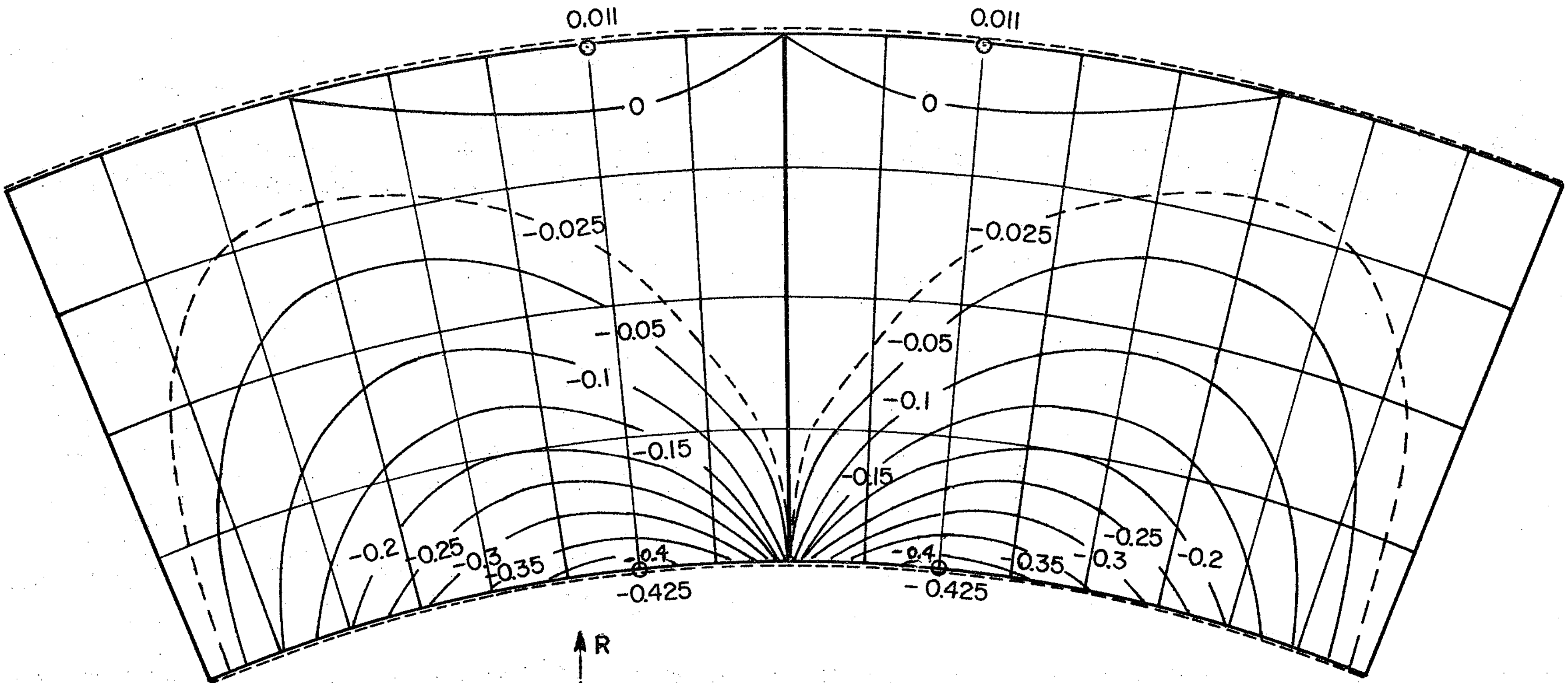

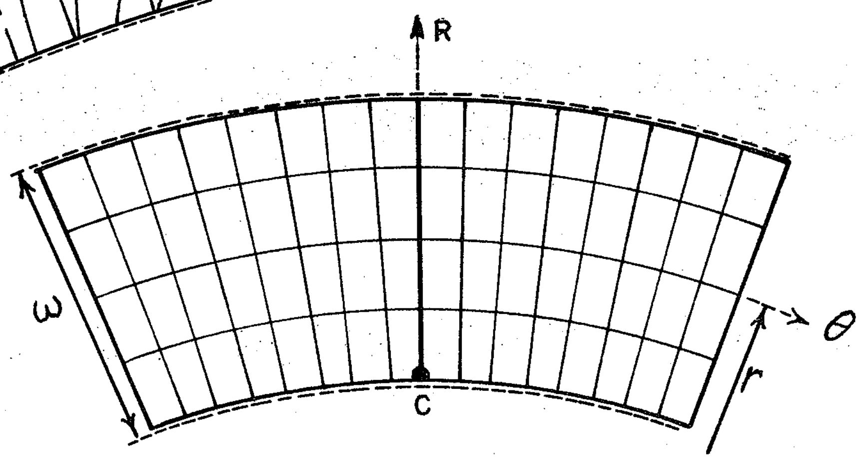

FIGURE I - 28

Influence Surface I_θ for the Reference Point C

$\theta_1 = \theta_2 = 22.5°$

$\frac{\omega}{r} = 0.3$

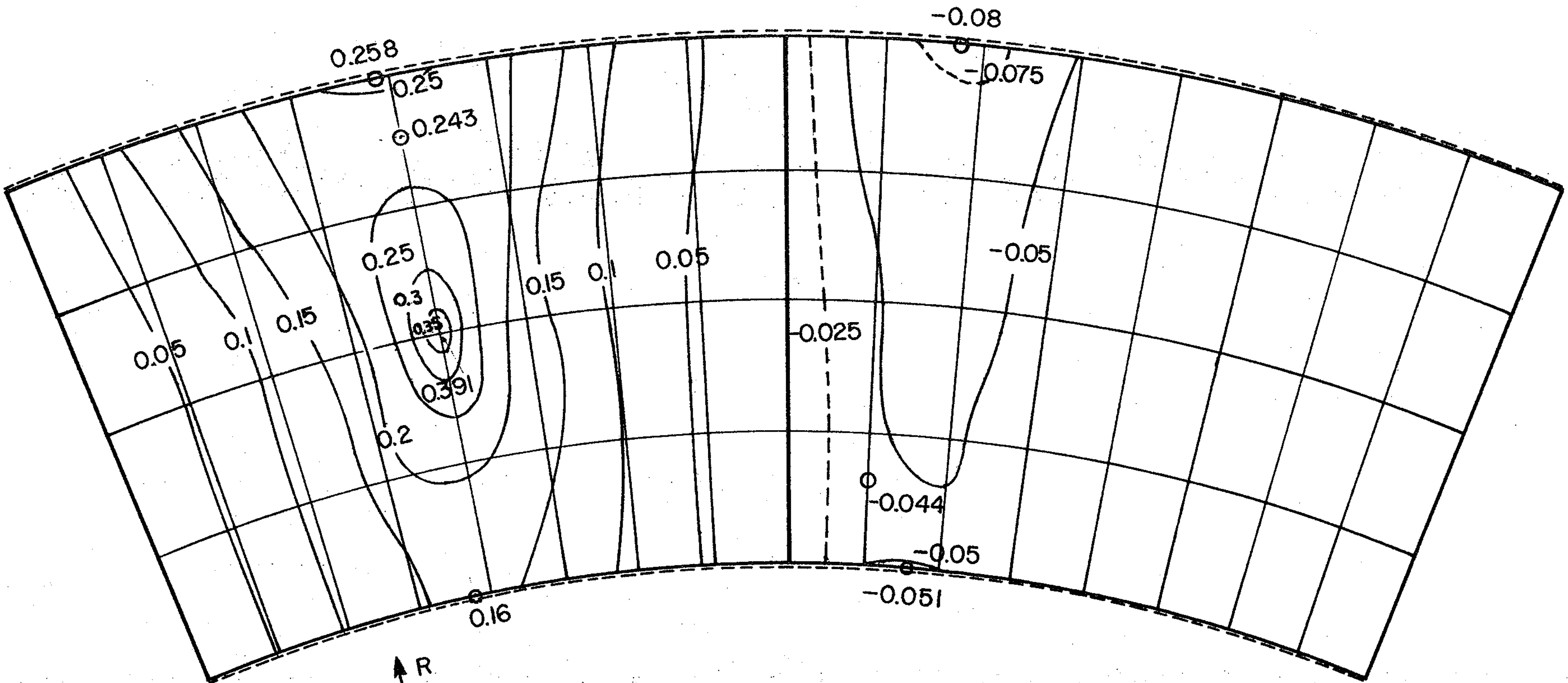

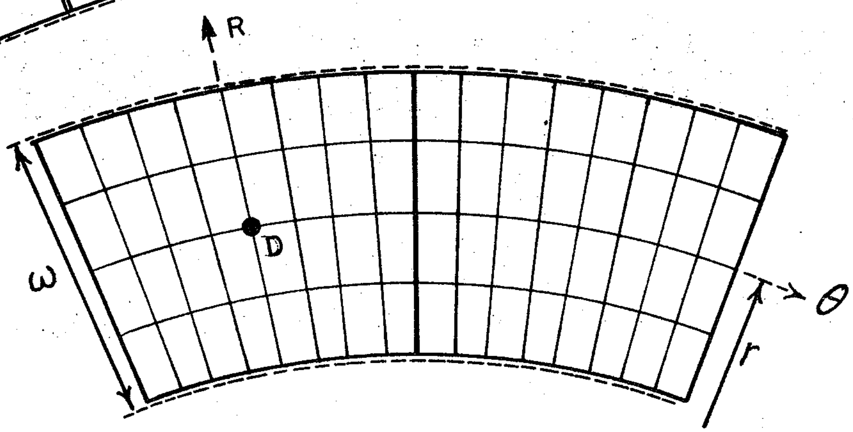

FIGURE I - 29

Influence Surface I_θ for the Reference Point D

$\theta_1 = \theta_2 = 22.5°$

$\frac{\omega}{r} = 0.3$

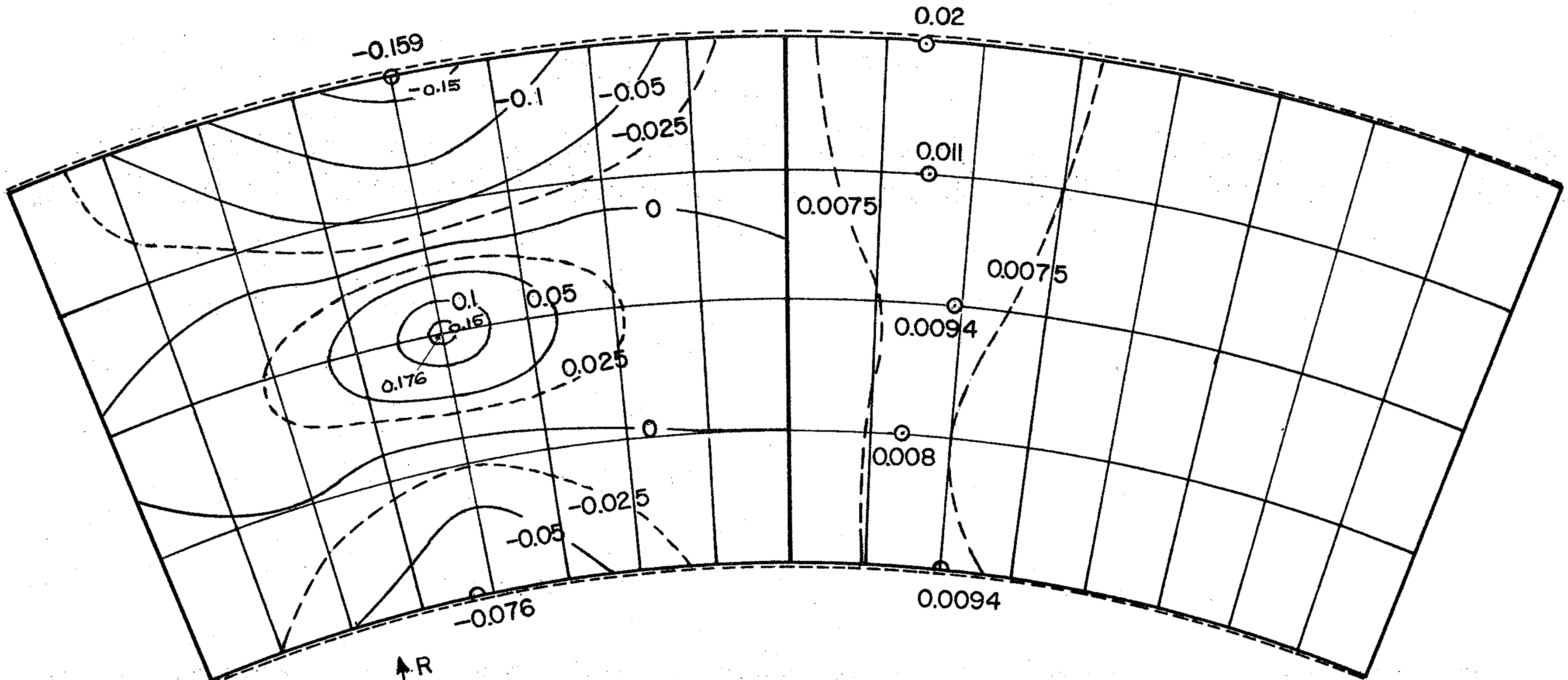

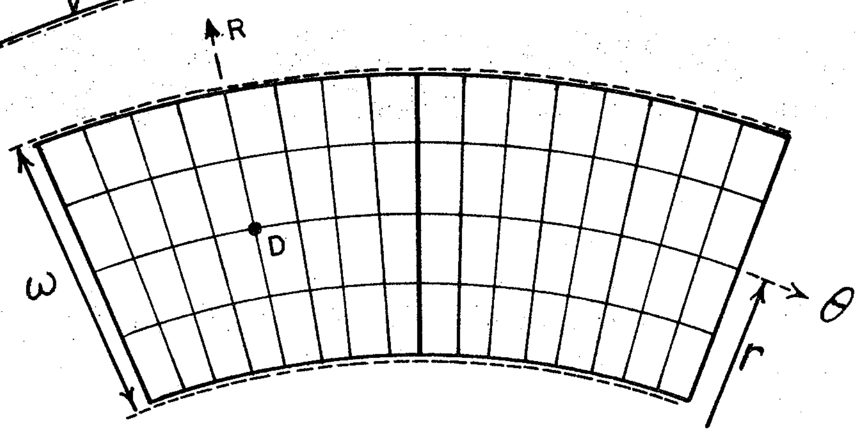

FIGURE I - 30

Influence Surface I_R for the Reference Point D

$\theta_1 = \theta_2 = 22.5°$

$\frac{\omega}{r} = 0.3$

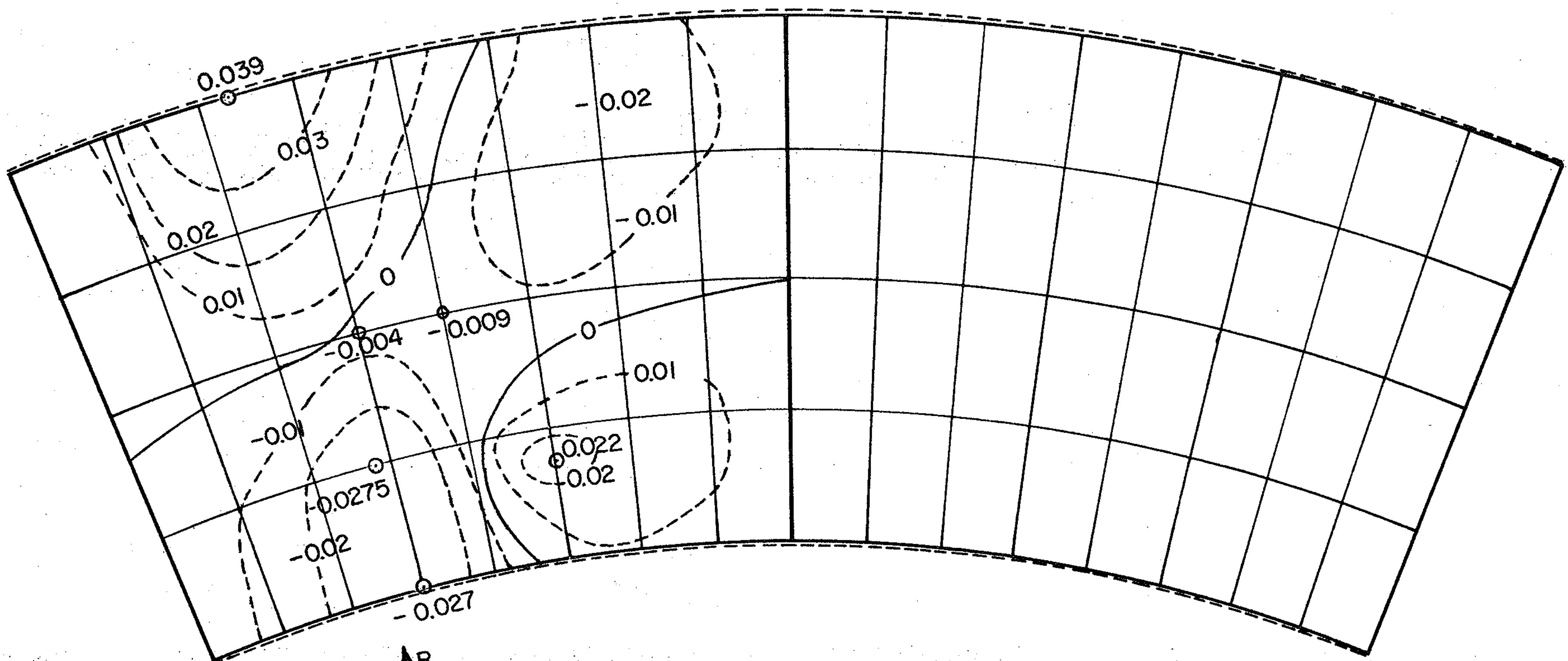

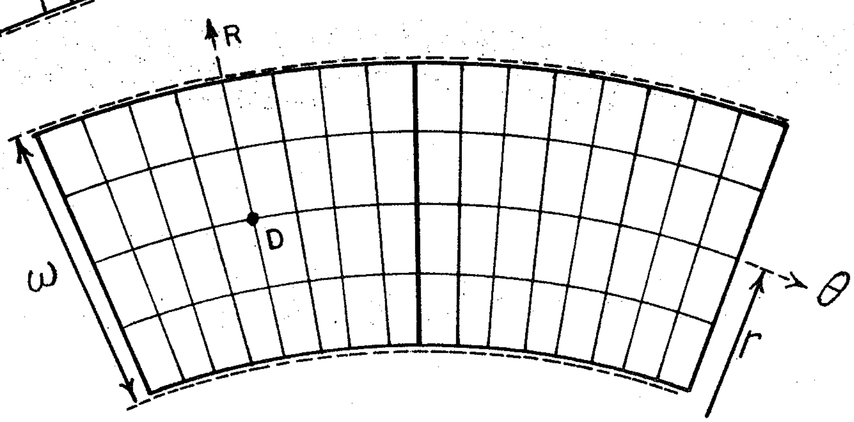

FIGURE I - 31

Influence Surface $I_{\theta R}$ for the Reference Point D

$\theta_1 = \theta_2 = 22.5°$

$\frac{\omega}{r} = 0.3$

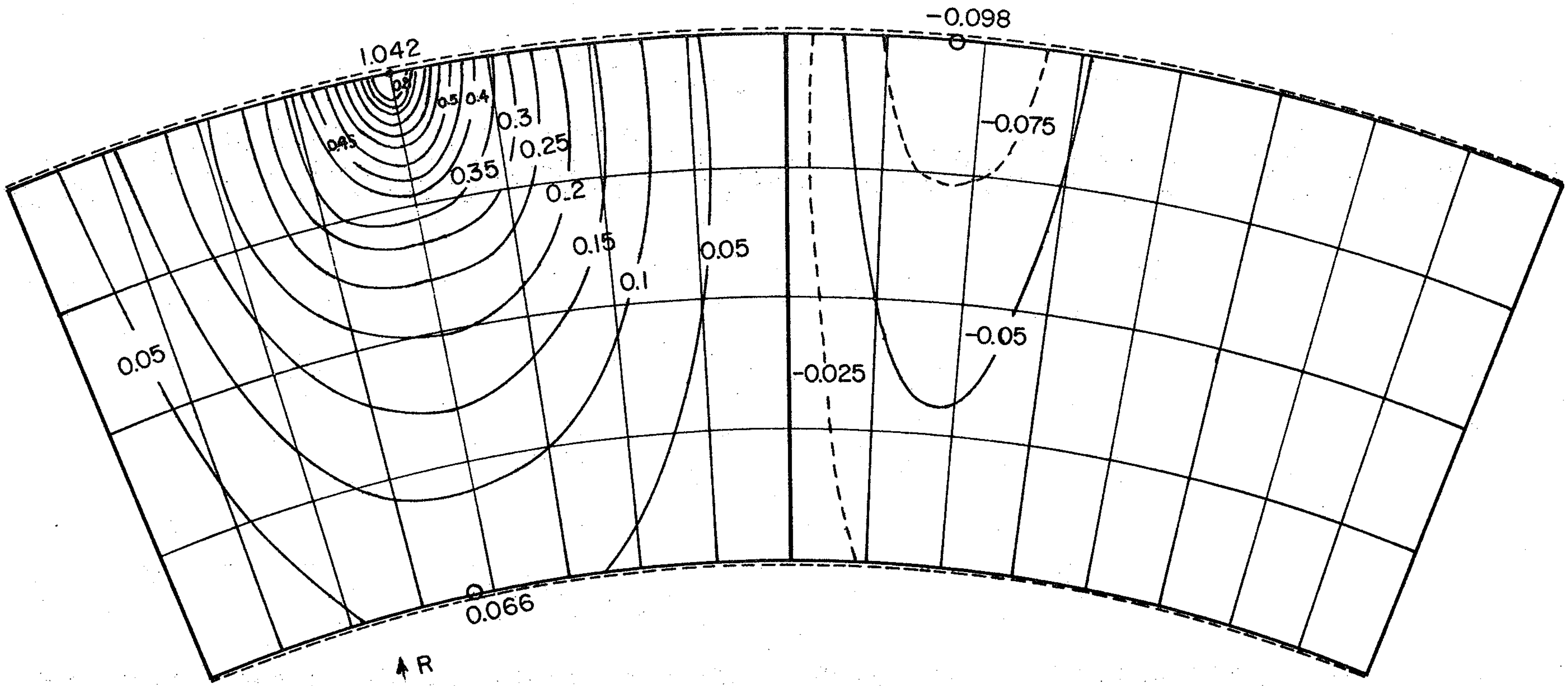

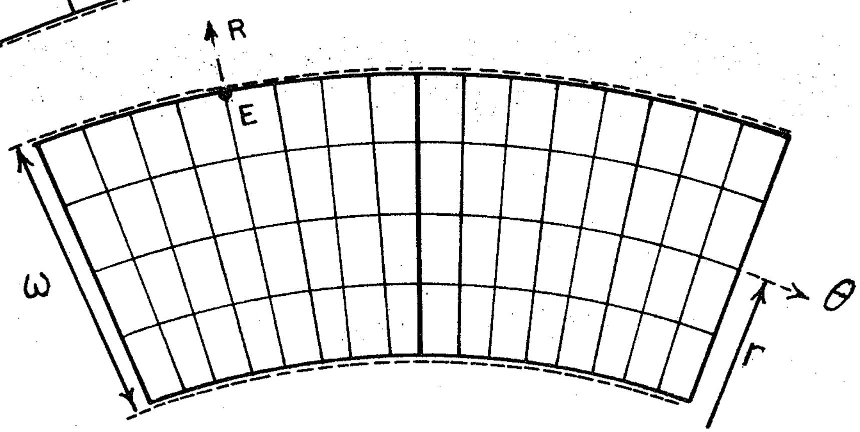

<u>FIGURE I - 32</u>

Influence Surface I_θ for the Reference Point E

$\theta_1 = \theta_2 = 22.5°$

$\frac{\omega}{r} = 0.3$

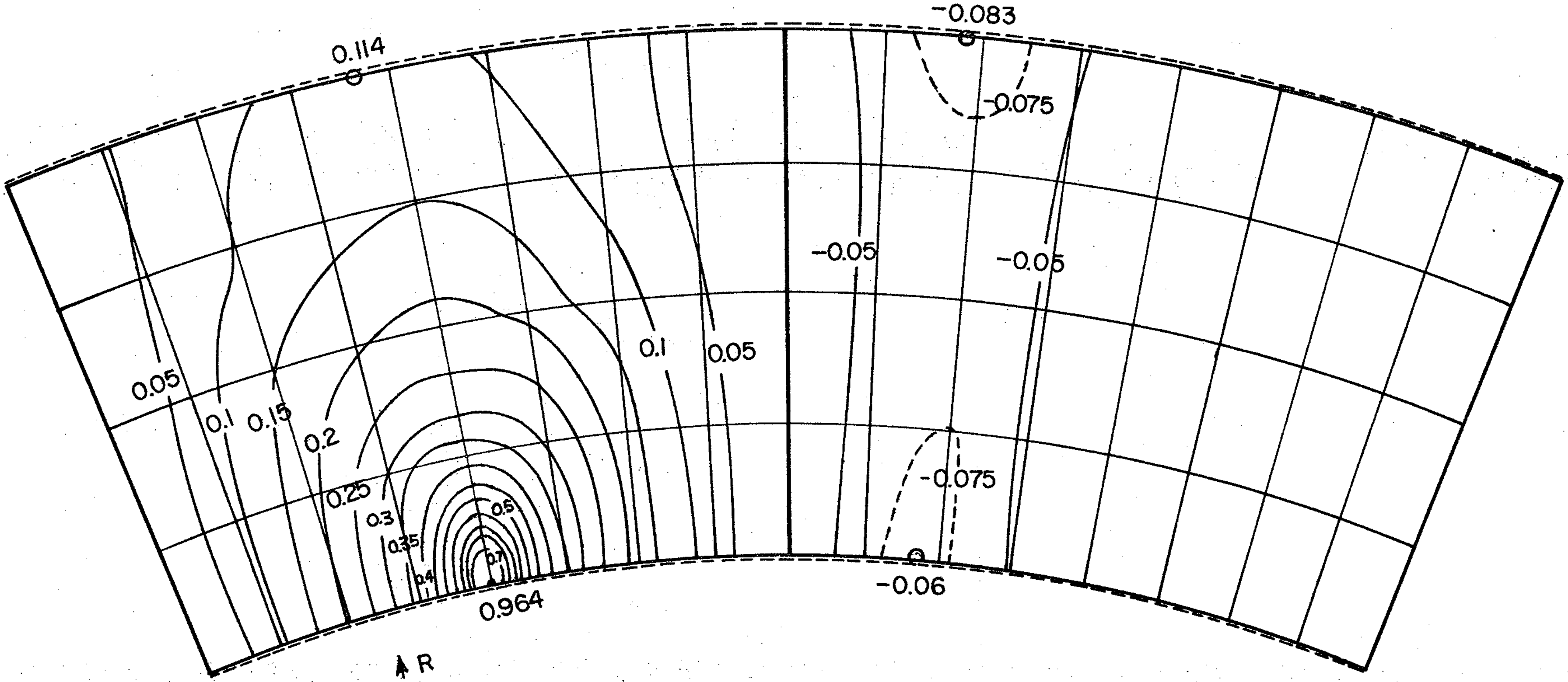

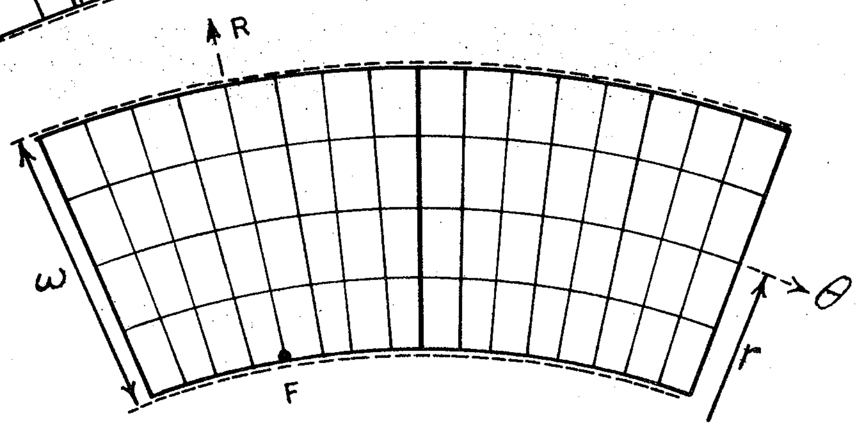

FIGURE I - 33

Influence Surface I_θ for the Reference Point F

$\theta_1 = \theta_2 = 22.5°$

$\frac{\omega}{r} = 0.3$

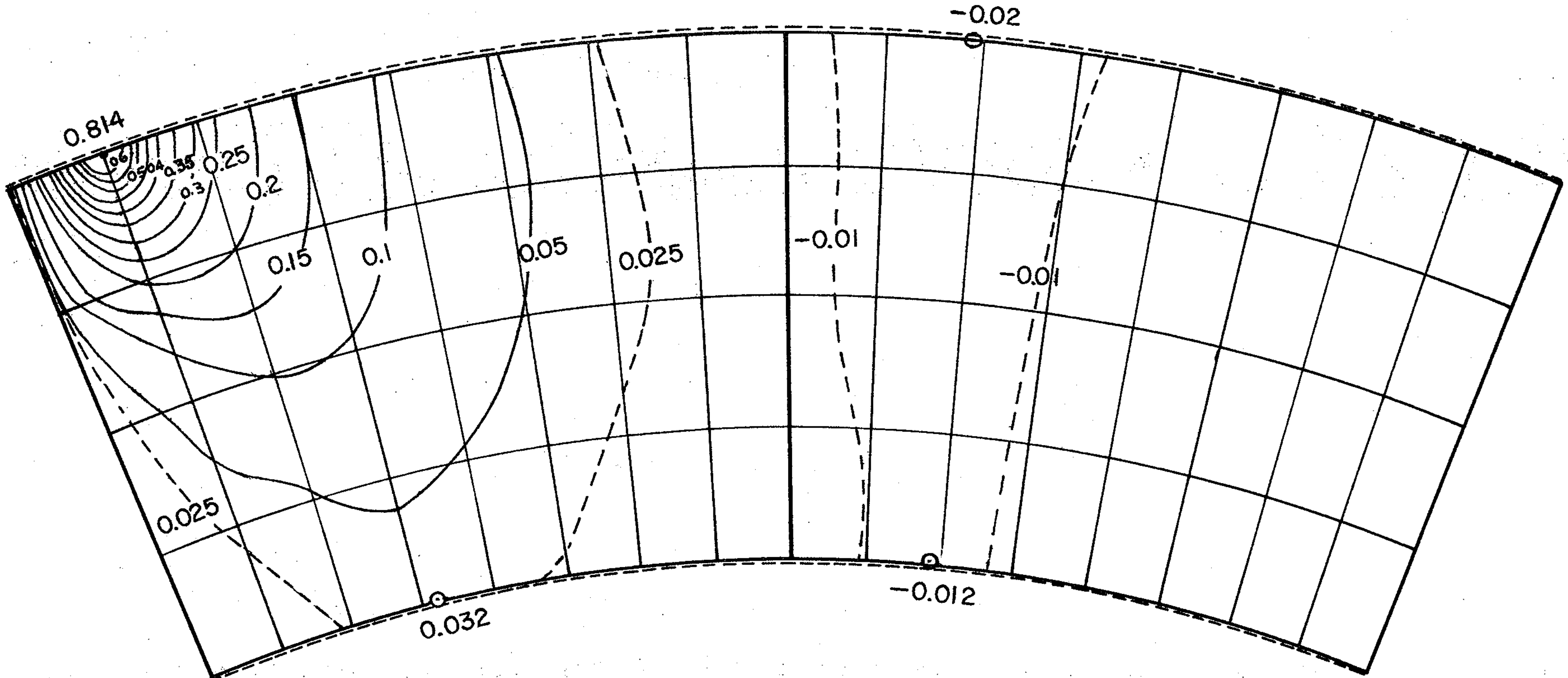

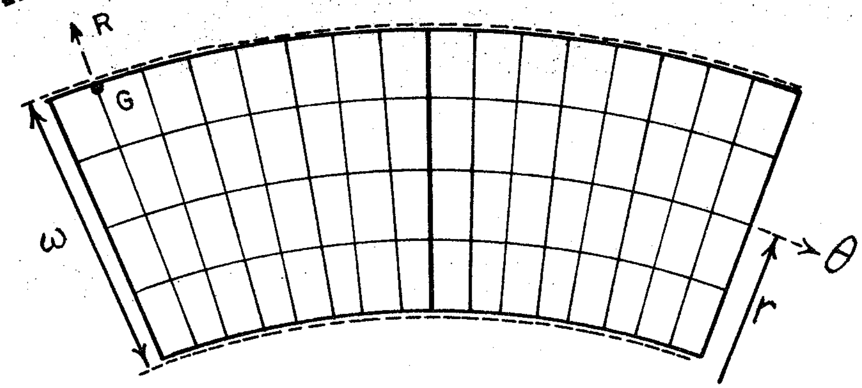

FIGURE I - 34

Influence Surface I_θ for the Reference Point G

$\theta_1 = \theta_2 = 22.5°$

$\frac{\omega}{r} = 0.3$

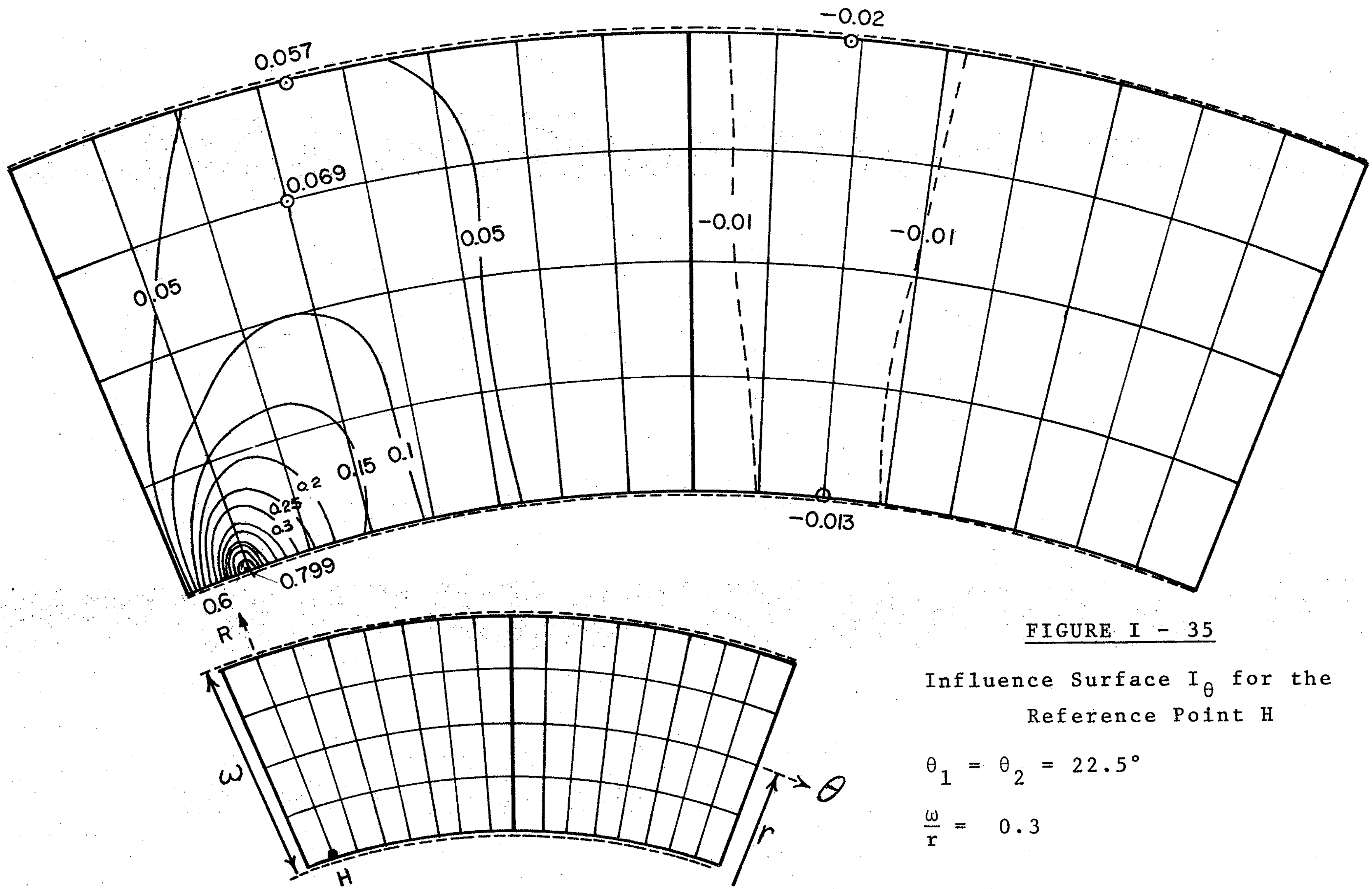

FIGURE I - 35

Influence Surface I_θ for the Reference Point H

$\theta_1 = \theta_2 = 22.5°$

$\frac{\omega}{r} = 0.3$